TAMPEREEN TEKNILLINEN YLIOPISTO
TAMPERE UNIVERSITY OF TECHNOLOGY

KEIJO PENTTILÄ

QUALITY IMPROVEMENT OF PLASMA SPRAYED CHROMIA COATINGS BY IN SITU DRY ICE PROCESSING

Master of Science thesis

Examiners: prof. Petri Vuoristo,
M.Sc. Jarkko Kiilakoski
Examiner and topic approved by the
Faculty Council of the Faculty of
Engineering sciences
on 7th December 2016

ABSTRACT

KEIJO PENTTILÄ: Quality improvement of plasma sprayed chromia coatings by in situ dry ice processing
Tampere University of Technology
Master of Science Thesis, 107 pages, 10 Appendix pages
May 2017
Master's Degree Programme in Materials Technology
Major: Surface Engineering and Ceramic Materials
Examiner: Professor Petri Vuoristo, M.Sc. Jarkko Kiilakoski

Keywords: thermal spraying, plasma spraying, chromium oxide, dry ice blasting

Atmospheric plasma spraying is a commonly used process to deposit ceramic coatings for applications of wear and corrosion protection. Feedstock materials include for example aluminium oxide, titanium oxide and chromium oxide. Plasma sprayed chromium oxide coatings are widely used in for example anilox rolls, pump seals and wear rings for their good surface quality, high hardness and wear resistance.

Chromium oxide is however challenging to spray due to its high melting point, low thermal conductivity and tendency to vaporize in high temperatures. The vaporization of chromium oxide during spraying creates extremely fine dust particles, which gather on the workpiece and are trapped inside the coating layers reducing the cohesion and mechanical properties of the coating.

Dry ice blasting has been used in the field to improve the quality of chromium oxide and many other plasma sprayed coatings by keeping the surfaces clean and helping with thermal management. The use of dry ice blasting during spraying was investigated by plasma spraying chromium oxide coating at TUT with two different commercial dry ice blasters attached to the spraying robot. Several parameters were tested and temperature monitoring was implemented. Metallographic specimens were prepared and analysed by SEM. Hardness, adhesion, gas permeability and wear tests were also conducted.

It was found that dry ice blasting modifies the temperature history of the substrate and coating dramatically having unexpected effects. Excessive cooling lessened splat to splat bonding lowering cohesion and wear resistance but adjusting the spraying parameters hotter eliminated some of the adverse effects. There were also great differences in different blaster models related to the size of the particles exiting the nozzle. While the other blaster sprayed only small dry ice dust that mainly cooled the substrate, the other sprayed larger pellets with greater kinetic energy having a much more positive effect on coating cohesion increasing wear resistance compared to non-dry ice blasted samples.

TIIVISTELMÄ

KEIJO PENTTILÄ: Plasmaruiskutettujen kromioksidipinnoitteiden laadunparannus kuivajääpuhalluksella
Tampereen teknillinen yliopisto
Diplomityö, 107 sivua, 10 liitesivua
Toukokuu 2017
Materiaalitekniikan diplomi-insinöörin tutkinto-ohjelma
Pääaine: Pinnoitustekniikka ja keraamimateriaalit
Tarkastaja: professori Petri Vuoristo, dipl.ins. Jarkko Kiilakoski

Avainsanat: terminen ruiskutus, plasma ruiskutus, kromioksidi, kuivajääpuhallus

Plasmaruiskutusta käytetään keraamisten pinnoitteiden valmistamiseen erityisesti kulutus- ja korroosiokestävyyttä vaativiin käyttökohteisiin. Lähtöaineena käytetään esimerkiksi alumiinioksidia, titaanioksidia ja kromioksidia. Plasmaruiskutettuja kromioksidipinnoitteita käytetään laajasti esimerkiksi painokoneiden teloissa, tiivisteissä ja kulutusrenkaissa niiden hyvän pinnanlaadun, korkean kovuuden ja kulutuskestävyyden vuoksi.

Kromioksidi on kuitenkin haastava materiaali ruiskuttaa sen korkean sulamislämpötilan ja matalan lämmönjohtavuuden vuoksi. Kromioksidi myös höyrystyy helposti korkeissa lämpötiloissa, joka johtaa hienon kromioksidipölyn muodostumiseen. Muodostuva kromioksidipöly jää helposti pinnoitekerrosten väliin heikentäen pinnoitteen koheesiota ja mekaanisia ominaisuuksia.

Alalla on käytetty kuivajääpuhallusta termisen ruiskutuksen yhteydessä kromioksidi- ja muiden plasmaruiskutettujen pinnoitteiden laadunparannukseen. Kuivajääpuhallus pitää työkappaleen pinnan puhtaana ja auttaa lämmönhallinnassa. Kuivajääpuhalluksen käyttöä plasmaruiskutuksen aikana tutkittiin TTY:llä ruiskuttamalla kromioksidia kahden erilaisen kuivajääpuhaltimen avustamana, siten että kuivajääpuhaltimen suutin oli kiinnitetty ruiskutusrobottiin plasmaruiskun kanssa. Useita eri parametreja kokeiltiin ja työkappaleen lämpötilaa valvottiin. Pinnoitteista valmistettiin metallografiset näytteet, jotka analysoitiin elektronimikroskoopilla. Näytteille tehtiin myös kovuus-, adheesio-, kaasunläpäisy- ja kulutuskokeet.

Näytteistä havaittiin, että kuivajääpuhalluksella oli odottamattomia seurauksia sen vaikuttaessa huomattavasti substraatin ja pinnoitteen lämpötilahistoriaan. Liiallinen jäähdytys heikensi pinnoitteen koheesiota ja kulutuskestävyyttä, mutta parametrien säätämisellä kuumemmaksi päästiin eroon joistain haitallisista vaikutuksista. Kuivajääpuhaltimien suuttimesta ulos tulevien kuivajäätpartikkelien koossa oli myös huomattavia eroja eri puhallinmallien välillä. Toinen puhaltimista suihkutti vain hienoa kuivajääpölyä, jolla vaikutti olevan lähinnä jäähdyttävä vaikutus. Kun taas toinen ruiskutti isompia kuivajääpartikkeleita, joiden suuremmalla kineettisellä energialla vaikutti olevan positiivisempi vaikutus pinnoitteen koheesioon parantaen kulutuskestävyyttä verrattuna ilmajäähdytettyyn näytteeseen

PREFACE

The long and arduous process that would culminate in this thesis started in the summer of 2015 and was eventually brought to an end at springtime 2017. This thesis was written in the Surface Engineering group at the Laboratory of Materials Science. I would like to thank Professor Petri Vuoristo and M.Sc. Jarkko Kiilakoski for their recurring guidance during the research and writing process, as well as senior laboratory technician Mikko Kylmälahti for his assistance.

I am also grateful of the pleasant working environment provided by the Surface Engineering group for all these years before and during the writing of this thesis. My final thanks go to Niina for her continued understanding and words of encouragement.

Tampere, 19.4.2017

Keijo Penttilä

CONTENTS

LIST OF SYMBOLS AND ABBREVIATIONS

316L	SAE 316L grade austenitic stainless steel
Ag_2O	silver(I) oxide
Al_2O_3	aluminium(III) oxide or alumina
APS	Atmospheric Plasma Spraying
Ar	argon
BSE	Back-Scattered Electrons, a type of signal in electron microscopy
C_2H_2	acetylene
C_2H_4	ethylene
C_3H_6	propene
C_3H_8	propane
CaF_2	calcium fluoride
CeO_2	cerium(IV) oxide
Co	cobalt, a binder used in hardmetals
CO_2	carbon dioxide
CoCr	cobalt-chrome, a binder used in hardmetals
c_p	specific heat capacity
CAPS	Controlled Atmosphere Plasma Spraying
Cr_2O_3	chromium(III) oxide or chromia
Cr_3C_2	chromium carbide, a carbide used in hardmetals
$CrO_2(OH)_2$	hexavalent chromium oxyhydroxide
CrO_3	hexavalent chromium
DE	Deposition Efficiency
F4-MB	plasma torch manufactured by Oerlikon Metco
Fe_3Al	iron aluminide, an intermetallic phase of iron and aluminium
FeAl	iron aluminide, an intermetallic phase of iron and aluminium
H_2	hydrogen
H_2SO_4	sulfuric acid
He	helium
H_u	net calorific value, energy released during fuel gas combustion
HV	Vickers hardness value
HVAF	High Velocity Air Fuel spraying
HVOF	High Velocity Oxy-Fuel spraying
MgO	magnesium oxide
Mohs	Mohs scale of mineral hardness
MoO_3	molybdenum trioxide
N_2	nitrogen
NaOH	sodium hydroxide
NiCr	nickel-chromium, a binder used in hardmetals
NiCrAlY	nickel-chromium-aluminium-yttrium, commonly used as bond coats
NiCrBSi	nickel-based super alloy
NIOSH	The National Institute for Occupational Safety and Health (USA)
OSHA	Occupational Safety and Health Administration (USA)
$p(H_2O)$	partial pressure of water vapour
$p(O_2)$	partial pressure of oxygen
PEL	Permissible Exposure Limit
PSZ	Partially Stabilized Zirconia

REL	Recommended Exposure Limit
RoHS	Restriction of Hazardous Substances, Directive 2002/95/EC
RPM	Revolutions Per Minute
SE	Secondary Electrons, a type of signal in electron microscopy
SEM	Scanning Electron Microscope
SiC	silicon carbide
SiO_2	silicon dioxide or silica
slpm	standard litre per minute
SOFC	Solid Oxide Fuel Cell
stddev	standard deviation
TiO_2	titanium dioxide or titania
T_m	melting temperature
WC	tungsten carbide, a carbide used in hardmetals
VPS	Vacuum Plasma Spraying
wt%	weight percent
XPS	X-ray photoelectron spectroscopy
Y_2O_3	yttrium(III) oxide or yttria
YSZ	Yttria-Stabilized Zirconia
ZrO_2	zirconium dioxide

1. INTRODUCTION

Ceramic coatings have a wide range of applications in the industry ranging from wear and corrosion protection to thermal protection and electrical insulation. Chromium oxide is a high hardness ceramic material and it is widely used in coatings for its excellent tribological properties such as high wear resistance. Atmospheric plasma spraying is often the preferred technology for applying chromium oxide coatings due to its extremely high flame temperature capable of readily melting ceramic materials [1]. Chromium oxide is however quite volatile at high temperatures vaporizing easily and creating fine dust that may cause problems when trapped inside the coating structure. In relatively recent studies [64]-[75], simultaneous dry ice processing has been found to improve the quality of plasma sprayed coatings across multiple different materials, including chromium oxide. As a result, the microstructure and mechanical properties of the coatings were noticeably improved according to the studies.

This thesis builds on past work done in the field with dry ice processing of plasma sprayed coatings and aims to assess further the viability of auxiliary dry ice blasting as a technology for improving the quality of plasma sprayed chromium oxide coatings. A dry ice blaster was implemented in a plasma spraying process to provide cooling and to clean the workpiece simultaneously while spraying. Several parameter combinations were tested with the setup and after careful optimization, some benefits of the dry ice process were eventually realized. High-speed imaging and thermal monitoring of the substrate was utilized to find the optimal processing parameters. The effect of dry ice blasting on the microstructure was evaluated using optical and electron microscopy. Additionally the coatings were tested for surface quality, hardness, adhesion, permeability and wear.

Chapter 2 begins with the basics of thermal spraying further explaining plasma and HVOF spraying technologies. Chapter 3 presents the most commonly used ceramic coating materials and introduces the reader to chromium oxide as a coating material. Chapter 4 delves deeper into the sprayability of chromium oxide and its challenges also covering the health issues related to its use. Chapter 5 explores the possibilities of auxiliary cooling in thermal spraying processes and the different technologies available. Chapters 6-9 cover the experimental portion of this thesis along with the results, discussion and conclusions.

2. THERMAL SPRAYING

Thermal spraying is a widely used thermomechanical coating process used to deposit a multitude of different materials as coatings on various substrates materials. Most metals and metallic alloys can be thermal sprayed as well as ceramics, composite and cermet materials. Coating thicknesses are typically in the range of 50-500 µm but with certain applications thicker or thinner coatings may be applied [1]. In thermal spraying the raw material is introduced into a heat source as a powder, wire, rod or as a liquid suspension. The molten or semi-molten droplets are then propelled towards the substrate by a gas stream. Upon contact, the droplets deform and conform to the surface forming what are referred to as splats. The individual splats solidify and form the coating. An exception to the above description is the cold spray process, which does not take advantage of heat but relies on high particle velocities (up to 1100 m/s) to deform the powder particles plastically instead of melting them. Naturally, only easily deformable metals and alloys can be deposited with the method. The thermal spray process is illustrated in Figure 1.

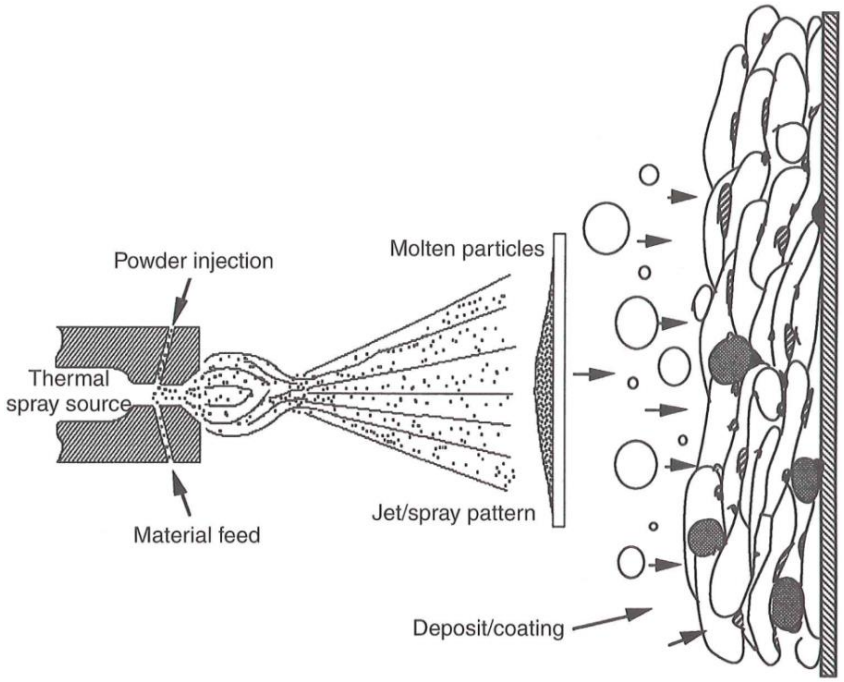

Figure 1. *Typical thermal spray process and coating structure. [1] (p. 33)*

Thermal spray processes are commonly classified by heat source, which include electric arc, plasma arc and combustion. In electric arc spraying two metallic wires are fed at an angle towards each other and an electric arc is struck between them. The arc melts the wires as they are fed closer to one another. An atomizing gas coming from behind the

electric arc atomizes the melting material into droplets and propels them towards the substrate. Feedstock is limited to wires, which are made of a malleable conductive metal, but cored wires containing even cermets are available expanding the choice of materials. [1] The plasma spray process will be described in more detail in subchapter 2.1.

Combustion processes consist of conventional flame spraying, detonation guns and high velocity oxy-fuel spraying. Flame spraying uses fuel gases to heat and accelerate the feedstock material, which can be introduced as powder, wire or rod. Particle velocities are usually less than 200 m/s. Feedstock materials include plastics, metals and alloys as well as some ceramics. In the detonation gun process feedstock powder, fuel and oxygen are injected into a chamber in which the mixture is ignited and the resulting detonation heats and propels the particles out of the spray gun at a very high velocity (~1200 m/s) imparting more kinetic energy on the particles than conventional flame spraying. The process is discontinuous and operates at a frequency of 1-15 Hz. Sprayable materials include metals, cermets and ceramics. [1] The high-velocity oxy-fuel process is akin to a continuous detonation gun process and will be described in subchapter 2.2. Different thermal spraying process temperatures and velocities are shown in Figure 2.

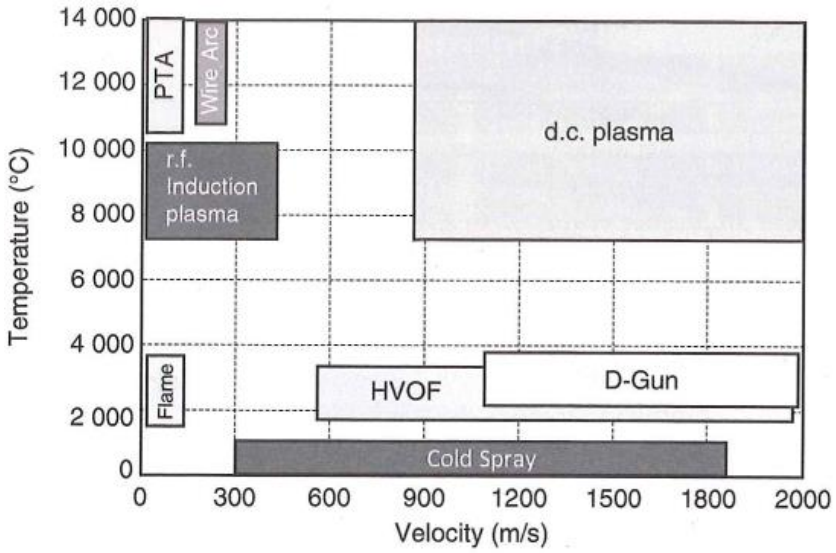

Figure 2: *Thermal spraying techniques by gas temperature and velocity. [2] (p. 6)*

As mentioned earlier, the coating forms through impacting, spreading and solidification of individual spray particles. The splats that form are typically 1-20 µm thick depending on spraying parameters and have a columnar grain structure. In addition to molten and resolidified particles, the resulting lamellar structure also consists of pores, oxide inclusions and unmelted particles. The amount of porosity in thermal spray coatings is in the range of 2-15 % depending on the material and process applied, with modern advanced processes even smaller levels of porosity can be achieved. Porosity is natural for the process as droplets do not always flow to fill all the crevices. Especially in ceramics, some porosity is formed by horizontal or vertical cracks during cooling. [1]

Oxidation is a common problem in metallic coatings; particles oxidize during flight but also after coating formation between passes. In the case of ceramics, they can occasionally be partially reduced to metallic form resulting in metallic inclusions. Another unwanted feature is unmelted particles, these are particles that do not melt during flight and wind up embedded into the coating as they are surrounded by incoming molten particles. All of the aforementioned defects typically result in reduced coating properties. [1]

Thermal spray coatings are often used to improve the wear resistance, corrosion resistance and thermal resistance of components in multiple applications in a wide variety of industries. They are also used for clearance control in machinery, for their electrical and other special properties. As a technique, thermal spraying can also be applied on worn or damaged components to restore them back to working condition. [1] Some examples of thermal spray applications include: turbine engine components, valves and pumps, piston rods, paper machine rolls as well as medical implants. [3]

Compared to alternative coating methods the advantage of thermal spraying is its versatility as a technique: ability to deposit almost any metallic, ceramic or plastic material in a wide range of thicknesses onto small or large components without inflicting a lot of additional heat. Deposition rates are also high, stripping and reapplication of coatings is relatively easy (depending on material) and capital costs are relatively low. As a downside, thermal spraying is a line of sight process meaning it cannot be used for complex geometries or for example the interior of small cylinders. The spray torch has to be nearly perpendicular to the substrate surface to guarantee maximal coating properties. In addition, as mentioned earlier, coating porosity can present problems in some corrosive environments if corrodents can seep through the coating and damage the substrate. Finally, coating adhesion is always related to how the substrate-coating interface is prepared, typically the surfaces have to be grit-blasted to enhance adhesion which results in additional work. [1]

2.1 Atmospheric plasma spraying

Atmospheric plasma spraying (APS) is the most common variant of the plasma spraying processes. In plasma spraying an electric arc is formed between an axially aligned tungsten anode and a ring like copper anode which is part of the nozzle interior. The high-temperature arc heats the flowing gases causing them to ionize and form a plasma jet. Feedstock powder or liquid is fed into the plasma jet, which heats it and propels it towards the substrate. As the name suggests, APS operates in a normal air atmosphere, while other variations like vacuum plasma spraying (VPS) or controlled atmosphere plasma spraying (CAPS or CPS) operate in controlled environments. [1]

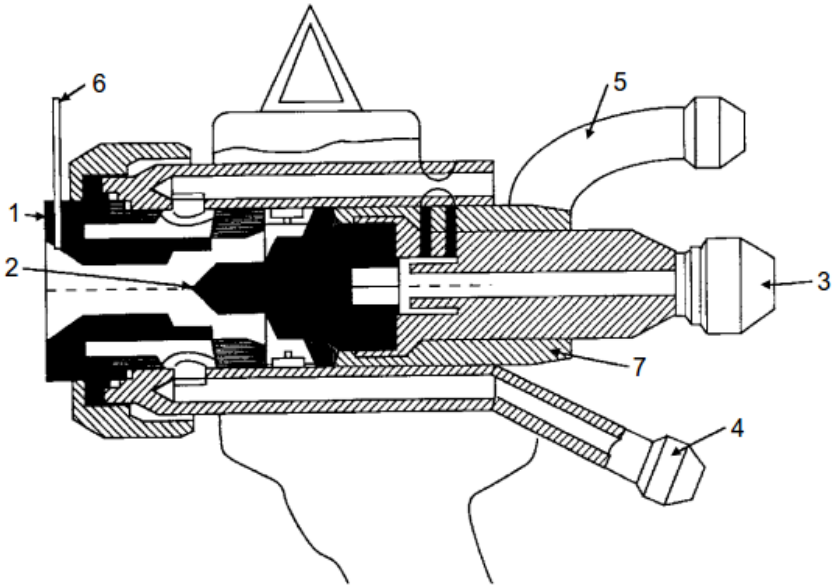

Figure 3: *A cross-section of a plasma torch. 1) anode; 2) cathode; 3) water outlet and cathode connector; 4) water inlet and anode connector; 5) working gas inlet; 6) internal powder injector; 7) electrical insulation. [4] (p. 75)*

A plasma torch with internal powder feed is illustrated in Figure 3. The torch can be divided into three key systems: electric circuit, cooling water circuit and gas feed. Direct current flows through the positive connectors to the anode where it forms an arc, jumping to the cathode, which is connected to the negative connector. Insulation between the anode and cathode is necessary to facilitate arc formation, thus some components have to be fashioned out of non-conductive materials. [3]

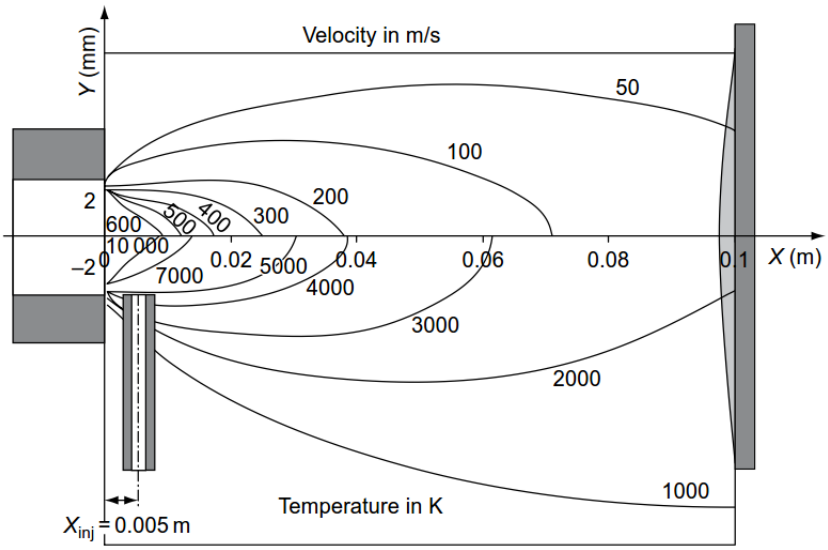

Figure 4: *Calculated velocity and temperature distribution for the F4 plasma torch. [4] (p. 176)*

Typical torch powers range from 30 to 90 kW but high-powered torches can reach electrical power over 250 kW. Powder flow rate for typical torches is 3-6 kg/h with deposition efficiency around 50 %. Arc voltages range from 30-80 V with a current of 300-1000 A. The plasma jet can reach temperatures of 12000-15000 °C with velocities up to 500-2500 m/s at the nozzle exit. However, the velocity and temperature drop after the nozzle exit is significant as can be seen from Figure 4, this happens mainly due to turbulent mixing with the surrounding air. [2] Actual particle velocities and temperatures are noticeably lower.

Cooling water is required due to high thermal loads especially on the cathode but also on the anode. High flow rates and pressures are essential to prevent water vapour formation, which would result in a lowered heat transfer rate ultimately resulting in electrode overheating and melting. The working gas is fed to the back of the spray torch where it passes through a gas distributor ring, which evens and redirects the flow. Often a gas vortex is formed inside the arc chamber. The rotating gas keeps the arc in motion to prevent the anode from eroding locally. As the gas is ionized, it expands and exits the spray torch. [1]

An internal radial powder feed is shown in Figure 3 (p. 11) but external radial powder feed is also common. For radial feeding, one port is typically used but multiple port designs are available [4]. In advanced systems that utilize three electrodes instead of one, the powder feed can also be located axially between the electrodes. When injected directly along the centreline of the plasma, uniform heating can be achieved. Another advantage of the 3-electrode design is the reduced thermal load on the electrodes as the energy is divided which leads to a longer service life and makes higher power levels possible. [3] With internal powder feeding, both axial and radial, a great advantage is the longer particle dwell time in the plasma jet. However, internal powder feeding requires a tighter size distribution for the feedstock powders. [1]

When using radial powder injection, care must be taken to optimize the powder feeding parameters as they affect the final powder velocity and degree of melting, which translate to the coatings characteristics. Powder size distribution, carrier gas velocity, powder feed port diameter and position determine the initial trajectory of the powder when it enters the plasma. When feeding the powder with enough velocity, larger particles have enough momentum to penetrate to the plasma centre while smaller particles remain in the cooler areas where they still heat up sufficiently. Too high or low carrier gas and powder flow rate and the powder feed will miss the centre of the plasma jet. A typically used powder size for plasma spraying is 10-45 µm. [1]

Powder feed should be aimed towards the centre of the plasma jet, when using external feeders they should be positioned precisely every time adjustments are made. A straight 90° angle to the plasma axis is commonly used but directing the port upstream of the plasma jet will result in longer dwell times, which may be beneficial for high melting

point materials, similarly directing the port downstream results in less heating. A small diameter powder feeding port creates higher velocities and therefore port erosion. Wear should be monitored, as even slight wear will result in decreased powder injection velocities. [1]

The type of gas used in a plasma torch defines the plasma characteristic. Different plasma gases can be evaluated based on the achievable plasma jet temperature and the plasmas thermal conductivity. Helium reaches high temperatures and has good thermal conductivity, but is often too expensive. Argon also produces a high temperature plasma but conducts heat poorly making it ineffective at heating powder particles. Hydrogen is an effective secondary gas as it increases the enthalpy and heat conductivity of the plasma also increasing the arc voltage. Nitrogen on the other hand is challenging to ignite and use. [3] In some applications, pure argon is used but combinations such as $Ar+H_2$, Ar+He and $Ar+N_2$ are used for their combination of high temperature and good heat conductivity. Nitrogen can be also utilized alone but it is also used together with hydrogen as a mixture. Ternary mixtures of $Ar+He+H_2$ or $Ar+He+N_2$ are also used. [4]

The torch nozzle and anode design is one of the determining factors of the plasma jets characteristics. Generally, smaller diameter nozzles increase the plasma temperature, though the increase is not as drastic as with changing the plasma gas composition. With small diameter nozzles velocity increase is however twofold: a smaller channel diameter on its own increases the flow but the raised plasma temperature increases it even further. Cylindrical nozzles are common in plasma spraying but diverging Laval-type nozzles have been found to create a more uniform velocity and temperature and reduce turbulence with the surrounding air. The cathode shape has an effect mainly on the velocity. A sharper cathode tip provides faster axial velocities but due to increased erosion rate the shape changes thus altering the velocity distribution. [2]

Arc current and plasma gas flow are the main parameters that are adjusted and tweaked to create the optimal plasma characteristics; their effect is illustrated in Figure 5. Increasing the arc current increases both the velocity and temperature of the plasma jet and particles. Increased current however creates more heat thus decreasing electrode life. A higher plasma gas flow rate results in higher velocities but in return, the plasma and particle temperature is decreased. To maximize coating quality further a plasma jet with certain characteristics has to be matched with the correct spraying distance. If the distance is too short, the higher impact velocities lead to porosity whereas too long distances lead to particles re-solidifying mid-flight. [2]

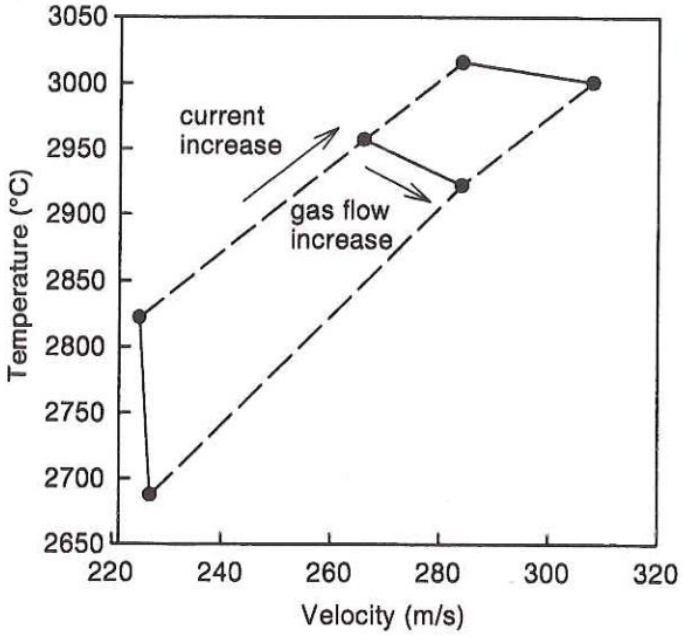

Figure 5: *The effect of current and plasma gas flow rate on YSZ particle temperature and velocity in an Ar-He plasma. [2] (p. 423)*

Plasma spraying with its wide range of jet temperatures is capable of depositing coatings of virtually any material as long as its melting point and evaporation or decomposition points are not too close. Operating atmosphere presents some limitations though as some metals, cermets and non-oxide ceramics sprayed with APS tend to oxidize or decompose during flight due to exposure to surrounding air. For oxide critical applications, vacuum (VPS) or controlled atmosphere plasma spraying (CAPS) is used. [2]

APS sprayed metals include various iron, nickel and cobalt based alloys as well as other superalloys and molybdenum. These are typically for low or high temperature corrosion applications but wear resistant coatings are also applied. Cermets can also be sprayed in regular atmosphere, however especially WC and WC-Co coatings are easily oxidized or decomposed resulting in lower hardnesses. Cr_3C_2-NiCr is more resistant to oxidizing and is easier to spray with APS. [2]

Non-oxide ceramics are easily oxidized or decomposed so they are usually deposited with VPS or CAPS. Oxide ceramics on the other hand are the most popular material deposited by APS. Most common are aluminium oxide, titanium oxide, chromium oxide and zirconium oxide and their various mixtures. Aluminium oxide and titanium oxide are mainly for wear and corrosion resistance as well as dielectric applications; these are often used as mixtures of varying compositions as they provide better properties than pure oxide coatings. The main applications of chromium oxide are also wear and corrosion resistance, it is also sometimes alloyed with aluminium oxide or titanium oxide. Zirconium oxide is primarily used in thermal barrier coatings due to its low thermal conductivity and high thermal shock resistance. [2]

The range of possible coating characteristics is wide, but for typical plasma sprayed coatings thicknesses are in the range of 300-1500 µm [3] with 2-8 % porosity and bond strengths over 40 MPa. With suspension plasma spraying for SOFC applications coatings as thin as 10 µm are however possible. [1] Usually low porosity levels are desirable but for thermal barrier coatings much higher porosity levels are advantageous and are achieved with the right parameters. Higher bond strengths are also achieved in some cases. [1]

2.2 High velocity oxy-fuel spraying

In high velocity oxy-fuel spraying (HVOF) a gas or liquid fuel is continuously injected with oxygen into a combustion chamber in the spray gun, the mixture is ignited to initiate the combustion process. The combustion generates high-pressure gases, which exit through a narrow barrel. Feedstock powder or liquid is injected into the stream heating and accelerating it tremendously. The jet exits the spray gun nozzle at supersonic speed. [1] A variation of the HVOF process is high velocity air fuel spraying (HVAF), where oxygen is replaced by compressed air resulting in a far more economical process. Compared to HVOF, HVAF produces higher velocities but colder flame temperatures. [2]

HVOF guns come in a variety of designs, the differences are mainly related to fuel compatibility, combustion chamber design and powder feed systems. Guns can be classified into four categories based on these factors; the variations are illustrated in Figure 6. In a gun with an axially aligned powder feed and combustion chamber (Fig. 6a) the powder injection port is located in the back of the combustion chamber and the combustion gases and powder feedstock exit through a water cooled nozzle. The next design (Fig. 6b) is similar to the one described earlier but the oxygen-fuel mixture in injected into a combustion chamber at a right-angle in relation to the axial powder feed direction. In another gun variation (Fig. 6c) the combustion is not confined into a nozzle and is similar to a flame spray torch. In systems utilizing liquid kerosene (Fig. 6d) the powder is often injected into the nozzle radially. [1]

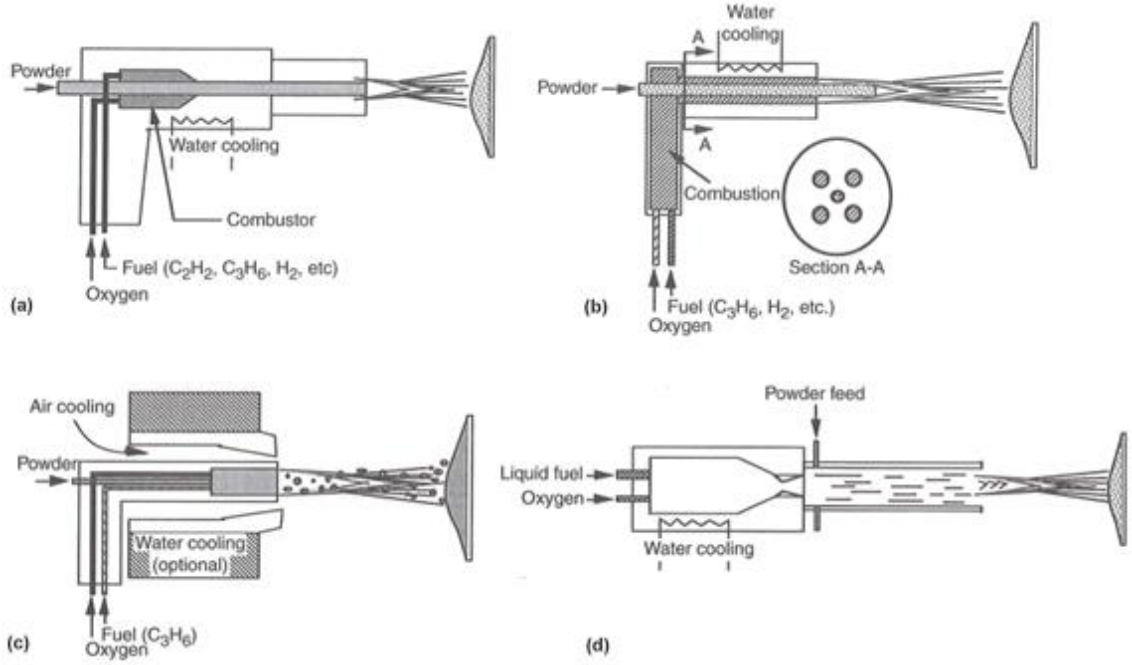

Figure 6: *Different commercially available HVOF torch models. a) HV 2000 b) JetKote c) Diamond jet d) JP-5000 [1] (p. 40)*

Table 1: *Fuel properties. [3] (p. 94)*

Fuels	Max. flame T [°C]	Mixing ratio at max. flame T [m^3/m^3]	Calorific values (H_u) [MJ/m^3]
Acetylene	3160	1:1,5	56,5
Ethene	2924	1:2,4	93,2
Hydrogen	2856	1:0,42	87,9
Propylene	2896	1:3,7	56,5
Propane	2828	1:4,3	10,8
Natural gas (as methane)	2786	1:1,8	33,9
Kerosene	~2800	1:2,9	38 (MJ/l)

The following fuels are typically used in HVOF processes together with oxygen: acetylene (C_2H_2), ethene (C_2H_4), hydrogen (H_2), propylene (C_3H_6), propane (C_3H_8), natural gas (consisting mostly of methane) and liquid kerosene. The type of fuel used has little effect on the spraying velocities but their effect on flame temperature is much greater. Fuel properties, including maximum attainable temperatures and optimum mixing ratios and calorific values are compiled into Table 1. The fuel is selected according to the torch being used and the material being sprayed to optimize coating quality. [3] Power levels for guns using gaseous fuel is 100-120 kW with possible powder flow rates up to 7,2 kg/h, for liquid fuels power levels go up to 300 kW with a 12 kg/h powder flow rate. Deposition efficiencies are noticeably higher for HVOF compared to APS, 70 % for gaseous fuels and 60-80 % for liquid fuels. [2]

Compared to the plasma spraying process, HVOF spraying is relatively simple as far as different parameters go. Excluding acetylene, there is not much difference in the attainable flame temperatures of the fuels. The temperature can also be regulated by varying the mixing ratio, increasing the oxygen flow decreases the temperature but increases the velocity through increase of total gas flow. On the other hand decreasing the oxygen amount decreases the temperature as well as the velocity. For air-cooled systems, increasing the flow of compressed air cools the flame without affecting its flow. [3]

Throughout the development of HVOF torches, maximum combustion pressure has been constantly increasing resulting in higher velocities. With 1st and 2nd generation torches operating at 3-5 bars, particle velocities have been over 400 m/s. For the 3rd generation torches with 6-10 bar operating pressures velocities up to 650 m/s are possible [3]. Another method of increasing particle velocities is nozzle design; the capabilities of straight barrel nozzles are limited but the use of for example converging-diverging de Laval-nozzles has been shown to increase particle velocities tremendously [2].

Various metals and alloys have been successfully sprayed with the HVOF process including: nickel and cobalt alloys, high alloyed steels as well as molybdenum, copper and aluminium alloys. Coatings exhibit low levels of porosity and good bond strength (>50 MPa) resulting in high quality anti-corrosion coatings. [2] The most HVOF sprayed material group is cermet-composites, most notable being WC-Co and Cr_3C_2-NiCr which are used extensively for their wear and corrosion resistance. Compared to plasma spraying, HVOF sprayed WC-Co exhibits less carbide decomposition due to lower spraying temperatures. [2] A typical particle size for powder feedstock is 5-45 µm [4].

HVOF spraying of chromium oxide, aluminium oxide, titanium oxide and their mixtures has been successfully executed with positive outcomes but it is challenging and requires optimization of particle heating due to extremely high melting temperatures of the materials. In one study titanium oxide was successfully sprayed and it was also found that having a narrow size distribution is crucial as large particles are easily left unmelted. [5] For example HVOF sprayed aluminium oxide, chromium oxide and their mixtures have been found to be harder, tougher and more wear resistant than their APS sprayed counterparts [6][7][8].

3. THERMAL SPRAYED OXIDE COATINGS

Thermal sprayed ceramic coatings are widely used in various industries especially for wear and corrosion protection, thermal and electrical insulation as well as other specialized applications. Oxides are most prominent ceramic group in thermal spraying due to their cost-effectiveness, stability and good material properties. [9] Thermal spraying of non-oxide ceramics is often more challenging due to their susceptibility to decompose or evaporate during processing. Some carbides, borides and nitrides can be sprayed but even then, they typically require a controlled atmosphere. [2]

The majority of the powders used in thermal spraying of oxides are manufactured by fusing and crushing or spray drying, powders made with both methods are shown in Figure 7. Fused and crushed powders start by fusing the raw material in a furnace above the materials melting temperature. The produced block of material is then broken up, crushed and milled to produce the powder. Fused and crushed powders are sharp and blocky with little internal porosity. The coarse shape makes for poor flowability, which can cause irregular powder feed during spraying; this can be addressed with a further spheroidization treatment in flame or in plasma but there is a risk of internal porosity formation. Another problem with fused and crushed powders, at least in the case of chromium oxide is the formation of metallic chromium through a high temperature reducing reaction. This can be detrimental to the coatings qualities, especially if electrical insulation is required. [4]

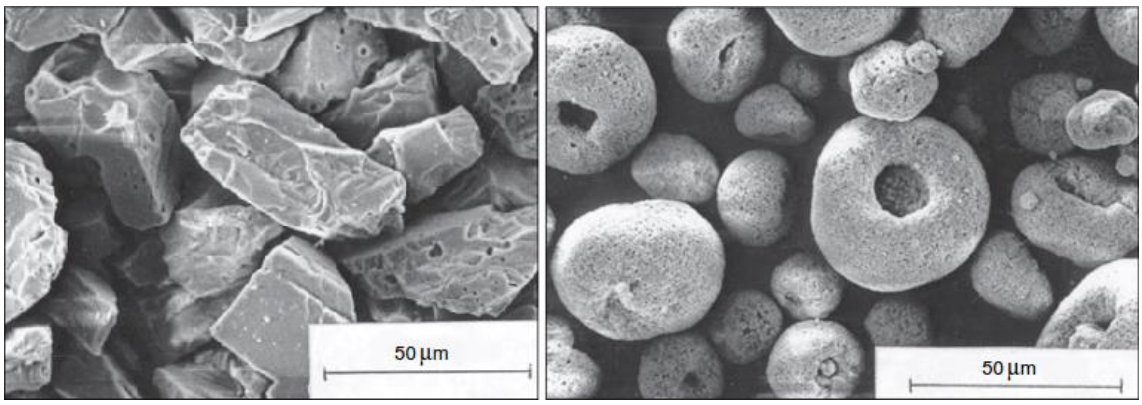

Figure 7: *Fused and crushed Cr_2O_3 powder (left), spray dried Cr_2O_3+SiO_2 powder (right). [4] (p. 11, 16)*

Spray drying starts with a slurry, which contains precursors to form the solid powder, an organic binder to bind together the agglomerates after drying and additives to enhance slurry or binder properties. The slurry is fed into an atomizer where it is sprayed with high pressure to form fine droplets. Atomizing is followed by drying with heated gas, which

evaporates the moisture leaving behind solid powder agglomerates. The resulting particles are globular with good flow properties but also porous and sometimes hollow which is caused by the rapid moisture evaporation rate. The morphology of the powder depends on the atomization and drying parameters as well as the slurry composition. Spray dried powders can be further densified by sintering, heating in an arc plasma or radio frequency plasma. This additional processing step creates much denser powders that heat and melt better during spraying. Due to this extra thermal processing step, phase changes are possible and should be taken into account. [4]

Oxide materials require very high temperatures to properly melt and deposit via thermal spraying, therefore plasma spraying is frequently utilized to deposit them. Although the particles properly melt in the plasma jet, their velocities are low resulting in porosity and poor cohesion. Within the last 15 years, progress has been made in the field of HVOF spraying enabling the utilization of HVOF spraying for deposition of high-quality ceramic coatings. It is best to use internal powder feeding so that the powder is fed straight to the hottest section maximizing heating. When proper particle heating is achieved, HVOF spraying provides ceramic coatings with better structures than APS. [3]

In a study to chart the effect of different microstructural characteristics on the properties of ceramic coatings chromia, alumina and alumina-titania coatings were plasma sprayed with a few different parameters. When comparing the wear properties of the coatings and bulk ceramics it was found that the coatings had markedly higher wear rates than ceramics of the same hardness level suggesting that the unique microstructure of thermal sprayed coatings greatly affects the coatings wear properties. Namely, a good connection was found between hardness, porosity and wear volume. A definite link was also found for vertical crack density and wear particle size. [10] Even though bulk ceramics and thermal sprayed ceramic coatings are chemically similar in composition, the processing route affects their properties to a great degree, emphasizing the need for careful process control and improvement. Besides wear resistance, the unique microstructure affects their corrosion properties as well. Ceramics are chemically quite inert materials but ceramic coatings are rarely dense with zero through porosity. This means that corrosive substances can often seep through the coating and corrode the underlying substrate. This can however be prevented with for example polymer impregnation of the coating. [4]

Alumina (Al_2O_3) is one of the most common and cost-effective oxides on the market as it is widely utilized in abrasives. Alumina coatings are good options for abrasion and corrosion in acidic environments but they are not suitable for alkaline environments. [3] Due to its dielectric properties, alumina is also used extensively as an insulating coating. The coatings are however relatively brittle which poses some limitations. During thermal spraying the α-alumina transforms to metastable γ-alumina during rapid cooling. The γ-phase is stable up to 950 °C where it transforms back to the α-phase. The resulting phase

change is accompanied by a change in volume resulting in coating failure; therefore, the high temperature applications of pure alumina coatings are limited. [2]

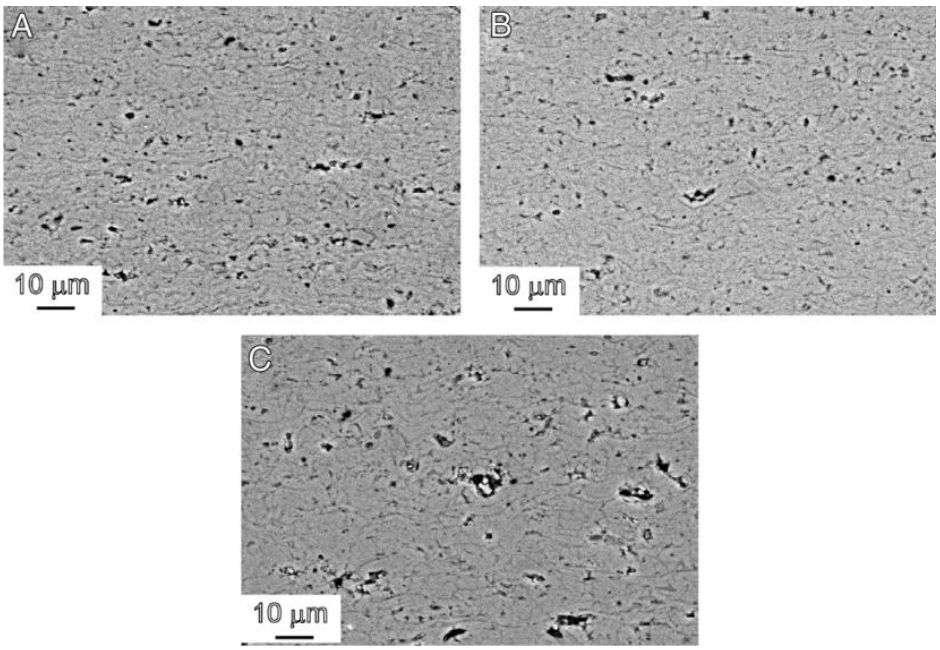

Figure 8: *A) HVOF sprayed conventional Al_2O_3, B) HVOF sprayed nano-Al_2O_3, C) APS sprayed conventional Al_2O_3. [11] (p. 4815)*

Alumina is often used with titania additions of 3-40 % to enhance its properties, titania additions up to 13 % increase the coatings wear resistance by improving its toughness even though hardness is usually decreased [2]. Chromia additions on the other hand have been successfully used to create stable α-phase in the as-sprayed state [12], which results in overall better properties than pure alumina [13]. HVOF spraying of alumina has been shown to improve its properties resulting in less porosity (see Figure 8), better cohesion, higher toughness and hardness and of course better wear resistance then their APS sprayed counterparts. Nanostructured feedstock powder increased the properties further but only slightly. [6][7]

Titania (TiO_2) and titania containing mixtures are amongst the easiest to spray as titania has the lowest melting point of the oxides at 1850 °C. [3] Titania is used in similar applications as alumina but overall its properties are inferior. Titania is commonly mixed with other oxides, coatings containing titania result in lower hardness but higher toughness and less porosity [4]. As with alumina, HVOF spraying of conventional titania and nanostructured titania powders also demonstrated significantly better abrasion resistance and coating adhesion compared to APS sprayed titania. [14]

Zirconias (ZrO_2) primary application lies in its thermal properties, for a ceramic material it has a very high thermal expansion coefficient, close to that of steel [3]. It also exhibits very high thermal shock resistance and a very low thermal conductivity, overall making

it an excellent choice as a thermal barrier coating. As other ceramics, pure zirconia also has other possible phases in high temperatures but zirconias phase structure can be stabilized with additions of yttria (Y_2O_3), ceria (CeO_2) and magnesia (MgO), yttria stabilized zirconia (YSZ) being the most widely used. It is also being used in solid oxide fuel cells as an electrolyte where it is applied as a thin layer. There are also reports of zirconia being successfully sprayed by HVOF. [2]

3.1 Chromium oxide coatings

Thermal sprayed chromium oxide coatings can ideally reach hardnesses in the range of 1900-2000 HV; they have excellent wear resistance and a good surface finish. Compared to other thermal sprayed oxides, chromium oxide has relatively low levels of porosity and is insoluble in acids, alkali or alcohol. This makes chromium oxide an appealing coating for applications such as anilox rolls (Figure 9), pump seals and wear rings. Pure chromium oxide consists of stoichiometric α-Cr_2O_3 and is green in colour but during spraying the stoichiometric Cr_2O_3 may partially reduce to a non-stoichiometric composition that appears darker in colour and has slightly inferior properties, partial reduction to metallic chromium is also possible, careful optimization of the spraying process is thus necessary. [2]

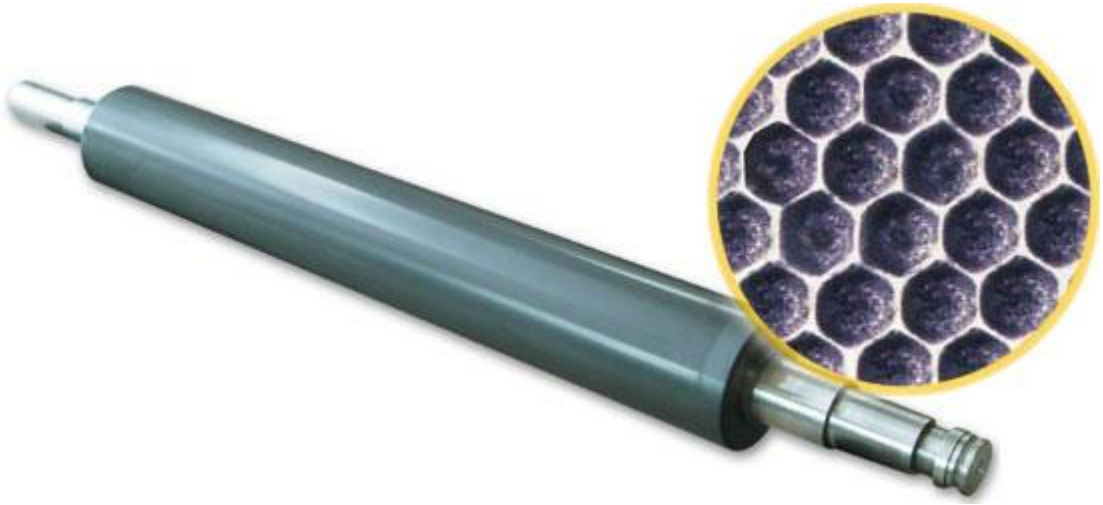

Figure 9: *An anilox roll with a chromium oxide coating laser engraved with dimples that transport ink. [15]*

Chromium oxide is not always used as a pure coating as other ceramic additions enhance the coatings properties. While pure APS sprayed chromia yielded a porosity of 2,15 % and a hardness of 1140 HV, a mechanically mixed composite powder with 10 wt% alumina only had a porosity of 0,77 % and a hardness rating of 1437 HV. A mixture containing equal parts of chromia and alumina on the other hand yielded the highest fracture toughness. [13] Titania is also commonly used with chromia to increase its toughness; varying compositions from 4,25 wt% to 40 wt% are available on the market. Silica (SiO_2)

is also used together with titania to enhance the toughness further. [16] Titania also helps reduce the oxygen loss during spraying [17].

Other more uncommon additives like MoO_3 [18], CaF_2, Ag_2O and ZrO_2 [19] have also been studied to some extent. MoO_3 was found to reduce the porosity and increase the hardness of the coating as well as lower the coefficient of friction in normal and elevated temperatures. Cr_2O_3-Ag_2O-CaF_2 (CAF) and Cr_2O_3-ZrO_2-CaF_2 (CZF) coatings had a lower hardness than pure chromia coatings and higher coefficient of friction at room temperature. Since CaF_2 is a high temperature solid lubricant, it lowered the composite coatings friction coefficient at higher temperatures. Of the two composite coatings, CAF performed better as Ag_2O improved the transfer films wettability whereas ZrO_2 hindered its formation.

Apart from additives and spraying parameters, another method of improving the properties of ceramic thermal sprayed coatings is the use of nanostructured powders. Plasma spraying of conventional fused and crushed chromia powders and a sol-gel produced nanostructured powders produced coatings with a remarkable difference in their wear resistance. In an oscillating wear test, the conventional coating had a wear rate 20-times higher than the nanostructured coating. [20] A similar study was also made with Cr_2O_3–3%TiO_2-powders, conventional and nanostructured. Nanostructured coatings had a higher hardness and resisted erosion and dry sliding better than the conventional coatings. [21]

Chromia is often selected for applications requiring good tribological properties, mainly wear resistance. Chromia is however not always an ideal solution for wear applications amongst thermal sprayed ceramic coatings. When tested in a dry sand-steel wheel test an alumina coating outperformed the chromia coating, both coatings were plasma sprayed and had a porosity of 6 %. Within the scope of the same study, same samples were also tested in a pin-on-disk tribometer, this time chromia experienced less wear than the alumina coating. The measured friction coefficients and pin material losses were also lower with the chromia coating than with any other tested coatings. Success of chromia was attributed to the formation of a compact tribofilm through plastic deformation. [22]

The tribofilms formed by plasma sprayed chromia coatings in dry sliding have been studied in another study in more detail. Cr_2O_3-3%TiO_2-5%SiO_2 coatings were tested in a reciprocating dry-sliding test at room temperature and at 450 °C. The total wear was higher in the 450 °C test; however, the coefficient of friction was lower. This was explained by the fact that due to the higher wear amount in the beginning of the 450 °C test, a more pronounced tribofilm with a higher hardness was formed. Through an XPS analysis it was discovered that the wear films differed also in chemical composition from the as-ground surfaces, films formed in the test at room temperature showed signs of CrO_3, while the test at 450 °C produced films with CrO_2. [23]

To investigate the abrasive wear behaviour of alumina and chromia coatings, a single point scratch test was utilized. With low contact pressures, the chromia coating had a high wear resistance, the primary material removal mechanism being microfracture originating from existing cracks and pores. However, when a critical contact pressure limit was exceeded, lateral cracks beneath the contact area formed causing macro-fracturing. [24] The macro-fracturing is most probably associated with weak cohesion between coating layers, often visible in plasma sprayed chromia fracture cross-sections as can be seen in Figure 10 [6].

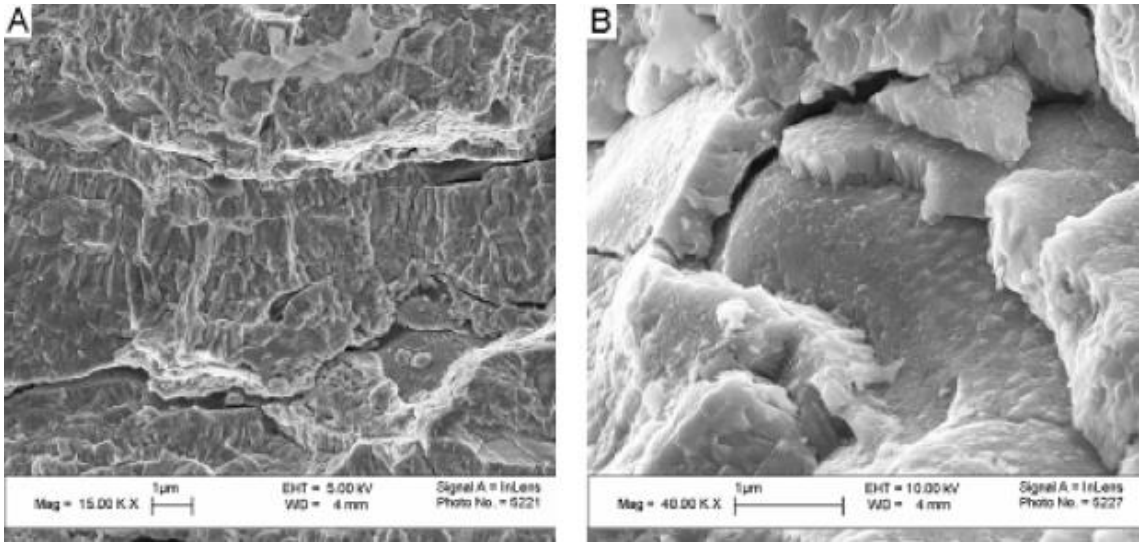

Figure 10: *APS sprayed chromia coatings fracture surfaces. [6] (p. 48)*

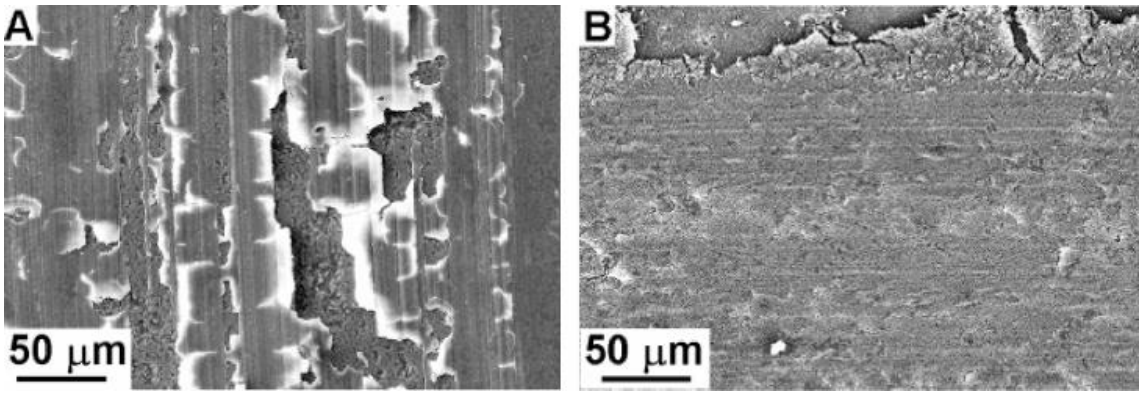

Figure 11: *Wear tracks on alumina (A) and chromia (B) coatings. [7] (p. 69)*

Wear tests conducted on HVOF sprayed chromia and alumina coatings demonstrated a significant improvement in wear properties over APS coatings. In dry sliding tests chromia coatings fared better due to the formation of a more uniform, durable tribofilm (see Figure 11). When the contact pressure was increased the influence of the higher toughness exhibited by the HVOF coatings became evident. Chromia coatings also worked better than alumina coatings against abrasive wear in the dry sand-rubber wheel test, the HVOF

sprayed chromia having the lowest mass loss. [7] HVOF and APS sprayed ceramic coatings were also studied in [25] and similar improvement in microstructure and properties were noted in HVOF coatings. HVOF and plasma sprayed chromia coatings were also tested in a cavitation erosion series with other sprayed coatings. Amongst all the tested specimens, including the cavitation resistant bulk stainless steels as reference samples, HVOF sprayed chromia had a mass loss in the same range as the bulk reference samples [26].

As a material on its own, chromia is resistant to acidic and alkaline solutions [2]. Various ceramic APS and HVOF coatings were tested in NaOH and H_2SO_4 solutions and chromia experienced very little mass loss being second only to the titania coating. In comparison the mass loss of the alumina coatings were several orders of magnitude higher. [27] Thermal sprayed ceramic coatings are not often used for corrosion protection as producing a ceramic coating absolutely free of cracks and through porosity is challenging. The use of a bond layer to increase the corrosion resistance of the coating system has been investigated, but the results with different bond coatings were similar: the bond coat corroded underneath the chromia layer resulting in failure at the interface. The bond coats that were chemically more corrosion resistant therefore naturally fared better. [28]

One possibility for improving the corrosion protection capabilities of chromia and other coatings is sealing the open porosity with organic or inorganic sealants. Organic sealants consist of resins, waxes and other polymeric materials. Inorganic sealants include sol-gel, aluminium phosphate and even molten metals. [4] Application of aluminium phosphate sealing has for example been studied with chromia coatings. The results indicated an improvement in corrosion resistance as well as in erosion and abrasive wear resistance. [29] A post-spraying treatment however requires an additional processing step increasing the cost of the components.

4. SPRAYABILITY OF CHROMIUM OXIDE

Thermal spraying of chromia and ceramics in general is not simple due to their high melting point, the use of plasma torches is a good start but having the correct operating parameters is even more vital and their optimization has been thoroughly researched. HVOF spraying is another alternative for processing chromium oxide; the reachable temperatures are not as extreme as with plasma spraying but the improved particle velocity makes processing of ceramics viable. HVOF spraying of ceramics has been experimented with for at least 20 years [26][36] but it still remains relatively challenging due to the higher melting points of ceramic materials.

4.1 Plasma spraying of chromium oxide

Spraying parameters found in literature for plasma spraying of chromia differ somewhat. Primary plasma gas is often argon, while hydrogen acts as the secondary gas, in some cases helium is used in place of hydrogen. Arc current ranges from 500 A to 750 A with a voltage of 45-75 V, this results in 34-45 kW power. The powders used are either sintered and crushed or agglomerated and sintered typical particle size being 10-45 µm, powder flow rates range from 15 g/min to 25 g/min. Spraying distance is usually kept near 100 mm. [18]- [22]

In earlier experimental studies regarding plasma spraying of chromium oxide, the effect of different parameters was investigated. High current intensity, 500 A being the highest tested value in this study, was deemed important for good adhesion and low porosity. [30] The effect of substrate preheating also appeared important as peak adhesiveness was achieved with preheating to 400 °C. [30] In a similar study, the parameters affecting adhesion were studied in further detail. The results supported the earlier study about the importance of high current intensity and clarified the influence of surface preheating. Evidently, the time between substrate grit blasting and spraying is a key factor. [31]

It was speculated that a longer time between grit blasting and spraying would allow the formation of a thicker absorption layer consisting of air, moisture and other impurities. If there had been a long time (2 h) between grit blasting and spraying, preheating increased the coating adhesion noticeably, most probably due to evaporation of impurities. If spraying was done immediately after grit blasting the need for preheating was not as significant. [31] Studies regarding single-splat behaviour of chromium oxide were not available but studies on zirconia indicate that the purity of the surface is vital for clean splat formation rather than the high substrate temperature, see Figure 12 for details. [32] As far as

other pre-spray treatment goes, correctly executed grit blasting is also necessary, as increasing the surface roughness from 2,5 µm to 4-5 µm improves coating adhesion. [31]

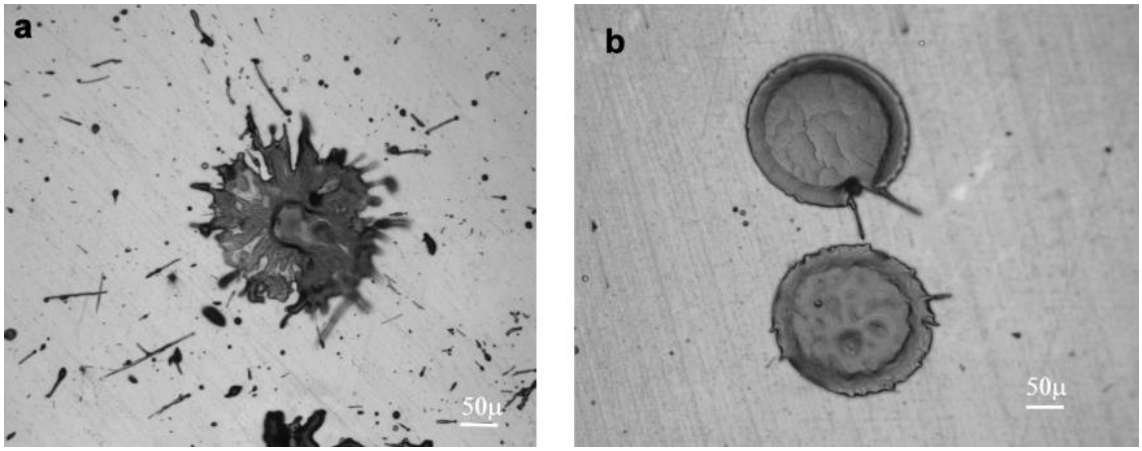

Figure 12: *Morphology of zirconia splats on polished substrates sprayed in a low-pressure chamber. a) Sprayed on a substrate at room temperature. b) Substrate was first heated to remove condensation, then cooled to room temperature, then sprayed. [32] (p. 149)*

It was also found that the effect of the cooling jets and their positioning was the most critical parameter for chromium oxide coating quality; this was attributed to their cooling and cleaning properties as they were claimed to blow away unmelted particles from the surface. The setup consisted of two compressed air jets parallel on both sides of the plasma jet; the optimal lateral distance in this case was 30 mm. Even though the cooling jets were said to cause turbulences in the plasma jet, their use was still deemed beneficial. [31]

Other plasma spraying techniques besides APS have potential to produce superior coatings. Chromia coatings were made with a high-power 250 kW plasma spray system with different parameters and the higher velocities created the best coatings. [33] The high-power plasma spray system is capable of particle velocities twice the velocities of conventional APS, the faster particle impact velocities result in coatings with a higher hardness and lower porosity [34]. The high-power plasma spray system is also capable of 2-3 times higher spray rates which creates significant cost savings in industrial use [35].

4.2 HVOF spraying of chromium oxide

The higher velocities related to HVOF spraying have typically produced coatings of much higher quality than typical APS, this fact is already well known in the case of cermet coatings. For spraying of chromia the temperature (and velocity) should be maximized to ensure proper degree of melting, combustion gases used in literature include hydrogen,

propylene [6][25], ethylene [8] as well as acetylene [36]. Hydrogen provides a wide process window with high temperatures, while propylene is able to reach higher velocities. Even though acetylene has the highest flame temperatures, which is why some of the earlier HVOF chromia spraying trials were done with it, its flow rate is limited due to pressure limitations in actual use [36].

The used powder size is kept smaller than in APS due to the limited heating capability of the HVOF system, the usual powder size for ceramics in HVOF spraying is 5-15 µm. A tight size distribution makes processing easier and provides a wider process window [5]. Spraying distance is generally longer than with APS, 100-150 mm being common. Powder feed rates are similar to the values used with APS. [6][8][36] In earlier trials the shorter spraying distance has created coatings with better wear resistance, this might have been related to particle cooling and solidification during the longer flight [36].

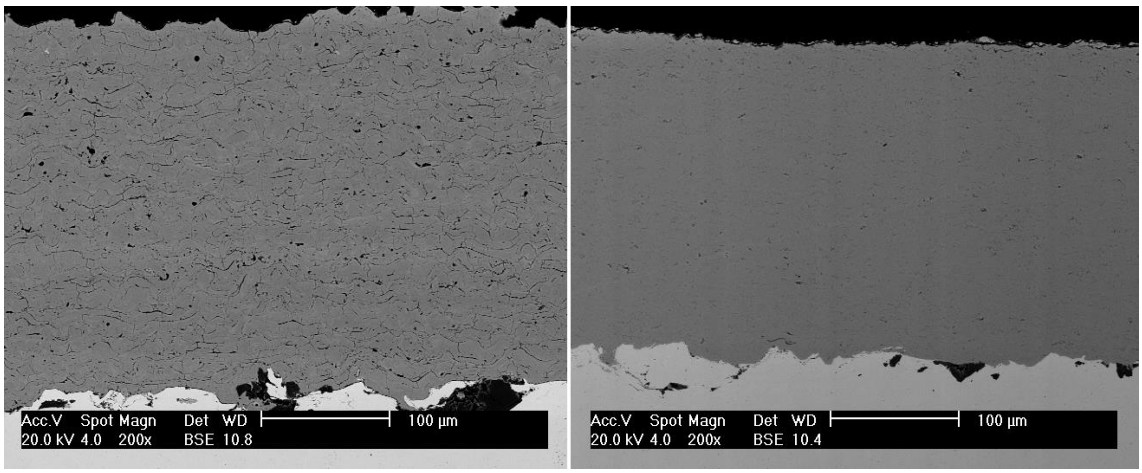

Figure 13: *SEM (BSE) micrographs of APS (left) and HVOF (right) sprayed 100 % Cr_2O_3 coatings, both sprayed at TUT.*

HVOF spraying of chromia has been shown to produce coating microstructures with lower porosity, less cracks and well-adhered splats compared to the APS sprayed samples, the existing pores are smaller and more evenly distributed. [25] These attributes of HVOF sprayed chromia are shown in Figure 13. Equiaxed and smaller columnar grains have also been examined in HVOF sprayed chromia; additionally, the same samples exhibited higher indentation fracture toughness and bending fracture behaviour similar to that of bulk materials. Vickers hardness and indentation fracture toughness was also improved in the HVOF samples compared to APS counterparts. [6]

The performance of HVOF systems for spraying chromia originate from the significantly higher velocities and cooler flame temperatures compared to APS. The degree of particle flattening is higher in HVOF sprayed samples, which makes for higher cohesion between splats. It is also postulated that due to nearly instantaneous flattening and high kinetic energy, solidification cannot start before flattening is complete, which results in higher

supercooling and the aforementioned equiaxed grains. [6] Due to the cooler flame, HVOF spraying reduces lesser amounts of chromia to metallic chromium. However, even though HVOF coatings had better properties, the deposition efficiency of the process was lower than with APS, this might however just be a matter of further process optimization. [8]

4.3 Vaporization of chromium oxide

There is little data related to the deposition efficiency (DE) of thermal spraying of chromia, which is possibly related to DE being challenging to measure reliably and therefore information is rarely published. Consensus within the research group suggests that chromias DE is low and what could be gathered from literature does support the claim. Deposition efficiency is inherently related to the spraying parameters and therefore will fluctuate greatly from process to process. In one particular study where the DE of plasma sprayed chromia was investigated in great detail the achieved DE values ranged from 26,6 % to 58,5 % depending on the torch parameters. [37] For HVOF using propane as fuel gas a 32 % DE has been reported. [38]

The low deposition efficiency is partially caused by unmelted particles when using low flame temperatures especially with HVOF systems, insufficient heating during flight often also leads to poor coating quality. Chromia has a relatively high melting point T_m = 2334 °C (2607 K [39]) and a low thermal conductivity, which is decreased further by the porosity of individual particles. As the particle dwell times in thermal spraying are quite low, it is necessary to use high flame temperatures to properly melt the particles. However, this leads to another challenge: the vaporization of the feedstock powder and the resulting drop in DE in high temperature flames. [40] According to computer simulations, the temperature on the surface of 35 µm chromia particles can well exceed the melting temperature while the core remains solid. As can be seen in Figures 14 and 15, porosity plays a significant role in how particles behave during spraying. [39]

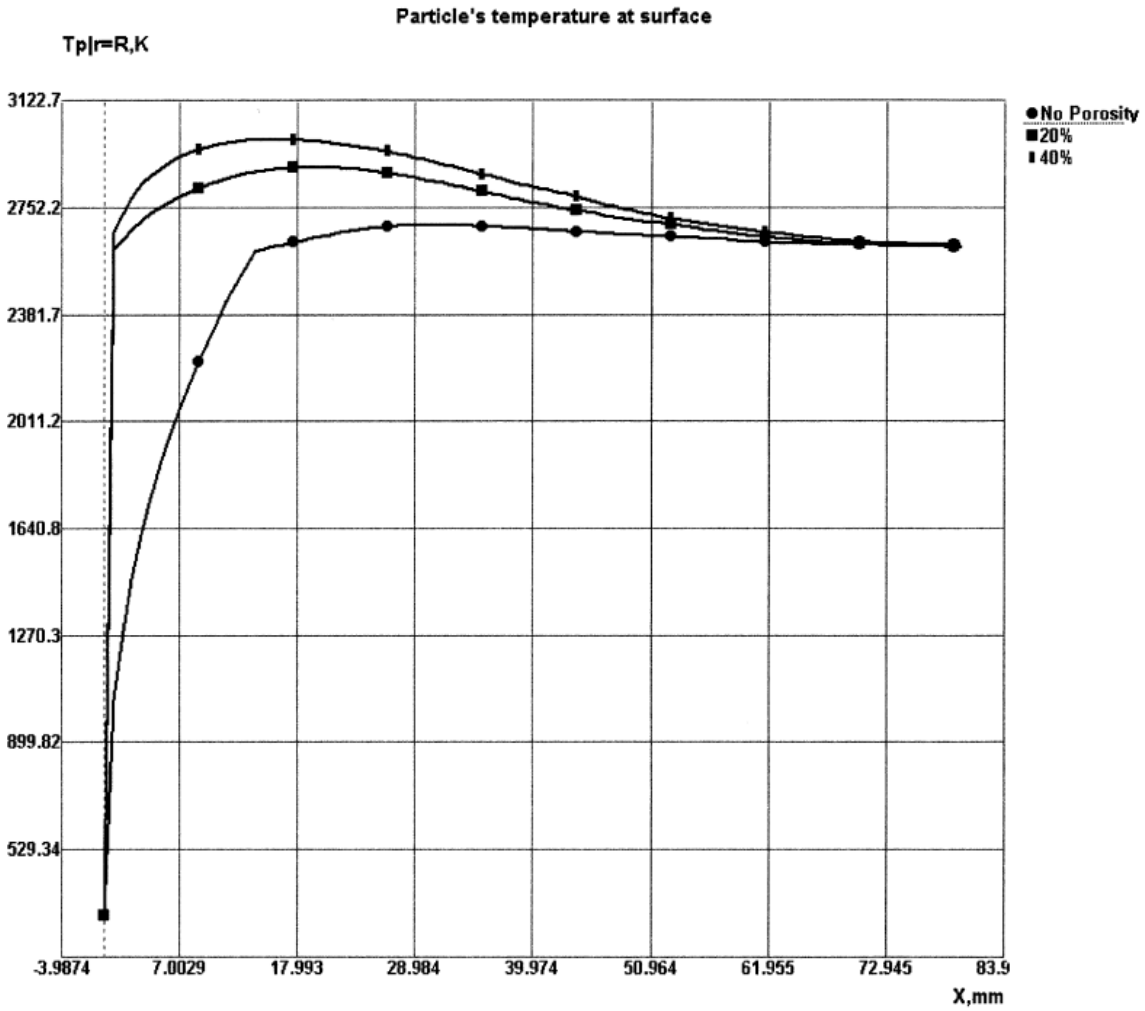

Figure 14: *Surface temperatures of sprayed Cr_2O_3 particles with varying porosities in a plasma flame. (X = distance from injection port) [39] (p. 373)*

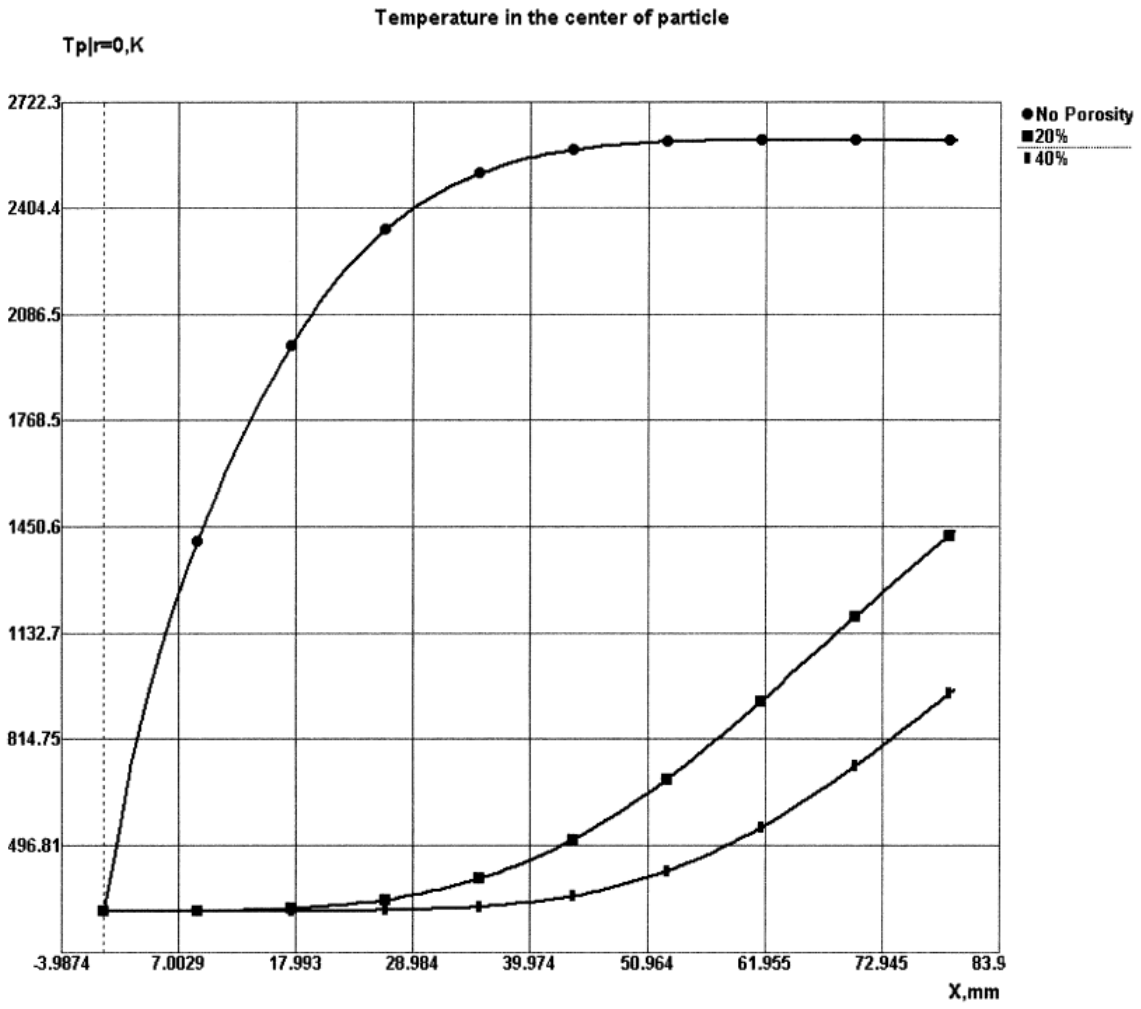

Figure 15: *Core temperature of sprayed Cr_2O_3 particles with varying porosities in a plasma flame. (X = distance from injection port) [39] (p. 374)*

Research on the vaporization of chromia in thermal spraying processes and its effect on deposition efficiency and coating microstructure is scarce and the problem is rarely addressed in literature. The actual amount of material vaporized from a stream of chromia particles is difficult to estimate and will always depend on the particle size distribution, internal porosity and flame parameters. The amount of vaporization in plasma spraying processes in general however, seems quite significant. Calculations have indicated that for iron particles (14-55 µm) the total amount of vaporized mass in plasma spraying can be up to 25 % with a high hydrogen content and high arc current. Lower plasma temperatures naturally reduce the amount of vaporization. It was also documented that as the formed iron vapour cools it condenses into submicronic particles [40].

The vaporization and the consequent condensation of vapours has also been demonstrated for ceramics in the case of yttria-stabilized zirconia (YSZ). The results were similar to those conducted with iron particles, the YSZ powder vaporizes and condenses to submicronic particles (dust). The concentration of particles was measured and it was found to

increase with increasing axial distance from the spray torch, meaning the dust concentration was higher closer to the substrate. [41] This dust can accumulate on the substrate itself along with unmelted particles and get trapped between incoming molten droplets, such a phenomena has been demonstrated with alumina elsewhere, see Figure 16 [42]. Similar behaviour has also been speculated for chromia [31]. The inclusion of fine dust between each pass creates a poorly adhered layer between each pass, which leads to poor overall coating cohesion and a layered porosity in thermal sprayed chromia coatings. These microstructural factors further deteriorate the coatings wear resistance amongst other properties.

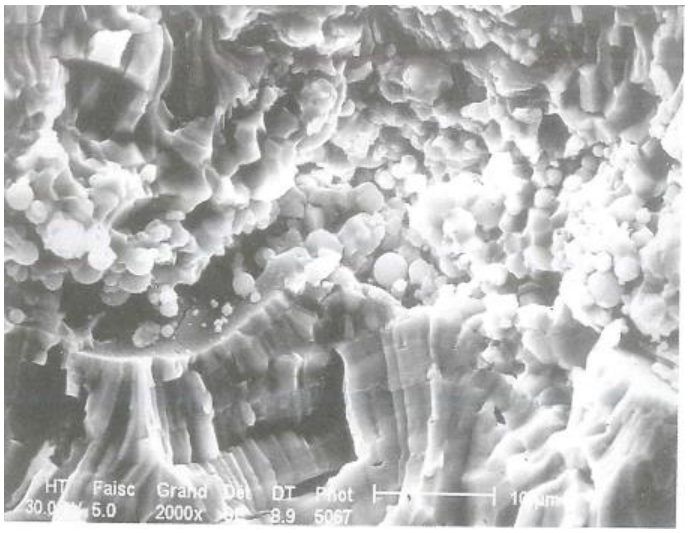

Figure 16: *Interface of alumina beads with small spherical particles trapped between columnar grains. [42] (p. 620)*

We have concluded that vaporization affects multiple materials in plasma spraying due to the extreme temperatures in the process but what makes vaporization even more significant for chromia is the chemical reactivity in high temperatures and the formation of hexavalent chromium compounds. While chromia melts at 2334 °C and starts vaporizing above that, toxic hexavalent chromia compounds start forming below 1000 °C and will vaporize at much lower temperatures, which adds to the total amount of material loss.

What actually happens to chromia in a thermal spraying environment has not been investigated but studies related to the behaviour of chromium oxide in solid-oxide fuel cells and in waste incinerators will give some ideas as to the possibilities even though the temperatures and atmospheres are not exactly the same. When sintered Cr_2O_3 was held in a furnace in temperatures of 1000-1200 °C and subjected to pure oxygen or argon with or without moisture, several phenomena were documented. In an oxygen atmosphere, the sample showed signs of weight loss, which nearly doubled in wet oxygen. In argon, wet or dry, however, weight loss was zero. [43]

This indicated that a chemical reaction is behind the evaporation of Cr_2O_3. Thermodynamically the most feasible compound was speculated to be hexavalent chromium oxide CrO_3 according to reaction 1.

$$Cr_2O_3(s) + 3/2O_2(g) = 2CrO_3(g) \quad (1)$$

CrO_3 is a metastable oxide but with high oxygen pressure its formation is likely. Its existence was not verified in the furnace trials as it typically decomposes back to Cr_2O_3. When a Cr_2O_3 sample was heated with an oxy-gas torch, CrO_3 was detected in the smoke that condensed on a cold surface. The CrO_3 was retained possibly due to the rapid quench. [43]

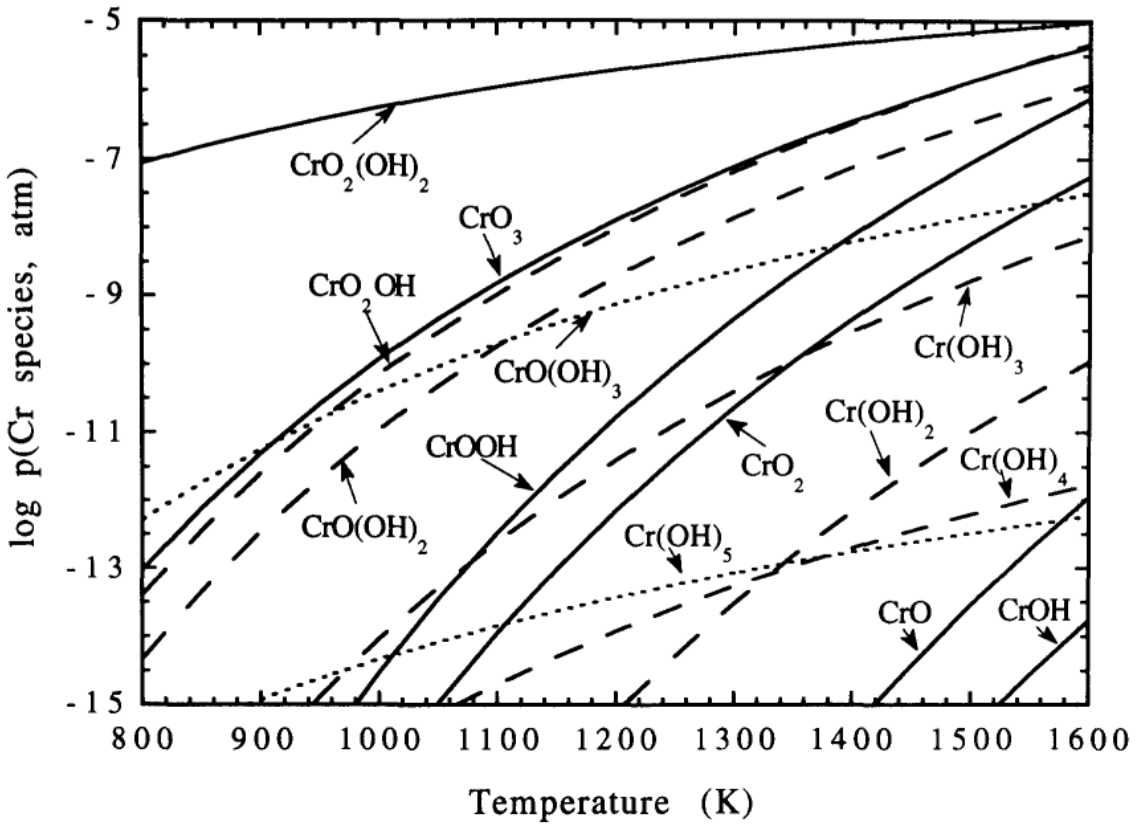

Figure 17: *Logarithmic plot of chromium species partial pressures as a function of temperature at $p(H_2O)$ = 0,10 atm and $p(O_2)$ = 0,10 atm. [44]*

Another possibility for the dominant chromium species that forms is hexavalent chromium oxyhydroxide $CrO_2(OH)_2$, which forms according to reaction 2 and is also attributed as the reason for increased weight loss in wet oxygen environments.

$$Cr_2O_3(s) + 2H_2O(g) + 3/2O_2(g) = 2CrO_2(OH)_2(g) \quad (2)$$

Calculations indicated that when $p(H_2O)$ = 0,10 atm and $p(O_2)$ = 0,10 atm chromium oxyhydroxide $CrO_2(OH)_2$ would be the dominant vapour species. CrO_3 is the second most

dominant in this system as illustrated in Figure 17.[44] With increasing temperature the relative amount of CrO_3 increases and considering the higher range of temperatures in the plasma spraying process CrO_3 may be the dominant species in that process. The formation of $CrO_2(OH)_2$ also necessitates the presences of moisture. In other computations done in a similar system where water vapour was not taken into consideration CrO_3 emerged as the dominant vapour species [45][46].

Actual experiments agree to some degree with the aforementioned calculation results. Experiments were done in a constant temperature of 950 °C by variating the partial pressure of water $p(H_2O)$ from 0,0007 to 0,3. At $p(H_2O)$ lower than 0,005 bar, vaporization of Cr_2O_3 was independent of water partial pressure. With $p(H_2O)$ higher than 0,005 bar, vaporization rate increased with increasing water partial pressure. With low $p(H_2O)$, CrO_3 was found as the dominating vapour species and it was claimed to be independent of $p(H_2O)$. Meanwhile $CrO_2(OH)_2$ was more prominent at higher $p(H_2O)$ and its partial pressure was strongly related to $p(H_2O)$. Additionally experiments done at constant $p(H_2O) = 0.02$ bar the evaporation rate of Cr_2O_3 increased with increasing temperature. [47] The effect of temperature on the formation of CrO_3 in dry air and $CrO_2(OH)_2$ in wet air is illustrated in Figure 18.

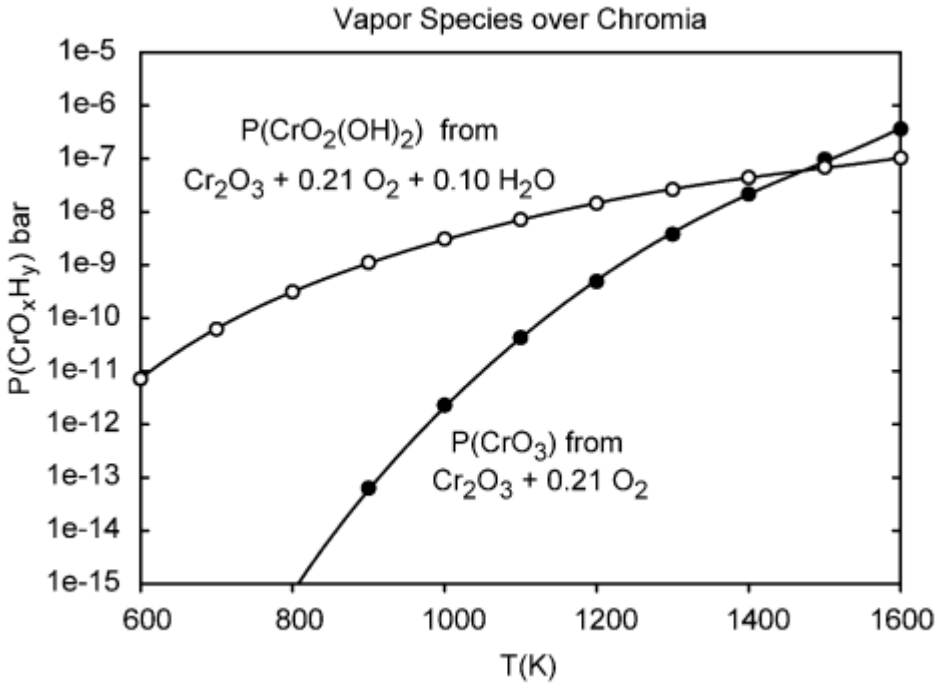

Figure 18: *Calculated vapour pressures of volatile chromia species in dry and wet air. [48]*

In other experimental studies, lower temperature ranges in wet oxygen were covered through a transpiration technique. At 600 °C and below, mainly brown liquid chromic acid ($CrO_2(OH)_2$) was found. At 700-900 °C in addition to the brown deposit, green Cr_2O_3

was also discovered. Hexavalent chromium being an unstable compound it was noted that it tends to decompose above 400 °C, indicating that at higher temperatures the hexavalent vapours decompose and deposit as Cr_2O_3. Additional experiments to determine the effect of CrO_3 on the total vaporization were also conducted at 900 °C in dry oxygen, it was concluded that its contribution was not more than 1 % in that temperature, once again emphasizing the dominance of $CrO_2(OH)_2$ at lower temperatures. [49]

What can be gathered from this array of experimental and theoretical studies is that, to minimize the vaporization of chromia, moisture has to be reduced in the spraying atmosphere as moisture promotes the formation of the more volatile oxyhydroxide. Another factor to monitor is the spraying temperature; high flame temperatures naturally increase the overall evaporation rate. In this respect, HVOF appears as a promising technique, but on the other hand, it is possible that the higher amount of oxygen in the HVOF flame will promote the oxidation of Cr_2O_3 regardless of the lower operating temperatures. In a plasma flame the oxygen available for the reaction is mainly entertained by the surrounding mixing air currents.

In actual plasma spraying operations the amount of hexavalent chromium in process fumes has been measured in a few cases. Plasma spraying of pure metallic chromium powder yielded a 26-30 % fraction of hexavalent chromium out of total chromium in the collected fumes [51][52]. In a separate analysis for plasma spraying of 100 % Cr_2O_3 the amount of hexavalent chromium formed was 8,9 grams per kilogram of sprayed material [53]. The amount of process fumes and the amount of hexavalent chromium formed would naturally vary and would be affected by starting powder and most importantly the process parameters.

4.4 Health effects of hexavalent chromium

As stated, the fact is that hexavalent chromium vapours are present in thermal spraying processes involving chromium and chromium oxide, which creates problems for work safety, ventilation and waste handling. Even though part of the fumes condense back to the much more harmless Cr_2O_3 some are still retained due to rapid quenching [43] or via the formation of stable compounds with alkali metal impurities present in the spraying powder [50].

It has been proposed that the use of extremely pure chromia with alumina additions can reduce the vaporization and formation of hexavalent chromium compounds. Even if the amount of hexavalent chromium was reduced through process optimization, its complete elimination is highly unlikely. Therefore, the health risks associated with hexavalent chromium should be recognized by personnel working with these materials and respective measures should be taken to reduce exposure as well as limit environmental emissions.

People working with chromium containing compounds and materials may be exposed to hexavalent chromium through inhalation, skin contact or ingestion [85]. For thermal spraying operations, inhalation of fumes and dust is possibly the most prevalent. Ingestion may occur if food, cosmetics or tobacco are handled in the same space and are contaminated as a result. The same dust may also land on the skin and get absorbed through it. [86] Overall, hexavalent chromium is not very easily absorbed through the lungs or the digestive system; it is however absorbed more readily than the trivalent form making it more hazardous. Hexavalent chromium is often reduced to its trivalent form by gastric liquids reducing exposure through ingestion. Absorption through skin contact is highly dependent on the compound and its form as well as the condition of the skin. [85]

Acute effects of hexavalent chromium exposure include skin ulcers and allergic reactions. Ingestion of large amounts may lead to stomach ulcers, gastrointestinal bleeding, vomiting, kidney and liver damage and in extreme cases death. In most cases, chronic exposure is more common in the workplace; effects of chronic toxicity include ulceration, skin irritation and hypersensitization to other metals resulting from dermal exposure. Inhalation may result in nasal bleeding, loss of smell and taste as well as asthma. Hexavalent chromium is also classified as a carcinogen as an increase in lung cancer has been observed in people working in industrial facilities utilizing chromium compounds. [85][87]

There are different levels of exposure permitted by various health and safety organizations. In 2006, the Occupational Safety and Health Administration (OSHA) in the United States passed new regulations regarding hexavalent chromium exposure lowering the previous limits by a factor of 10. The permissible exposure limit (PEL) was set as 5 $\mu g/m^3$ as a weighted time average during an 8-hour shift. If the amount of chromium in air exceeds this limit, access to the area must be limited, air monitoring must be conducted every three months and respirators and special clothing is required for people working in said area. [88]

In addition to the PEL, OSHA also maintains a separate action level which is 2,5 $\mu g/m^3$. When the chromium content is between 2,5-5 $\mu g/m^3$ air monitoring must be implemented every six months and workers must be medically tested. [88] In 2013 the National Institute for Occupational Safety and Health (NIOSH) published its own recommended exposure limit (REL) of 0,2 $\mu g/m^3$ for hexavalent chromium [86]. Although the REL is only a recommendation, it indicates a clear trend towards lowering the limit gradually to reduce exposure. The regulations in Finland controlled by the Ministry of Social Affairs and Health are similar to the ones implemented by OSHA as the concentration known to be hazardous is the aforementioned 5 $\mu g/m^3$ weighted time average during an 8-hour shift [89]. Other related restrictions include the RoHS-directive (Restriction of Hazardous Substances) where the amount of hexavalent chromium in homogenous materials is restricted to 0,1 wt% [90].

5. AUXILIARY SYSTEMS FOR COOLING AND CLEANING

As a process technology, thermal spraying is still evolving, new and existing materials are being sprayed with new generation torches with optimized parameters providing coatings with longer lifetime and enhanced properties. Simply modifying the spraying conditions to reach higher or lower temperatures and higher velocities however is limited in terms of coating evolution. At times the desired coating properties require contradicting settings resulting in compromises, thus the introduction of auxiliary systems is necessary to incorporate more levels of freedom to process optimization [54].

One group of auxiliary systems that are used for pre- and post-processing include torches and lasers for preheating, surface cleaning and remelting. Preheating with a torch is a common practice to evaporate condensates and impurities off the substrate surface to improve coating adhesion. [2] This can be done with the spraying torch prior to spraying or with a secondary torch while spraying, lasers are capable of achieving the same effect as well, like in the HeatCool® process illustrated in Figure 19 [54]. Lasers can also be used to remelt the coating layers in succession with layer deposition.

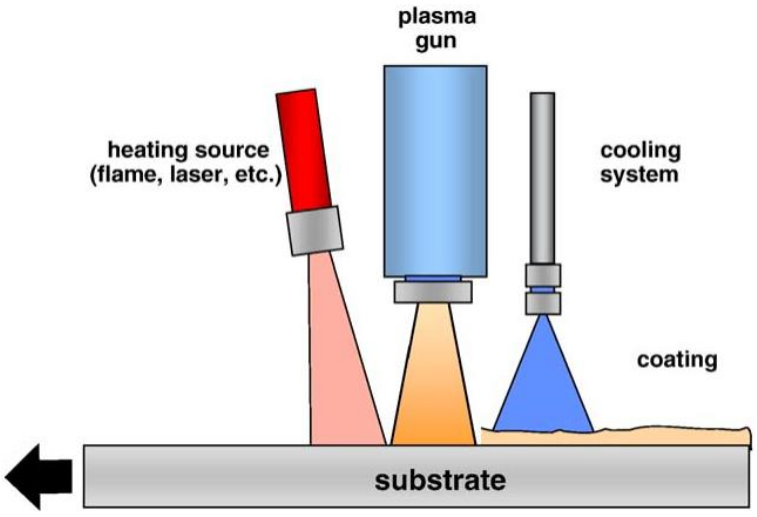

Figure 19: *Set-up of the HeatCool® process utilizing simultaneous preheating and cooling during plasma spraying. [54] (p. 1971)*

Another group which will be the main focus of this chapter is cooling systems, namely compressed air, liquid nitrogen and carbon dioxide based systems. Compressed air is already used especially with high power spray systems such as plasma and HVOF as they can induce significant heat strain on the components. Without the use of air cooling, cooling breaks would sometimes be necessary resulting in loss of productivity [3]. Cooling

systems have two primary functions: temperature control and removal of dust and overspray. [2] The capabilities of compressed air are however limited and with modern high-power spraying systems even insufficient. Much more effective cooling can be achieved with the use of cryogenic nitrogen or carbon dioxide [55].

Not many comparative studies have been done with various cooling systems as most studies involve the use of a single method with standard air cooling as a reference. The systems available in the industry also come in different designs, newer models being more sophisticated and efficient than the ones studied in the past. Some basic evaluation can however be made according to the properties of the cooling substance alone. The specific heat capacity, the enthalpies of phase transitions and temperature all affect the cooling potential of the system. Some of these properties are listed in Table 2.

Table 2: *Thermodynamic properties of cooling mediums [56][57].*
N_2 values correspond to vaporization and liquid phase.
CO_2 values correspond to sublimation and solid phase.

Gas	Vaporization or sublimation temperature (°C)	Vaporization or sublimation enthalpy (kJ/kg)	Specific heat capacity c_p of liquid or solid (kJ/kg*K)	Specific heat capacity c_p of gas (kJ/kg*K)
Air	-	-	-	1,005
N_2	-195,8	**198,6**	2,06	1,039
CO_2	-78,4	**573**	0,519	0,845

When compressed air exits a nozzle and expands, it cools slightly but it is still close to room temperature, compared to the other cooling media this is still relatively warm. Nitrogen can be used in its liquid state below its evaporation temperature of -195,8 °C. Carbon dioxide is supplied as a liquid in high-pressure containers but does not exist in the liquid phase at atmospheric pressure, rather as it expands and cools it deposits directly into a solid from the gas state. Solid carbon dioxide, also known as dry ice, sublimates at -78,4 °C. Even though liquid nitrogen is significantly colder than dry ice, the sublimation enthalpy of carbon dioxide (573 kJ/kg) is noticeably higher than the vaporization enthalpy of nitrogen (198,6 kJ/kg). It should also be noted that the phase transitions enthalpies are over a hundred orders of magnitude higher than the specific heat capacities, making it evident that the phase transition enthalpy is a dominant factor when it comes to cooling efficiency in cryogenic systems.

In theory, solid dry ice sublimating on a hot surface has a better cooling capacity as it absorbs more heat energy in the process than liquid nitrogen. The heat energy absorbed by 1 kg of liquid nitrogen, dry ice and air heating from their starting temperature to 100

°C was calculated. The starting temperature of compressed air was chosen as 11 °C [55]. During the cooling process liquid nitrogen and dry ice start vaporizing and sublimating prior to contact, thus it was presumed that the temperature at moment of contact is near the corresponding phase transition temperatures. According to these calculations, the total cooling capacities are 89 kJ/kg for compressed air, 506 kJ/kg for liquid nitrogen and 722 kJ/kg for dry ice. If the cryogenic cooling media are in a gas state upon contact, the cooling capacity is only 150 kJ/kg for carbon dioxide and 307 kJ/kg for nitrogen.

There is also another issue related to liquid nitrogen, namely the Leidenfrost effect. When liquid comes in contact with a surface with a temperature significantly higher than the liquids boiling point, an insulating gas cushion is formed from the rapidly vaporizing liquid. This is a common occurrence for example in water quenching of metals. The insulating layer of vapour isolates the hot surface from the cooling liquid preventing direct contact and thus decreasing the rate of heat transfer. In the end, the cooling capacity of liquid nitrogen is not fully utilized the moment it makes contact with a hot surface. Dry ice particles impacting and sublimating on a hot surface do not face the same limitations. [59]

Table 3: *Studied cooling media and test parameters. [55]*

Cooling	Nozzle [mm²]	Pressure [bar]	Internal T [°C]	Nozzle exit T [°C]	Bond coating T [°C]	Top coating T [°C]
No cooling	-	-	-	-	200	330
Air cooling high flow rate	12,5*2	5 (60 m^3/h)	11	11	120	170
Cryogenic CO_2	2*2	20	20	-74	80	180
	2,5*2	60	-20	-74	80	140
Gaseous N_2	2*2	20	-196	8	180	250
	2*2	60	-196	8	150	230
Liquid N_2 high flow rate	12,5*2	5 (60 m^3/h)	-196	-140	40	140

As mentioned, the specific cooling system, its design and operating parameters determines the cooling efficiency, thus a direct comparison of different cooling media is challenging. Only one article [55] that featured all three different cooling media was found for reference. In the study, the cooling efficiency of different gases was experimentally tested for high-power plasma spraying of metallic bond coats and ceramic thermal barrier

coatings. The compared cooling systems and their data are listed in Table 3 along with the temperatures measured from NiCrAlY bond coat and PSZ top coat application experiments. All systems consisted of 2 nozzles on both sides of the plasma torch. It was not disclosed as to how the carbon dioxide behaved in the nozzle; whether the CO_2 stream consisted of just cold gas or a mixture of cold gas and small solid snow like particles.

Out of all the methods high flow rate liquid nitrogen had the best cooling efficiency, cryogenic CO_2 at 60 bars being only slightly less efficient. The high flow rate air cooling proved itself to be surprisingly efficient. High flow rate air cooling was at least as good as or better than gaseous N_2 cooling and the 20 bar CO_2 cooling. Considering the additional costs that N_2 and CO_2 systems would require in most cases, their use may not be very cost effective. The cooling efficiency reflected on surface quality as coatings deposited at lower temperatures had lower roughness and less defects.

5.1 Compressed air cooling

The air that is used for cooling in spraying operations should be dry and free of any grease that may be incorporated into some systems, dryers and filters may thus be required [3]. Compressed air works by removing heat via convection so its cooling capabilities are strongly related to the flow rate as the air is typically near room temperature. Cooling systems based on compressed air can be divided into two categories: air jets directed straight towards the substrate (Figure 20a) and air knives aimed perpendicular to the thermal spray jet (Figure 20b). [2]

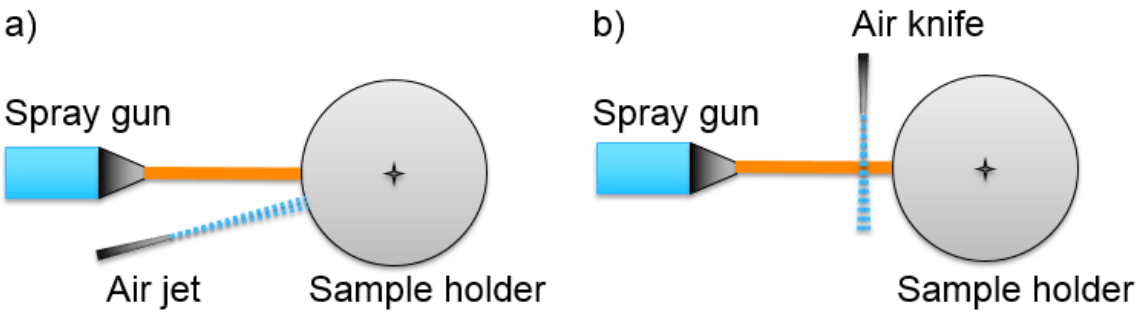

Figure 20: The use of air jets and air knives during thermal spraying.

Air jets directed at the substrate may be affixed to the torch or located in a separate, fixed position. For stationary cooling a single air jet may be used for example on the backside of a rotating work piece, alternatively a cooling strip with several holes covering the entire length of the work piece can be implemented for more uniform cooling [3]. For cooling systems fixed to the torch, a possible configuration is two nozzles on both sides of the spray torch. [2] The use of two air cooling nozzles during plasma spraying of chromia was found beneficial to coating quality, the cause was claimed to be their cooling and

most of all cleaning effect; it was also found out that a shorter distance of 30 mm between the nozzles and the torch was better than 50 mm [31].

The perpendicular air jets that intercept the spray jet are often referred to as air knives, air barriers or air curtains as the nozzles used often create a thin, wide air jet. The function of these air knives is to cool the hot gases minimizing their heating effect and blow slow moving, solid particles and dust off their trajectory so they do not deposit on the work piece. The downside to this is a noticeable reduction in temperature (200-300 °C) and velocity (20-30 m/s) of the hot particles as well. [2] This cooling and deceleration of particles mid-flight may lead to a decrease in coatings quality if the particle surface solidifies and they fail to adhere properly. The successful use of air knives especially with ceramics may thus require high-power spraying systems that can produce high quality coatings regardless of the drop in particle temperature and velocity. An air barrier has however been successfully used during plasma spraying of alumina to eliminate inclusions of small particles (Figure 16, p. 25) between spray beads [42].

5.2 Liquid nitrogen cooling

There are a few different methods for liquid nitrogen as a cooling medium in thermal spraying. The most typical way is to spray the sample with liquid nitrogen during spraying, often with a separate nozzle attached to the robot along with the spraying torch. The nozzle may also be located in a fixed position on the sample, for example on the opposite side to prevent the cooling spray from affecting the actual thermal spray plume [81]. There are also cases where an actual quench in a liquid nitrogen bath was utilized after a few spraying passes to achieve a martensitic structure [82].

The simplest liquid nitrogen cooling utilizes a spray of 100 % liquid nitrogen; some more technologically advanced equipment however may use a combination of liquid nitrogen and compressed air. Most notable in thermal spraying research is the so-called LIN-GAN system (Figure 21), which utilizes a proprietary nozzle that mixes liquid nitrogen with room temperature compressed air [83]. The ratio of liquid nitrogen to compressed air is controlled electronically making it a very adaptive system. It has been demonstrated as being an efficient cooling system when used together with HVOF spraying.

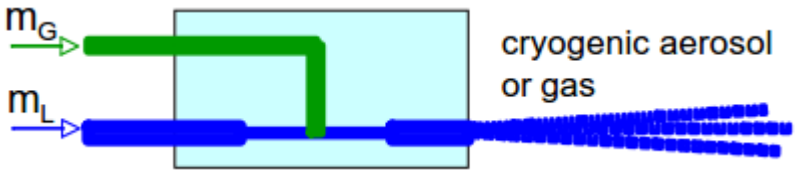

Figure 21: LIN-GAN cryofluidic nozzle.
m_G = gas stream, m_L = liquid nitrogen stream [84].

The hybrid cooling system was tested with HVOF spraying of WC-CoCr coatings on aircraft main axles. To retain the substrate properties on strict required levels the process temperature needs to be controlled and retained below a certain level. Even with air cooling, cooling breaks were necessary to prevent overheating. During cooling breaks, the HVOF torch was kept on, resulting in not only wasted time but also wasted gases and powder. [84]

With the use of the LIN-GAN cooling system, the overall process time was cut in half as cooling breaks were no longer required to maintain the process temperature, this in turn resulted in significant cost savings. Efficient cooling also resulted in a slightly higher deposition efficiency, which was speculated as being due to reduced splat oxidation and increased splat adhesion resulting from it. Overall, the coatings were found to be as good if not better than the air-cooled coatings. In the LIN-GAN cooled samples the substrate also retained its properties better than with air cooling. [84]

5.3 Carbon dioxide cooling

For cooling purposes, carbon dioxide is supplied in two forms, in high-pressure containers as liquid carbon dioxide or in a thermally insulated container as solid dry ice. Liquid carbon dioxide is stored in pressurized containers and sprayed with specialized nozzles. This type of process is sometimes referred to as CO_2-snow blasting. Solid dry ice is commonly supplied as pellets which are used in dry ice blasting, a process very similar to grit blasting. [2]

In addition to cooling, carbon dioxide has potential at surface cleaning. The cleaning effects of dry ice, CO_2-snow blasting and a few other methods were evaluated in a tensile lap-shear strength test [60], where specimens were pretreated and bonded with two-component epoxy resin adhesive. Pretreatment with dry ice yielded results on the same level with corundum blasting, results from snow blasting were slightly inferior but still provided an improvement over solvent degreasing. Even though dry ice is not very abrasive, it was found to texture soft aluminium lightly, potentially promoting adhesion via mechanical interlocking [61].

5.3.1 CO_2-snow blasting

CO_2-snow blasting is used primarily for cooling purposes in high-temperature processes when faster cooling rates are required. In the process, liquid CO_2 is supplied from containers at 18 or 57 bars through a hose to a specialized convergent-divergent nozzle (shown in Figure 22). As the CO_2 pressure decreases in the divergent section at the nozzle, the CO_2 partially solidifies into small snow like particles, which are sprayed out of the

nozzle by the expanding gases. The solid CO_2 particles sublimate on contact with the workpiece cooling it along with the gases. [3]

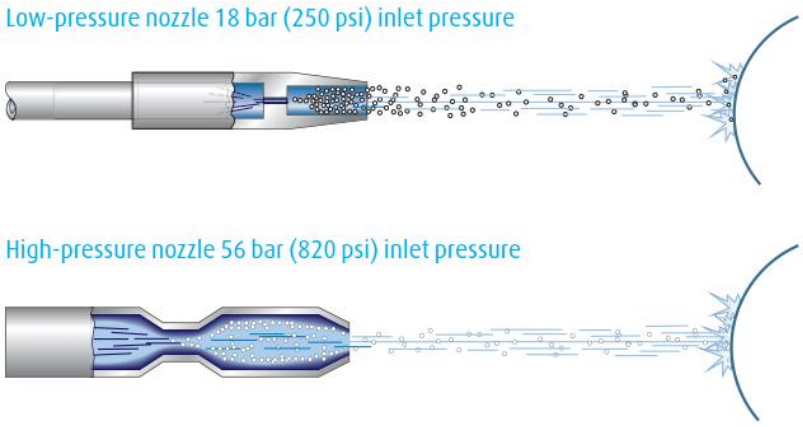

Figure 22: LINSPRAY® CO_2-snow blasting nozzle design. [77]

This type of CO_2-snow blasting is much more effective than air cooling simply due to the thermodynamic properties discussed earlier. In experimental trials, CO_2-cooling outperformed air cooling by cooling a heated component 5 times faster [59]. It can however be argued that the amount of air consumed has the greatest effect on air cooling and similar cooling efficiency might be achieved with higher air flow rates. The CO_2-cooling system was also compared to liquid nitrogen cooling. According to the results, a 2 kg/min nitrogen cooling was still less efficient than CO_2-cooling with a 730 g/min consumption.

Based on the reported benefits, CO_2-cooling does seem more appealing than air and liquid nitrogen cooling. The CO_2-cooling system does however have a limitation in its customization possibilities. At least in the LINSPRAY®-system the only way to adjust the amount of CO_2 consumed and the achieved cooling is by switching the nozzle as its size controls the CO_2-consumption [77]. Apart from the material produced by the companies marketing the cooling systems, very little information is available as to their benefits in thermal spraying.

While the LINSPRAY® CO_2 cooling –system is mainly marketed towards cooling in thermal spraying applications, similar systems utilizing CO_2 particles created in the blasting nozzle are also made for manual and automated cleaning applications [77]-[80]. As the systems make use of solid CO_2 particles, they exhibit a cleaning effect similar to dry ice blasting. These systems are actually often marketed as an alternative to dry ice blasting but the size of the particles being blasted and therefore the cleaning efficiency may be markedly different compared to real dry ice blasting. However due to the smaller size of the snow particles and the lower kinetic energy it is inherently a gentler process than dry ice blasting, making it better suited for certain cleaning applications.

5.3.2 Dry ice blasting

Dry ice consists of solid carbon dioxide at a temperature below -78,4 °C, typically supplied as pellets 1-6 mm in diameter and 5-15 mm in length for blasting applications. They are made by relieving liquid carbon dioxide to atmospheric pressure in a low temperature chamber creating carbon dioxide snow. The snow is compacted mechanically in moulds to create the pellets or any other desired form. The process is illustrated in Figure 23. [62]

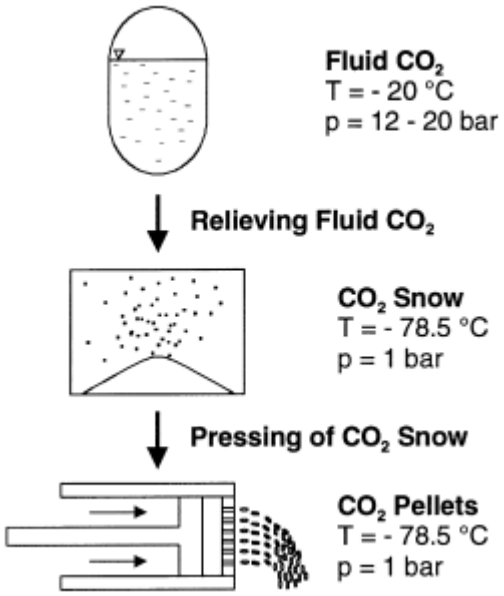

Figure 23: *Manufacturing process of dry ice pellets. [62] (p. 403)*

Dry ice blasting uses similar equipment as other media blasting: it consists of an insulated storage unit, a feeding system which doses the pellets into the compressed air stream, which transport the pellets through an insulated hose to the blasting nozzle. The operating parameters such as pressure and particle flow rate vary depending on the specific equipment. Dry ice blasting is suitable for cleaning and removal of rust, paint, lacquers, resins and oils. [62]

Only a part of the cleaning effect comes from the kinetic energy of the particles and the gas. During dry ice blasting the particles sublimate as they hit the surface cooling it rapidly inducing superficial thermal shocks. This in turn induces cracking and delamination of the contaminant layer due to difference in thermal expansion coefficients of the layers. Furthermore as the particle turns into gas, it goes through a volume change expanding rapidly. The expanding gas can penetrate under the partially delaminated contaminant layer promoting its removal. [2] The cleaning effects are illustrated in Figure 24 below.

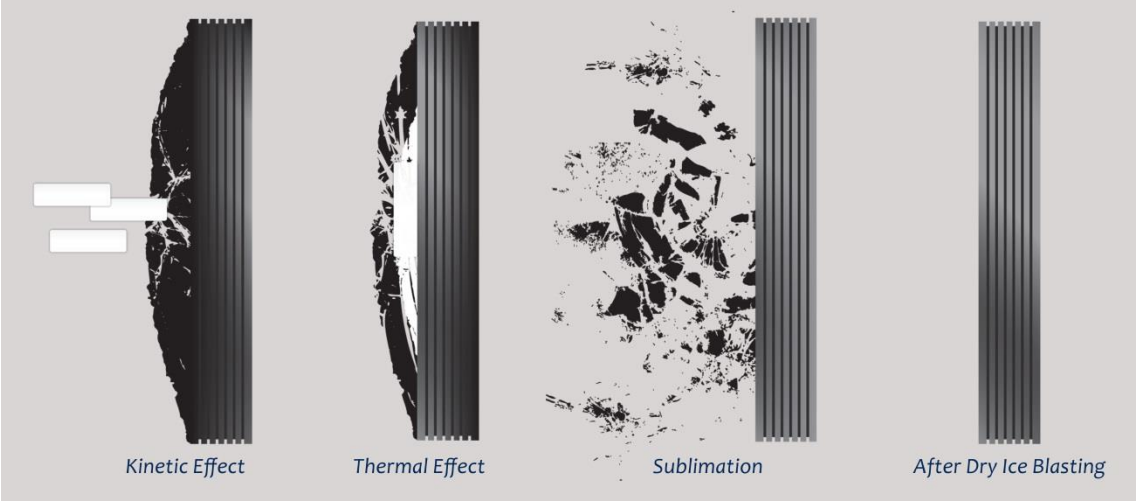

Figure 24: *Dry ice blasting cleaning principle. [76]*

Compared to other mechanical or chemical cleaning methods, dry ice blasting provides noticeable benefits. Since the blasting media evaporates, it leaves no residue requiring further removal by drying or cleaning making further processing operations easier. Dry ice particles have a low hardness (2-3 Mohs) and are only lightly abrasive, making them a suitable blasting medium for a variety of materials and contaminants. As the particles damage the surface only very lightly, further surface finishing requirements are minimal compared to grit blasting. The main limitations of dry ice blasting are the high noise level and the requirement for ventilation to prevent carbon dioxide build up. [62]

Dry ice blasting has been shown to be even capable of removing thermal barrier coatings, this process however required high-pressure blasting (over 16 bars) and preheating of the component to maximize the thermal shock effect. With the process, the ceramic thermal barrier coating was removed while the metallic bond coat remained intact. The metallic bond coat retained its surface topography and was ready for a new thermal barrier coating without any further processing. [63]

The vast majority of the studies related to the application of dry ice blasting during thermal spraying operations is by Dong et al. [58][64]-[75]. The studies have focused on various plasma sprayed coatings, both metallic and ceramic, plasma spraying parameters have varied according to material but the dry ice blasting parameters are constant between studies and are listed in Table 4. The nozzle utilized was of the divergent type but its exact dimensions were not disclosed in the papers. The dry ice blasting nozzle was fixed to a robot next to the plasma torch and they operated simultaneously during spraying operations.

Table 4: *Dry ice blasting parameters used during plasma spraying [58].*

Parameter	Value
Nozzle exit dimensions	9x40 mm
Dry ice mass flow rate	42 kg/h
Dry ice particle diameter	3 mm
Dry ice particle length	3-10 mm
Air pressure	6-8 bar
Nozzle distance from substrate	25 mm
Nozzle distance from plasma torch	20 mm

The results acquired from plasma spraying and dry ice blasting have been positive throughout the studies (data compiled in Table 5 on next page). For all of the coatings studied, the porosity of the coatings had always decreased when dry ice blasting was used, for most of the processes a significant reduction in working temperature was also measured in comparison to conventional air cooling. When reported, the oxide content and average surface roughness of metallic coatings was reduced. In the case of some alloy and alumina coatings hardness also increased noticeably with dry ice blasting. The effects of dry ice blasting on steel coatings are shown in Figure 25.

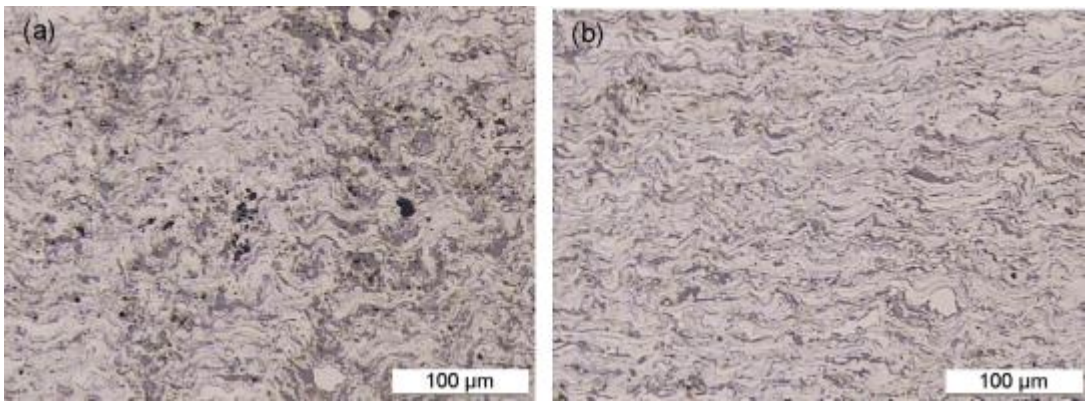

Figure 25: *Optical micrographs of steel coatings sprayed with APS (left) and APS with dry ice processing (right). [58] (p. 6)*

The effect of dry ice processing on adhesion was generally also positive. There are some differences whether dry ice blasting was only used during plasma spraying or whether it was also applied as a pretreatment. For example, the steel coatings benefitted from the additional pretreatment as the adhesion increased further. The pretreatment consisted of 4 passes over the sample holder with both the torch and the dry ice blasting nozzle. The function of the dry ice blasting was to clean off impurities and the plasma torch was used to prevent condensation related to excess cooling [66].

The exact mechanism behind coating quality improvement by dry ice blasting was not established, this was mainly due to the overlapping effects of the process. In the case of

porosity, part of the densification could be attributed to the shot peening effect on the coating [71], according to calculations in [62] the maximum impact force of dry ice blasting is in the order of 150 N. The other possible mechanism behind porosity reduction could be the cleaning effect, which improved splat adhesion [68]. The cleaning effect is most likely the dominating factor behind better adhesion as indicated by single splat studies. Dry ice blasting was shown to effectively clean impurities from polished surfaces and encourage the formation of disk like splats [69].

Table 5: *Properties of coatings produced with air cooling, with dry ice blasting and with pre- and during treatment by dry ice blasting. [58][64][65][66][68][70][71][75]*

Coating	Process	T [°C]	Hardness [HV]	Porosity [area. %]	Oxide [area. %]	Adhesion [MPa]	Ra [µm]
Steel	Air cooling	170	-	0,55	9,46	46	16,54
	Dry ice blasting	85	-	0,23	4,23	46	7,21
	Pretreatment + dry ice blasting	-	-	0,19	5,05	52	5,30
Al	Air cooling	-	-	3,45	-	40	18,08
	Pretreatment + dry ice blasting	-	-	0,35	-	53	11,14
CoNiCrAlY	Air cooling	160	-	(higher)	(higher)	54	-
	Dry ice blasting	80	-	(lower)	(lower)	52	-
	Pretreatment + dry ice blasting	-	-	-	-	56	-
FeAl	Air cooling	170	185	9,50	2,40	-	-
	Dry ice blasting	85	320	3,80	1,60	-	-
NiCrBSi	Air cooling	120	449	1,30	-	37,5	-
	Pretreatment + dry ice blasting	60	550	0,80	-	47,7	-
Al_2O_3	Air cooling	160	764	9,30	-	46	-
	Dry ice blasting	95	1035	6,80	-	60	-
Cr_2O_3	Air cooling	-	1211	6,60	-	13	-
	Pretreatment + dry ice blasting	-	1460	2,00	-	46	-

As far as oxidation in metallic coatings goes, the cooling effect reduces the surface temperature thus potentially reducing the rate of oxidation of solidified splats. The increased amount of carbon dioxide in the atmosphere surrounding the workpiece may also contribute to this. Additionally the dry ice jet could be capable of cleaning off oxidation that has already formed on the splats. [68] The increased hardness and smoother as-sprayed surfaces can be linked to the general improvement in microstructural characteristics of the coatings such as reduced porosity and oxide content.

One relatively surprising phenomena related to the cleaning mechanism is the apparent decrease in deposition efficiency. Aluminium sprayed with dry ice processing experienced a drop in coating thickness (269 µm versus 219 µm) compared to spraying without dry ice blasting even though spraying parameters stayed the same. [71] The calculated deposition efficiency of tool steel coatings was also lower with dry ice processed samples [74]. The cause for this was said to be densification via the shot peening effect as well as the removal of loose particles from between passes, which was verified in microstructural studies. In this case, the apparent drop in deposition efficiency resulted in coating quality improvement. The aluminium coating microstructures are illustrated in Figure 26.

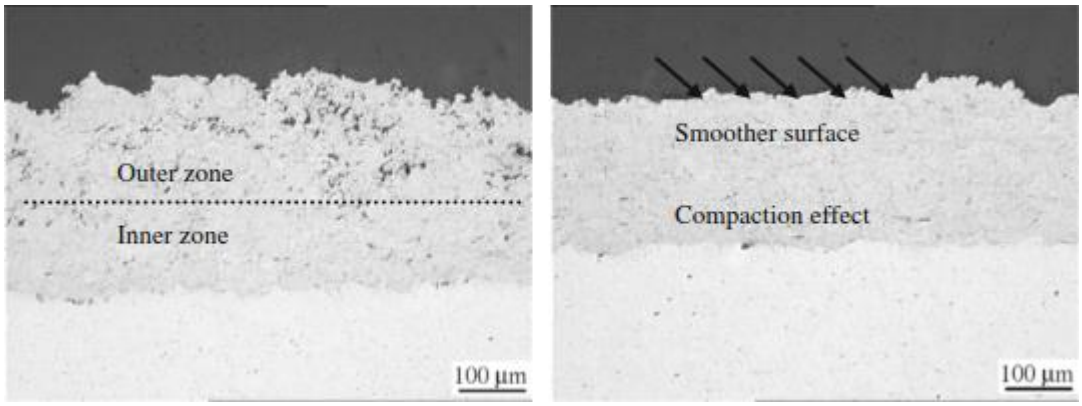

Figure 26: *Aluminium coating microstructures. Coating sprayed with APS (left) and coating sprayed with APS with dry ice processing (right). [71] (p. 1225)*

Another benefit of the increased carbon dioxide content arising from the sublimating particles may be realized while spraying high-carbon tool steel powders. It was found that a powder with 1,16 wt% carbon suffered severe decarburization having only 0,46 wt% carbon after spraying with conventional plasma spraying process. In comparison, the dry ice processed coating had retained a significantly higher fraction of carbon at 1,03 wt%. [74]

Improved microstructural characteristics commonly lead to improved properties and longer lifetimes; this was realized with a few coatings during wear testing. While the friction coefficients of the different tool steel coatings were similar, the wear amount in a sliding wear test was nearly half for the dry ice processed sample. The low wear resistance of the conventionally sprayed coating was attributed to propagation of cracks through oxide veins and subsequent fragmentation; the dry ice sprayed coating had a lower oxide content and thus a higher cohesion [74]. In the case of NiCrBSi coatings, the higher hardness of the dry ice processed coatings lead to a slightly lower friction coefficient and similarly lower wear [75].

Other coating specific quality improvements were also reported. According to phase analysis, the FeAl coating produced without dry ice blasting contained Fe_3Al and Al_2O_3 phases, which were the result of oxidation and selective evaporation. These phases were

not present in the coatings produced with dry ice blasting due to better cooling efficiency. The faster cooling and solidification was also credited for the higher hardness with these coatings [68], similarly a higher proportion of amorphous phase was found in NiCrBSi coatings sprayed with dry ice blasting [75].

Processing by dry ice blasting seems to also offer prolonged lifetimes for thermal barrier coatings [73]. Three types of multi-layered thermal barrier coatings were manufactured: one without dry ice blasting, one with dry ice processed bond coat and one with dry ice processed bond coat and top coat. The coating with dry ice processed bond coat and top coat gave the best performance in thermal cycling experiments. The improved lifetime was attributed to the reduced porosity and oxide content in the bond coat and increased vertical porosity in the top coat. Bond strength between the bond and top coat was also higher.

For the purpose of this thesis, the most significant paper by Dong et al. relates to plasma spraying of chromia with dry ice processing [70]. The plasma spraying parameters used in the study are listed in Table 6, dry ice blasting parameters were the same as listed earlier (Table 4). Since adhesion was a significant focus of the study, the samples were pretreated with dry ice blasting prior to spraying with the procedure described earlier in this chapter.

Table 6: *Plasma spraying parameters used in the dry ice experiment. [70]*

Parameter	**Value**
Powder	Amdry 6410
Powder composition	Cr2O3
Powder size	-45+22 µm*
Plasma torch	F4
Current	630 A
Voltage	68 V
Power	42,8 kW
Argon flow rate	32 slpm
Hydrogen flow rate	12 slpm
Carrier gas (Ar) flow rate	3,4 slpm
Spraying distance	115 mm
Holder rotation speed	150 RPM
Holder diameter	160 mm
Calculated surface speed	75,4 m/min
Line speed	15 mm/s
Calculated forward speed	6 mm/rev

*D10=20,52 µm, D50=35,24 µm, D90=59,14 µm

The difference between the sample coatings made with the two processes is quite significant as can be seen from the optical micrographs (Figure 27). The calculated porosity of the APS sprayed sample was 6,6 ± 1,1 % while the dry ice processed coating only had a porosity of 2,0 ± 1,1 %. Most likely as a result of improved microstructure, an elevated hardness was measured in the dry ice processed samples. Adhesion was also improved immensely from 13 ± 2 MPa to 46 ± 5 MPa with the application of dry ice blasting. Samples were also tested for sliding wear, friction coefficients were similar for both samples but the wear rate was lower for the dry ice processed coating. In addition to lower wear in the coating, the WC-Co counterbody also experienced less wear against the dry ice processed coating. [70]

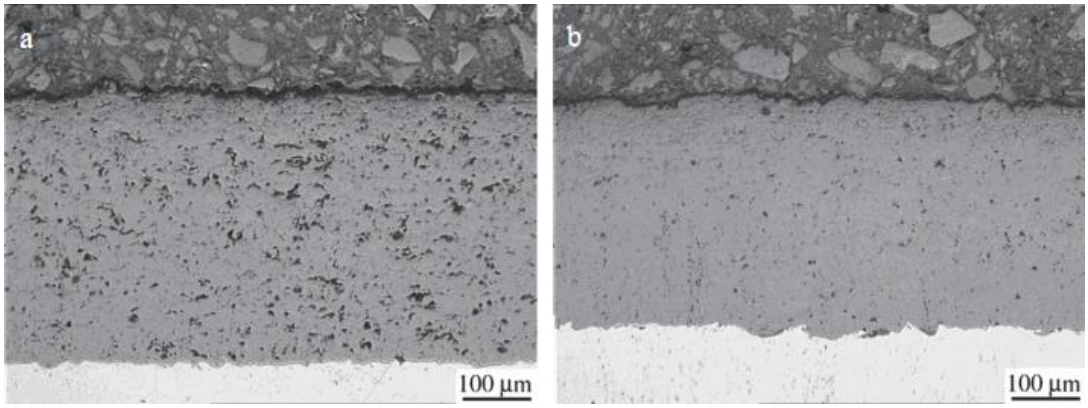

Figure 27: *Cr_2O_3 coatings sprayed with APS (left) and APS with dry ice processing (right). [70] (p. 60)*

As covered in the earlier chapter, the vaporization of chromia and the subsequent condensation of fine particles creates some challenges in its processing: they may gather between splats reducing adhesion and creating pores. It was suggested by Dong et al. that the improvement of coating quality by dry ice processing was mainly due to the elimination of fine particulates from the structure and from the substrate surface where they may accumulate before the first spraying pass. [70]

The exclusion of fine particulates was said to happen through two mechanisms. The first is the cleaning effect, as concluded in the case of other coatings; application of dry ice blasting can clean impurities in between spraying passes thus promoting coating adhesion and cohesion. This way fine chromia particulate could be removed so none get loosely embedded in between splats. The other way was related to the sublimation of dry ice, as the dry ice sublimates it expands and pushes the dust away from the workpiece along with the stream of compressed air. As evidence of the latter, the dry ice processed work piece was clean of fine chromia dust, which was found on the non-dry ice processed work piece. [70]

A third mechanism may have also been in effect: the higher carbon dioxide levels as a mechanism of oxide reduction. It is definitely more prominent in the case of metals, but its contribution should not be ignored here either. As summarized in chapter 4.3, the vaporization of chromia is a complex process and it is possible there are chemical reactions at play. Part of the vaporized chromia remains as Cr_2O_3 but part of it may be oxidized to CrO_3 according to reaction 1 (p. 32). In this case, the reduction of oxygen content could possibly reduce the amount of vaporized material thus reducing the total amount of process vapours and consequent dust.

6. EXPERIMENTAL STUDY

The purpose of the experimental part was to investigate the effects of auxiliary cooling systems on the structure and properties of plasma sprayed chromia coatings. The primary focus was the usage of dry ice blasting as a means to clean and cool the surface during spraying operations. Different parameters were used to examine their effect and find the optimal settings. Pretreatments were also tested as a means to investigate the cleaning effect of dry ice on the adhesion of the coating. Coatings were also made with only air cooling as a reference point. Due to unforeseen complications that arose at the end of the first spraying, more sprayings were necessary for the purpose of this study.

At the end of the first set of spraying trials while disassembling the equipment, it was discovered that a small stone was lodged in the dry ice spraying nozzle. It was presumed that the stone had been in the nozzle the entire time it was in use. The way the stone was positioned resulted in a significant blockage meaning that any dry ice particles passing through the nozzle would have been pulverized and the size of the particles exiting the nozzle would be significantly reduced resulting in lower kinetic impact energies and therefore lowered cleaning effect. In addition to the stone, it was also discovered later on that the spraying distance had been too long. Hence, additional sets of experiments were done. The spraying trials were done in TUT at the Laboratory of Materials Science.

6.1 Plasma spraying with dry ice blasting

In the first and second spraying trials, an IC 110-E dry ice blaster (Figure 28) by ICS Ice Cleaning Systems GmbH was used. The main unit consists of a dry ice tank, feeding system and control panel. It is a single-hose system so the dry ice is transported through an isolated hose at full pressure into the nozzle. The equipment is designed for manual cleaning operations but configuring the nozzle onto a robot arm was trivial. Multiple different nozzles are available depending on the application. [91]

Figure 28: IC 110-E (left) and IceBlast KG20 (right) dry ice blasters. [91][95]

In the third and final set of experiments another model was used due to a few unwanted features found in the IC 110-E. Firstly, the ice feed turned out to be slightly discontinuous and pulsating, especially with lower feed rates. Additionally the dry ice did not appear to exit the nozzle as pellets, but as a much finer dust. It is possible the pellets were crushed inside the machine prior to actually being injected into the hose.

IceBlast KG20 (Figure 28) by IceTech was the second machine used to get a second view of the process of dry ice blasting. This machine did appear to have a steadier dry ice feed even with low outputs and large dry ice pellets were visible even with the naked eye during blasting. Otherwise, it was similar to the IC-110 E being a single-hose system designed primarily for manual cleaning. Both machine specifications are presented in Table 7.

Table 7: Dry Ice Blaster specifications. [91][95]

	ICS IC-110 E	**IceBlast KG20**
Dimensions (L/W/H)	597x446x931 mm	480x520x850 mm
Empty weight	49 kg	58 kg
Dry ice capacity	17 kg	20 kg
Dry ice consumption	1-60 kg/h	16-55 kg/h
Blasting pressure	1-10 bar	2-10 bar
Air consumption	0,3-4,5 m^3/min	0,7-5,0 m^3/min

The thermal spraying equipment was an Oerlikon Metco F4-MB plasma torch with a radial powder feed, argon and hydrogen were used as plasma gases. The plasma gun and the dry ice blasting nozzle were both attached to a robot and the spraying was done on samples attached to a rotating drum. The plasma gun and blasting nozzle were aligned so that both the plasma gun and blasting nozzle were perpendicular to the sample drum. The vertical distance between the plasma plume centreline and the blasting nozzle exit was 25

mm while the blasting nozzle was positioned at a 25 mm distance from the substrate; the spraying setup is shown in Figure 29.

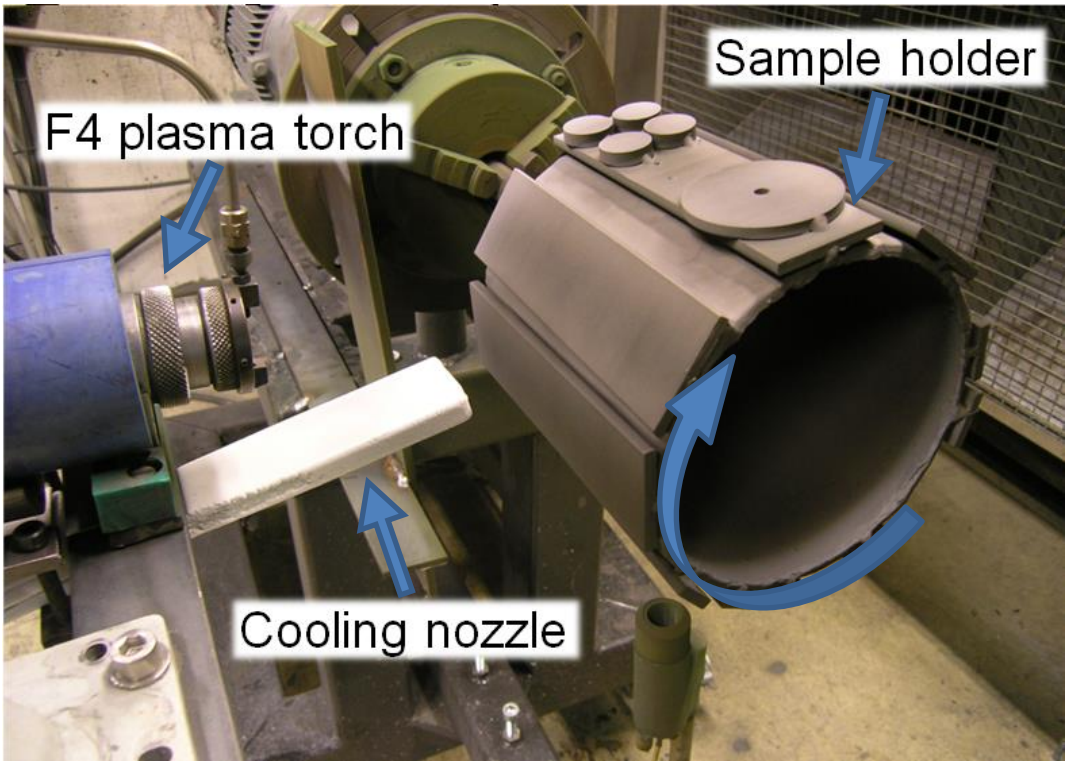

Figure 29: Spraying setup.

Table 8: Plasma spraying parameters

Parameter	**Value**
Powder	Amperit 704.001
Powder composition	Cr_2O_3
Powder size	-45+22 µm
Torch	F4
Current	630 A
Voltage	71,6 V
Power	45,108 kW
Ar	38 slpm
H_2	13 slpm
Carrier gas (Ar)	2,8 slpm
Spraying distance	130 mm
Holder speed	160 (& 100) RPM
Holder diameter	180 mm
Surface speed	90 (& 60) m/min
Forward speed	6 mm/rev

The plasma spraying parameters used for Cr_2O_3 are listed in Table 8, the same spraying parameters were used for all experiments. The powder used was a commercial Amperit 704.001 (99,5 % Cr_2O_3) from H.C. Starck with a reported particle size distribution of -45+22 µm (morphology in Figure 39). The bond coat found on a few samples was sprayed with Amperit 281 (Ni-5Al, -90+45 µm).

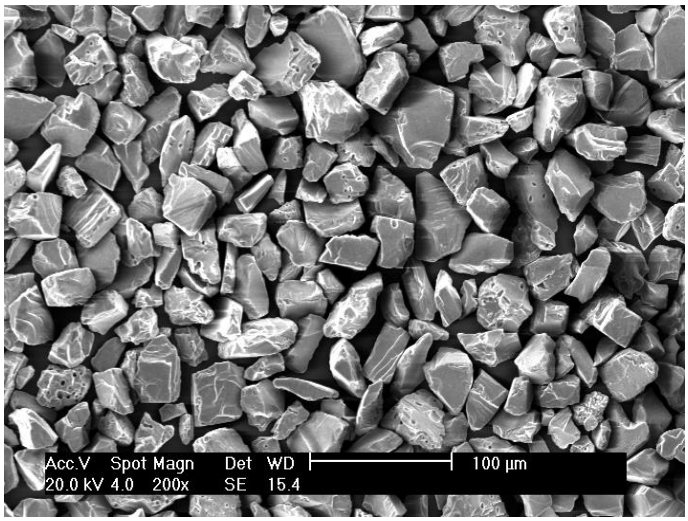

Figure 30: Amperit 704.001 Cr_2O_3 powder morphology (200x magnification).

In the first set, preheating (sample 2h) consisted of 4 passes with the plasma torch on without powder feed, dry ice pretreatment (sample 2i) was done similarly with the plasma jet and the dry ice blaster on. The sample holder rotational direction was also reversed for sample 2f to investigate whether the blasting should be before or after the plasma spray. The number of passes and the cooling parameters for the dry ice blasted samples are listed in Table 9. For reference, samples were made with air cooling utilizing the same nozzle as with dry ice blasting.

Table 9: First set of samples.

Sample	Spraying distance [mm]	Passes	Cooling type	Pressure [bar]	Pellet size [mm]	Feed rate [kg/h]	Other
1a	130	74	Air	6	-	-	Dry ice nozzle
1b	130	80	Air	6	-	-	Bond coat, 8 pass
2a	130	80	Dry ice	6	3	40	-
2b	130	80	Dry ice	6	3	30	-
2c	130	82	Dry ice	6	3	60	-
2d	130	51	Dry ice	6	1,5	40	-
2e	130	80	Dry ice	4	3	40	-
2f	130	80	Dry ice	4	3	40	Cooling after
2g	130	80	Dry ice	4	3	40	Bond coat, 8 pass
2h	130	80	Dry ice	4	3	40	Preheating, 4 pass
2i	130	80	Dry ice	4	3	40	Dry ice pretreatment, 4 pass

The second set of spraying trials was done with the same equipment in an identical setup as the first set, this time without a stone inside the nozzle. In addition to varying the cooling parameters, different spraying distances were also used; parameters are listed in Table 10. In addition to cooling with the same nozzle, a more spread out compressed air cooling was done with two compressed air nozzles located farther away from the sample holder.

Table 10: Second set of samples.

Sample	Spraying distance [mm]	Passes	Cooling type	Pressure [bar]	Pellet size [mm]	Feed rate [kg/h]	Other
0	110	60	Air	6	-	-	Spread out cooling
1c	110	60	Air	6	-	-	Dry ice nozzle
3a	130	61	Dry ice	4	3	40	
3b	110	60	Dry ice	4	3	40	
3c	110	60	Dry ice	4	1,5	40	
3d	110	60	Dry ice	3	3	40	
3e	110	60	Dry ice	3	3	60	
3f	90	60	Dry ice	4	3	40	
3g	90	60	Dry ice	4	3	40	Cooling after
3h	90	60	Dry ice	3	3	40	
3i	70	60	Dry ice	4	3	40	
3j	90	60	Dry ice	6	3	40	
3k	110	60	Dry ice	6	3	40	

The third and final set of samples was approached slightly differently, as a dry ice blaster of different make and model was used. Additionally, a slower surface speed was explored. All samples in the first and second set were sprayed with a holder speed of 160 RPM corresponding to a surface speed of 90 m/min. In addition to samples sprayed with 90 m/min surface speed a few samples were also made with a surface speed of 60 m/min (100 RPM). A slower surface speed results in higher surface temperatures, which were deemed beneficial due to auxiliary cooling. Overall, the dry ice blasting parameters were also adjusted lower than before. Parameters are listed in Table 11.

Table 11: Third set of samples

Sample	Spraying distance [mm]	Passes	Cooling type	Pressure [bar]	Pellet size [mm]	Feed rate [kg/h]	Other
0a	110	30	Air	6	-	-	90 m/min, spread out cooling
4a	110	40	Dry ice	4	3	40	60 m/min
4b	110	40	Dry ice	4	3	20	60 m/min
4c	110	40	Dry ice	2	3	20	60 m/min
4d	110	30	Dry ice	4	3	40	90 m/min
4e	110	30	Dry ice	2	3	20	90 m/min

All samples were sprayed on grit blasted low-carbon steel with a few pieces of stainless steel 316L for each set meant for cavitation test samples. In the first set the aim of each spraying was to do 80 passes, but due to human error or consumables running out mid process, the number varied slightly in a few samples. In the second set of samples 60 passes was deemed adequate due to higher thickness per pass. In the third set only 40 passes were made with 90 m/min surface speed and 30 passes with the slower 60 m/min surface speed.

6.2 Specimen preparation

Cross-section samples were prepared by cutting and sectioning with Discotom-10 cutting machine. After washing in the ultrasonic cleaner, the samples were mounted in epoxy under vacuum. The mounted samples were ground and polished with Phoenix 4000 semi-automatic grinding and polishing machine using SiC-foils and diamond suspensions, the detailed grinding and polishing parameters are presented in Table 12.

Table 12: Cross-section sample grinding and polishing parameters.

Surface	Suspension	Lubricant	Load (N)	Time (min)
SiC 200	-	water	30	1 *)
MD-Largo	Allegro Largo 9 µm	-	35	5
MD-Largo	Largo 3 µm	-	30	5
MD-Dac	Dac 3 µm	-	25	5
MD-Nap	Nap ¼ µm	-	20	5

*) Repeat step when necessary to expose the entire cross section.

In addition to the cross section samples, other sample pieces were also cut and prepared for surface hardness measurements and wear testing. Surface hardness and cavitation test samples were ground by hand with Struers Piano diamond grinding discs and polished with Dac 3 µm diamond suspension to a mirror finish. Dry-sand rubber wheel test and erosion test samples were ground up to a P1000 finish with the same Piano discs.

6.3 Research methods

This subchapter presents the research methods used within the scope of this thesis including process monitoring and different sample analysis methods. All studies were in TUT with the equipment at the Laboratory of Materials Science.

6.3.1 Dry ice particle measurements

Oseir HiWatch imaging system was used to characterize the stream of dry ice particles during blasting. The system is composed of a pulsing diode laser that illuminates particles

in an 8,94 mm by 6,69 mm area, which are then detected and recorded by the camera. The software simultaneously analyses the imaged particles for size and velocity. The measurements were done with the IC 110-E on two occasions, with (set 1) and without (set 2) the stone lodged inside the nozzle and once with the IceBlast KG20 (set 3).

6.3.2 Surface temperature monitoring

The surface temperature was monitored during spraying utilizing an Omega OS37-20-K infrared thermocouple and an Amprobe TMD-56 multilogger thermometer. The thermocouple was positioned beneath the sample holder and aimed at the centre. The temperature was logged at one second intervals and saved for later analysis.

6.3.3 Microstructural characterization

Cross section samples were imaged first with a Leica DM 2500 optical microscope for a preliminary study of the microstructures, a more detailed microstructural analysis was done with a Philips XL-30 scanning electron microscope (SEM), both secondary electron (SE) and back-scattering electron (BSE) images were obtained. Prior to SEM imaging, the polished samples were gold sputter coated for conductivity.

An image analysis was also conducted on 500x magnification SEM BSE images to calculate the average porosity of the different samples. ImageJ-software was used to apply a threshold on the image to produce a binary black and white image differentiating the cracks and pores from the solid material; subsequently the software calculated the amount of black in the image.

6.3.4 Hardness testing and surface roughness measurements

Vickers hardness measurements were taken with Matsuzawa MMT-X7 micro hardness tester from the cross section samples as well as from polished coating surfaces. Cross section hardness was tested with 300 gf (HV0.3), surface hardness test load ranged from 25 gf (HV0.025) to 1000 gf (HV1). Surface roughness was measured from as sprayed sample plate surfaces using a Mitutoyo Surftest SJ-301 portable surface roughness tester, R_a, R_y and R_z values were obtained.

6.3.5 Wear testing

The dry-sand rubber wheel test is an adaptation of the ASTM G65 "Standard Test Method for Measuring Abrasion Using the Dry Sand/Rubber Wheel Apparatus" [93], setup shown in Figure 31. The equipment consists of a rotating rubber coated steel drum, 5 sample holders that apply the contact load and sand hoppers that feed sand between the rotating wheel and the sample surface. Samples are 20x50 mm in size and are ground to a P1000 level finish to minimize effect of varying surface roughness, 3 pieces per sample are tested. The load per sample for ceramic coatings is 13 N. Sand hoppers are calibrated to feed sand at a rate of 20-30 g/min per sample, the sand is quartz with a particle size of 0,1-0,6 mm. The test is run 12 min at a time for a total time of 60 min. After each 12 min set the samples are removed, cleaned with pressurized air and weighed. The samples spend each 12 min test in a different holder to mitigate any variation caused by different holders. Drum diameter is 550 mm and it is rotating at 60 RPM resulting in a total distance of 6220 m traversed for each sample.

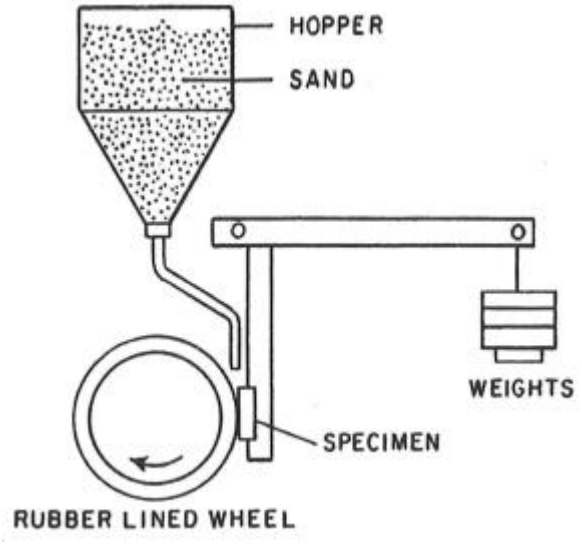

Figure 31: Schematic diagram of the rubber wheel test apparatus, adapted from [93].

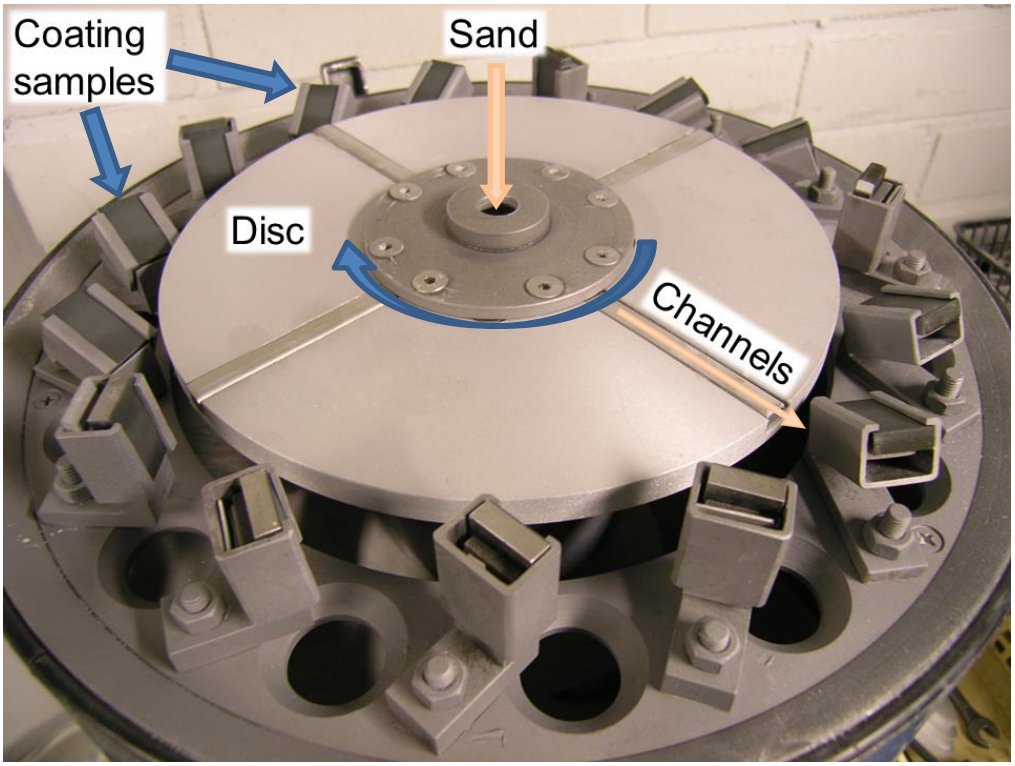

Figure 32: Solid particle erosion tester.

The centrifugal solid particle erosion tester consists of a sand funnel placed above a spinning disc and sample holders positioned around said disc (Figure 32), the disc and sample holders are enclosed during the test. The sand flows from the funnel into the centre hole of the spinning disc where it is accelerated by the centrifugal force and propelled outwards through the channels built into the disc. The sand impacts on the samples positioned at various angles, 30˚ and 90˚ angles were used here, 3 pieces per sample per angle were tested. Samples are 20x15 mm in size, are ground to a P1000 finish and weighed before and after testing. The discs speed is 3000 RPM and a total of 3 kg of sand was used during each test, the sand is the same as in the rubber wheel tests.

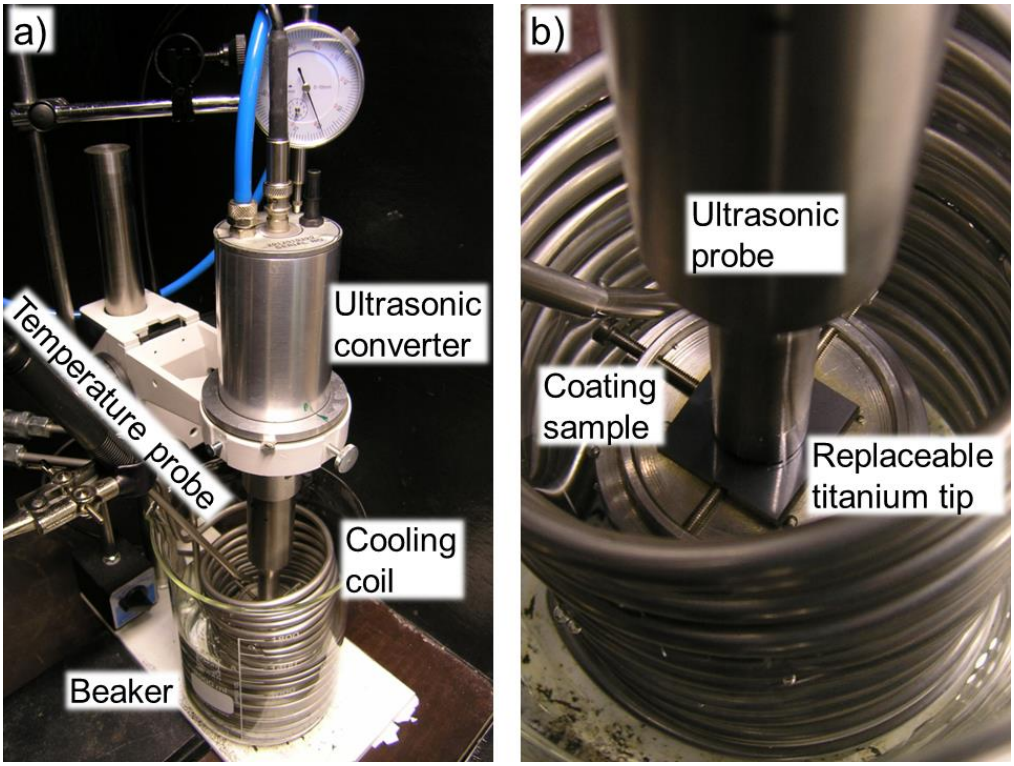

Figure 33: a) Cavitation test setup b) Sample close-up

The cavitation erosion test used at TUT complies to the ASTM G32 "Standard Test Method for Cavitation Erosion Using Vibratory Apparatus" [94]. The test utilizes a VCX-750 ultrasonic vibrator, which functions with a frequency of 20 kHz and maximum power of 750 W, the horn or velocity transformer is made of titanium alloy Ti-6Al-4V with a replaceable round tip with 15,9 mm in diameter. Amplitude is set to 50 µm. The test setup uses a stationary sample holder immersed in the beaker in de-ionized water with a mirror polished sample (25x25 mm) fixed onto the holder (Figure 33). The tip of the horn is lowered to a distance of 0,5 mm to the sample surface; water level is kept 15 mm above the test sample surface. A water cooling/heating-unit and coil are used to maintain the water temperature at 25±2 ˚C. The samples were cleaned with ethanol, dried properly and weighed at set intervals; the total test time for the chromia coatings was 90 min.

6.3.6 Adhesion tests

Adhesion tests were done according to ASTM C633 "Standard Test Method for Adhesion or Cohesion Strength of Thermal Spray Coatings" [92]. Coatings were sprayed on steel discs with a diameter of 25 mm. The backside of the discs and the mating surfaces of the test rods were grit blasted for gluing. Sample discs were placed between two rods with FM1000 Adhesive Film between the opposing surfaces. They were assembled in V-groove jigs and pressure was applied on the sample and rods to prevent misalignment during epoxy curing. The jigs were placed in an oven for 2 h at 180 ˚C.

After oven curing and cooling, the samples were removed from the jigs and excessive glue was removed by grinding with SiC-papers or scraped off with a sharp knife. The samples were tested with Instron 1185 tensile testing machine until failure occurred. The peak tensile load was recorded and the bond strength was calculated by dividing the load with the sample surface area. Four specimens per sample were tested.

6.3.7 Gas permeability measurements

The gas permeability measurements were carried out via the pressure drop method on samples sprayed on porous metal disc substrates. The samples were placed inside a chamber with insulating seals; the coated side was then pressurized with nitrogen to various pressures while the non-coated side would remain at atmospheric pressure. The pressure on the coated side was then recorded along with the gas flow rate on the other side of the sample. From the gathered data, the permeability k (m^2) of the coating is calculated with the Darcy's law [96]:

$$Q = k\frac{A\Delta P}{\eta e} \tag{1}$$

where Q is the air flow rate (m^3/s), A is the cross sectional area of the sample (m^2), ΔP is the pressure drop (Pa), η is the air kinematic viscosity (Pa*s) (in this case of nitrogen) and e is the coating thickness (m).

7. RESULTS

The results of the process monitoring and sample analysis are presented in this chapter.

7.1 Dry ice particle in-flight properties

All measurements were taken at a 25 mm distance from the nozzle exit (blasting distance) to measure the particle properties at moment of impact. A lower feed of 20 kg/h was used to make the imaging clearer. Set numbers indicate which spraying set the measurements correspond to: set 1 indicates the clogged nozzle, set 2 clear nozzle and set 3 with another dry ice blaster.

Table 13: HiWatch results

Set	Blaster model	Pressure [bar]	Particle velocity [m/s]	Pellet size [mm]	Average particle size [µm]	Maximum particle size [µm]
1	ICS 110-E	6	184,6	3	20,9	28,8
1	ICS 110-E	4	115,4	3	21,1	34,8
2	ICS 110-E	5	222,8	3	21,8	56,1
2	ICS 110-E	4	197,0	3	21,7	43,8
2	ICS 110-E	4	199,0	1,5	21,8	59,1
2	ICS 110-E	3	150,2	3	21,7	59,8
3	IceBlast KG20	4	156,1	3	22,9	126,4
3	IceBlast KG20	2	78,7	3	23,0	158,7

The particle velocity is not a direct average value as the data was scattered very unevenly. Instead, a histogram was formed from the velocity data, a Gaussian curve was fitted and the highest peak was chosen as the value that best represents the particle velocity. This should mitigate the effect of the faster and smaller particles. The achieved particle velocities are all quite high in relation to what the modelling results [58] indicated. This can however be explained with the different nozzle and dry ice feed configurations of the blasters used in this study and by Dong et al.

Judging by the measured average particle sizes, it would appear that the equipment is not ideal for measuring dry ice blasting. In all cases, some of the pellets will be crushed and pulverized as they travel through the hose to the nozzle; hence, the stream will be full of fine dry ice dust. The software seems to mainly register the fine dust excluding most of the actual pellets as irregularities. Due to the limited imaging area (8,94 mm x 6,69 mm)

and low imaging depth, it would actually be challenging to capture and image particles larger than 1 mm even with the right parameters.

The minimum measured particle size ranged from 13 µm to 16 µm but the real differences lie in the maximum particle size. The clogged nozzle effect is best visible in the maximum particle size as removing the blockage nearly doubles the maximum size from 34 µm to 59 µm. The even greater difference between the maximum particle size of the two blasters is probably due to the differences in the feeding systems. During the IceBlast KG20 measurements, individual pellets could be seen raining down after they had hit the spraying booth wall, similar observations were not made during the IC 110-E measurements.

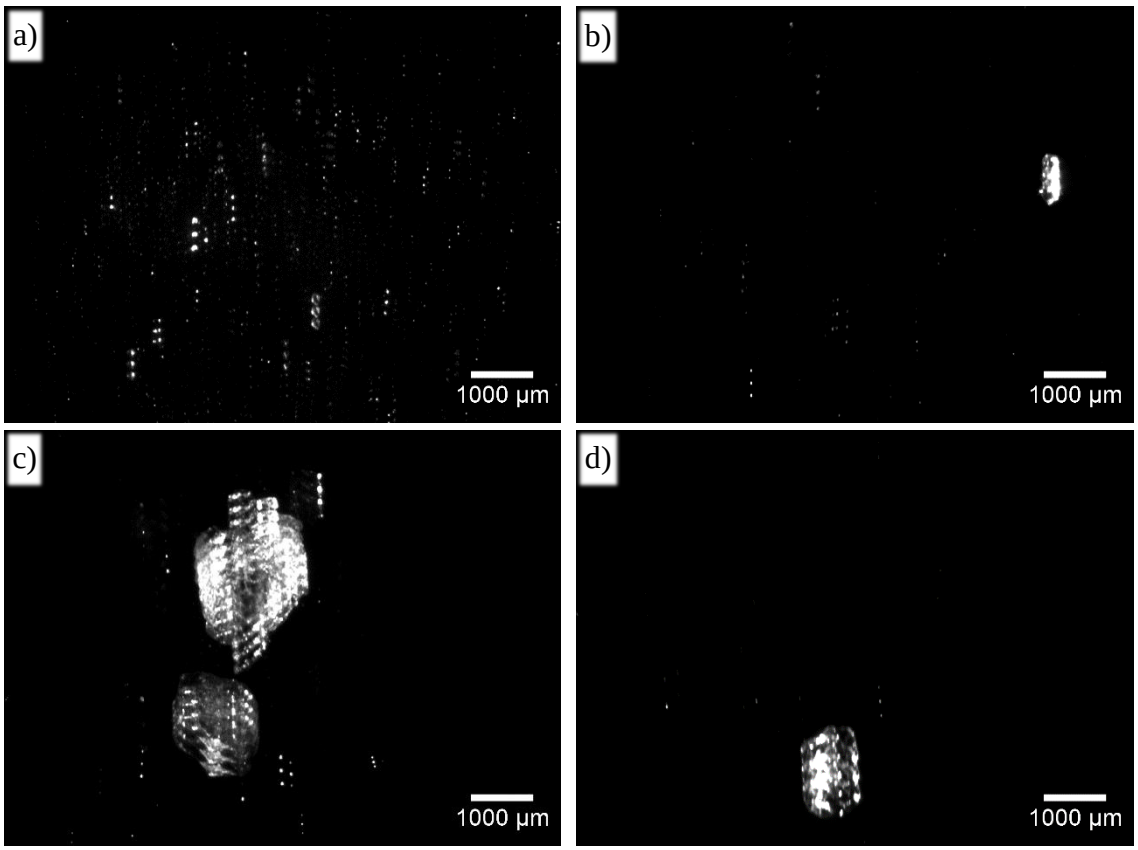

Figure 34: Largest particles found in the IC 110-E (a, b) and in the IceBlast KG20 (c, d) images. Particle diameters: a) 102 µm, 143 µm, b) 333 µm, c) 1804 µm, 1388 µm, d) 944 µm.

The HiWatch software captures images during the measurements and going through these images manually revealed significantly larger particles in the KG20 blasting stream that the software did not measure due to their size and image overlap (Figure 34). It must be noted however that images like these were few in numbers. The images of the IC 110-E measurements were also browsed but even with the greater number of measurements and images, no particles quite as large were found amongst them.

7.2 Surface temperature

It was noted during spraying that the temperature readings from the thermocouple were unusually low. At the end of spraying, the temperature was checked with a handheld infrared thermometer. It turned out that the handheld thermometer often gave a reading twice as high as the thermocouple when the sample holder was noticeably warmer than room temperature (>50 ˚C). Due to the thermocouple and thermometer not being calibrated according to the surface being measured, the temperature readings recorded were lower than the actual temperature by a great margin. All temperatures were however recorded with the same configuration and should therefore be comparable even if the absolute values are unreliable. The surface temperature graphs are presented below.

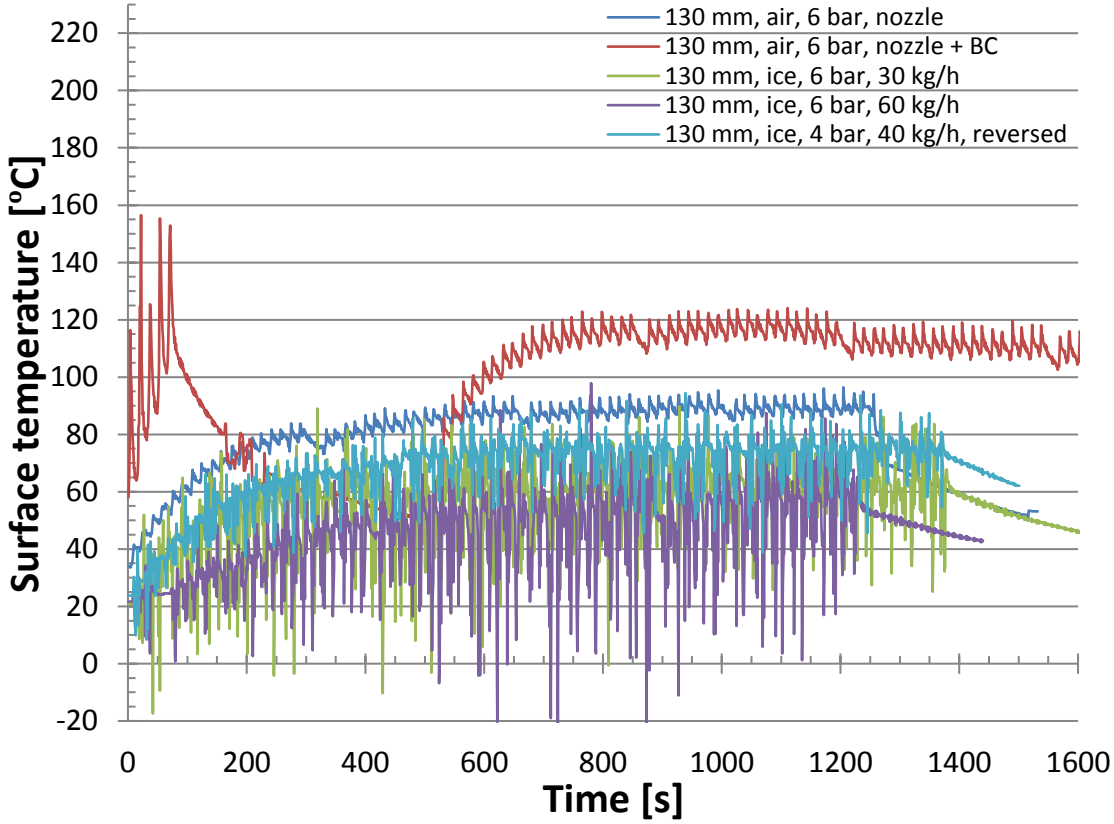

Figure 35: Surface temperatures of select samples with 130 mm spraying. (1st set)

At 130 mm distance (Figure 35), the temperature remained much steadier with air cooling as indicated by the smaller fluctuation of the two curves. 6 bar dry ice blasting has the greatest fluctuation with the 30 kg/h running slightly hotter than the 60 kg/h. 4 bar blasting with the reversed rotation averages slightly higher than the 6 bar samples being very close to the other 4 bar blasted samples (Figure 36).

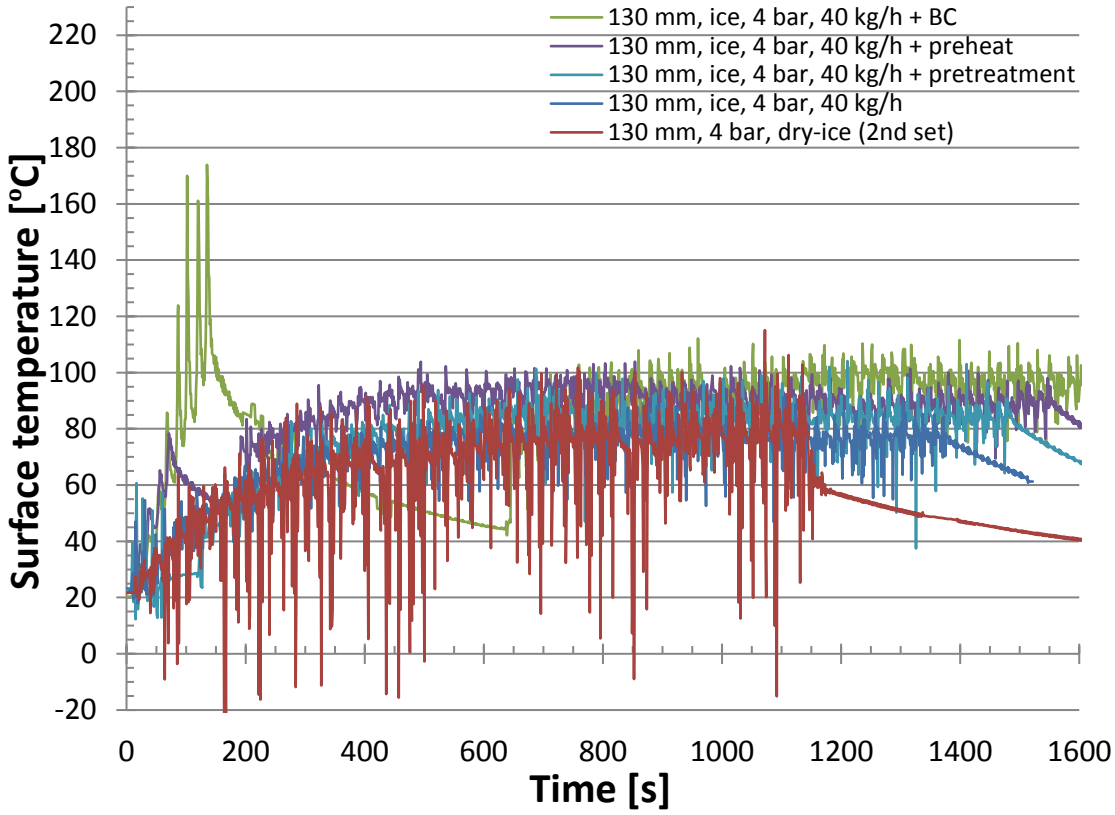

Figure 36: Surface temperatures of samples with 130 mm spraying distance and 4 bar blasting pressure. (1st set)

In the other 4 bar blasted samples (Figure 36) there was only slight differences in the average temperature resulting from the pretreatments while the temperature fluctuation is quite similar. The only differing sample is the one sprayed during the second set without the clogged nozzle, due to an uninterrupted flow the cooling seems to have been more efficient resulting in slightly lower temperature and significantly more fluctuation in temperature.

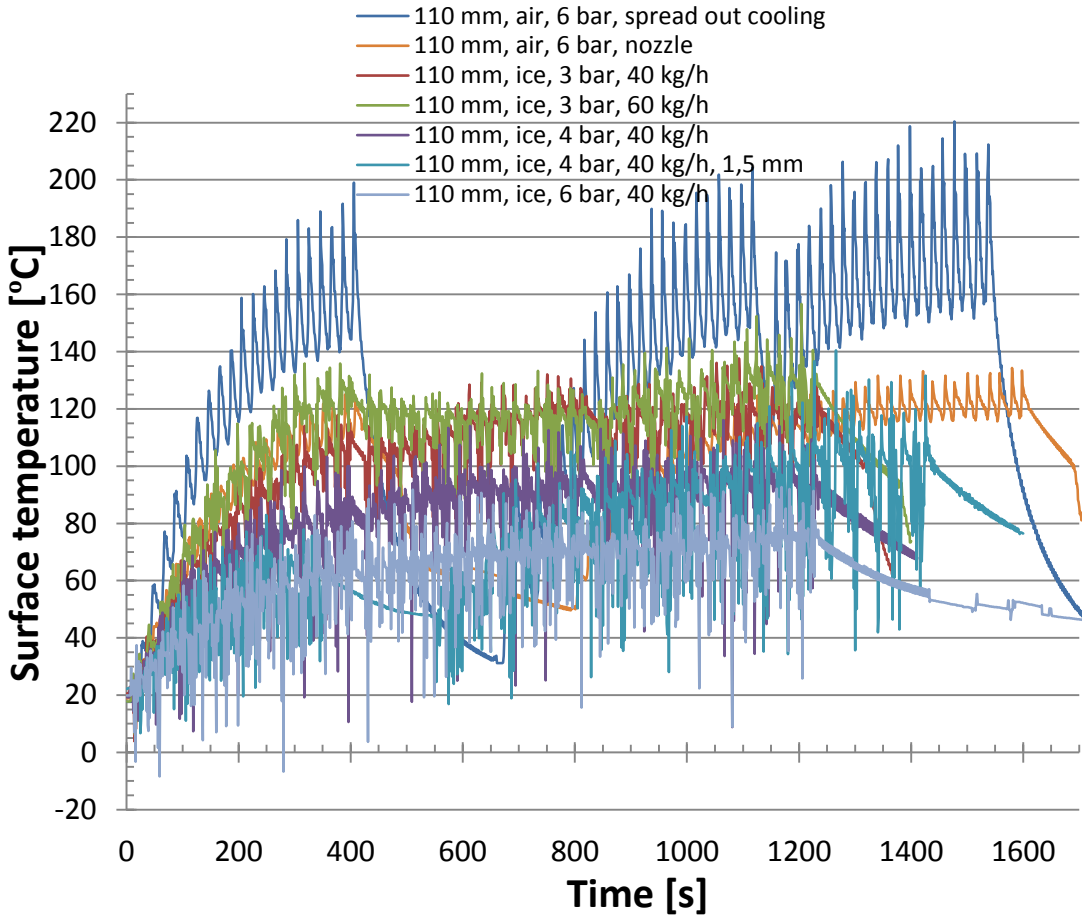

Figure 37: Surface temperatures of samples with 110 mm spraying distance. (2nd set)

Compared to the 130 mm samples the ones sprayed at 110 mm (Figure 37) have a higher average temperature as would be expected. As with the 130 mm samples, the air-cooled sample had the least fluctuation. The spread out air cooling however seemed to be quite ineffective as it had much larger temperature fluctuations and higher overall temperature. 3 bar dry ice blasting resulted in slightly higher temperatures than air cooling but also in a bit more fluctuation. Raising the blasting pressure drops the average temperature but also increases fluctuation.

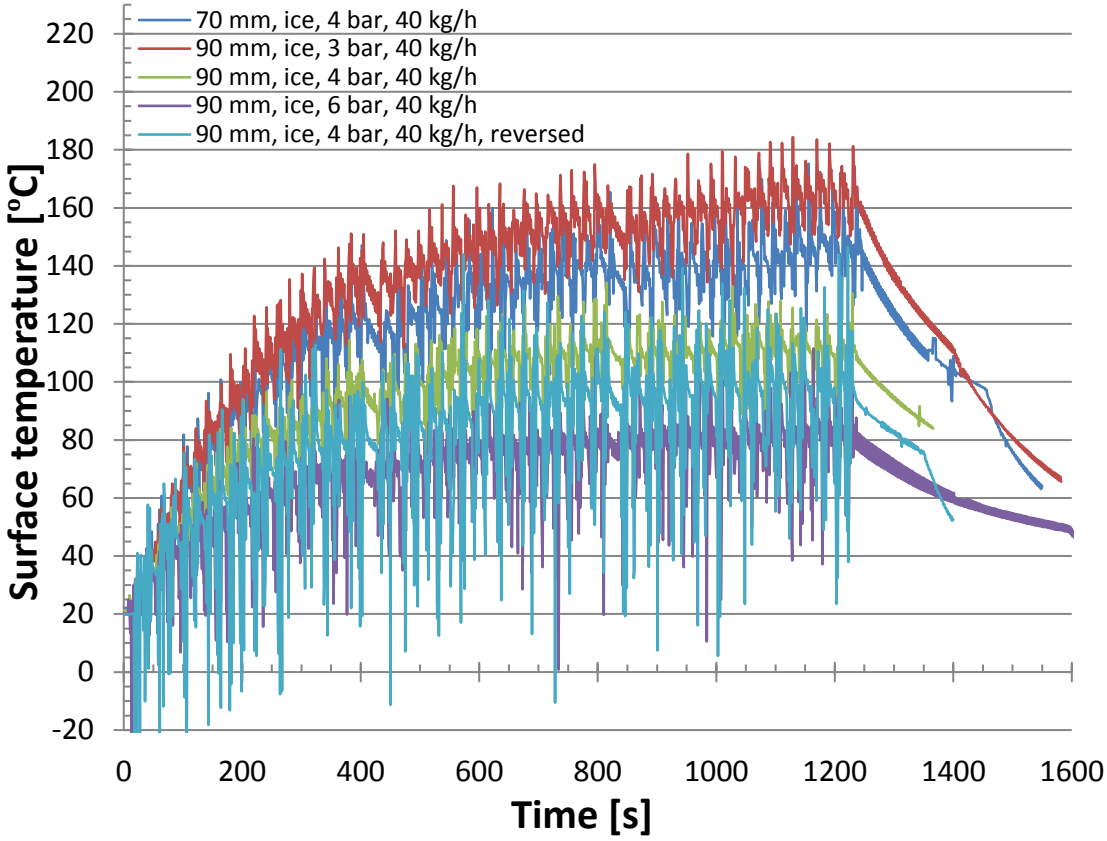

Figure 38: Surface temperatures of samples with 70-90 mm spraying distance. (2nd set)

By shortening the spraying distance to 90 mm and 70 mm, the surface temperature rises noticeably and as concluded earlier higher blasting pressures result in lower temperatures (Figure 38). Overall, the fluctuation of the curves is on the same level. However, with the reversed rotation the temperature fluctuation seems to increase drastically being even worse than with the 6 bar blasted sample.

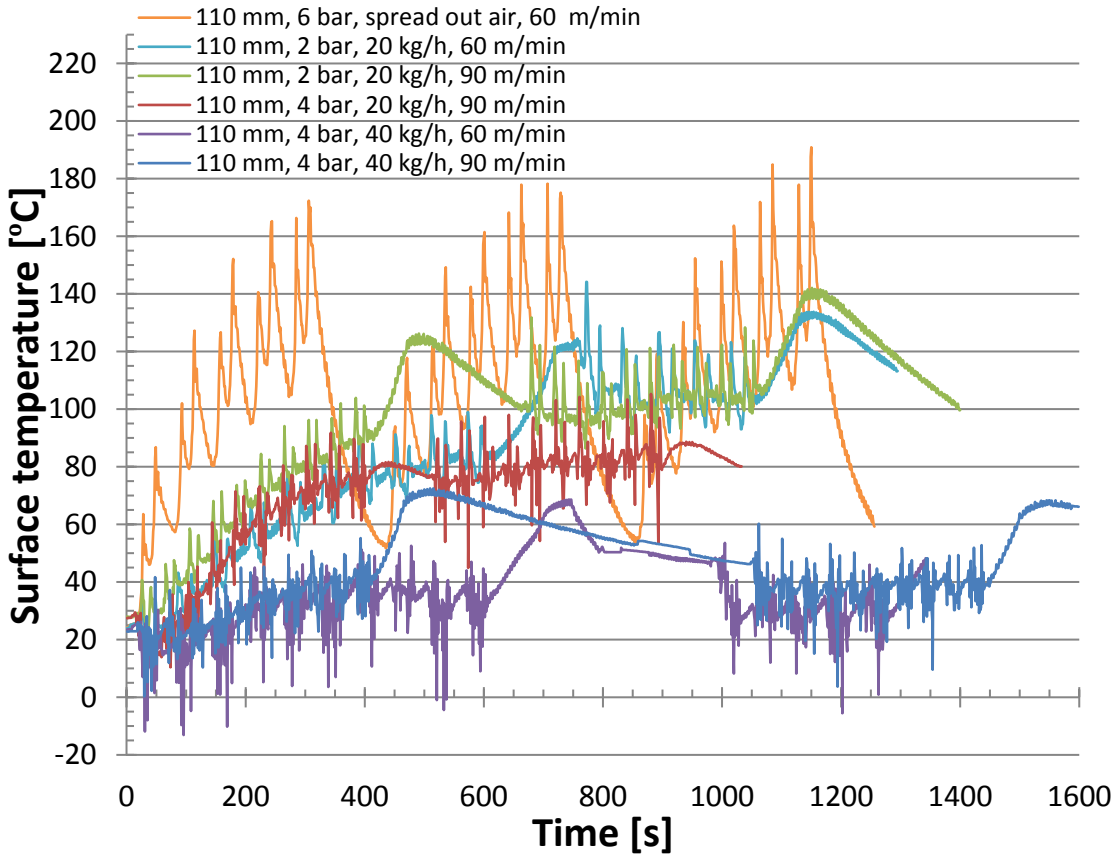

Figure 39: Surface temperatures of samples with 110 mm spraying distance blasted with IceBlast KG20. (3rd set)

The curves from the third spraying trials look slightly different (Figure 39) as a different dry ice blaster was used but also the amount of passes is different. As with the previous 110 mm sprayed samples the spread out air cooling was the least effective with quite noticeable temperature fluctuation. Compared to the previous 110 mm dry ice blasted sample curves the temperatures appear to be lower with similar blasting parameters. A curious feature in all the dry ice blasted sample curves is the temporary increase in surface temperature during the breaks and at the end of spraying. One possibility for this could be that this blaster cooled the surface very superficially while the spray gun heated it throughout, upon removal of the plasma and blaster the temperature begun to even out on the surface.

7.3 Microstructure

All of the coatings from both spraying sets initially appeared quite similar under the optical microscope with a clear lamellar structure and some porosity; further SEM studies did however reveal slight differences. All samples from the first spraying set presented with rather pronounced splat boundaries regardless of cooling method, although air-cooled samples (Figure 40 and 41) did appear denser than dry ice blasted samples (Figure

42) as can be seen from the SEM images and from the average porosities listed in Table 14. Overall, the porosity numbers are relatively high mainly due to the highly pronounced splat boundaries. While the visible boundaries are not true voids or pores, they still indicate poor cohesion.

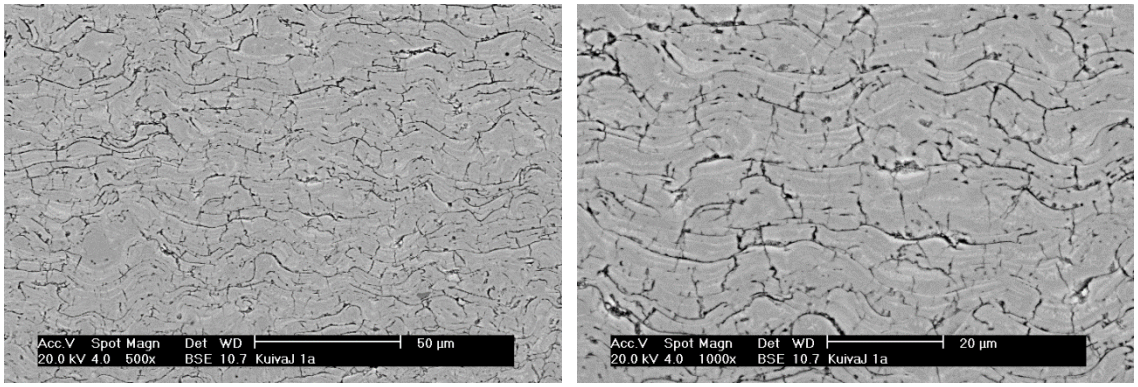

Figure 40: Sample 1a: 130 mm, air, 6 bar, nozzle (500x and 1000x magnification)

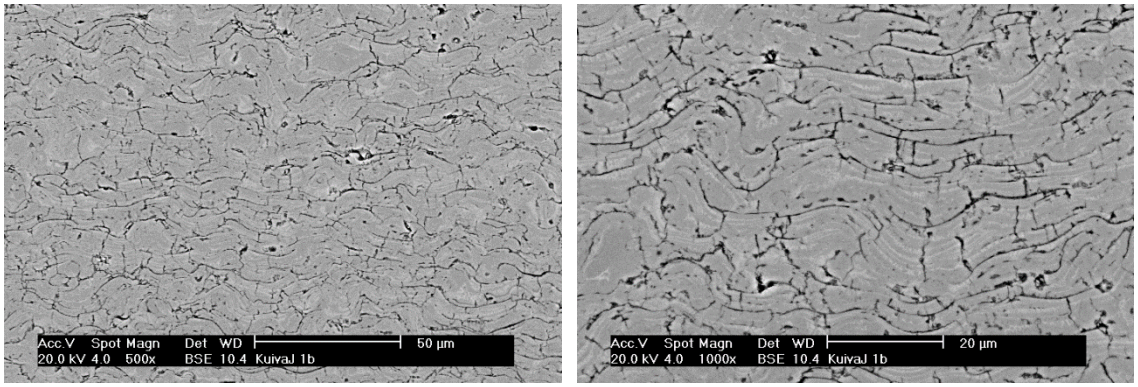

Figure 41: Sample 1b: 130 mm, air, 6 bar, nozzle + BC (500x and 1000x magnification)

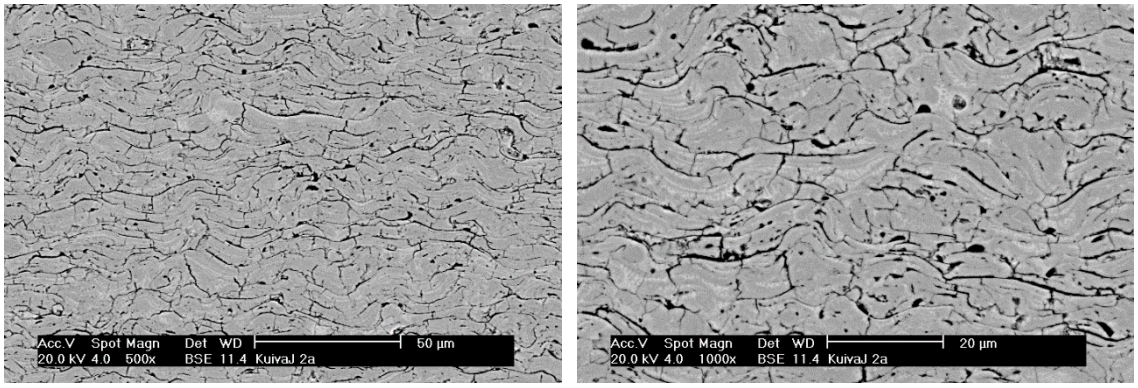

Figure 42: Sample 2a: 130 mm, ice, 6 bar, 40 kg/h (500x and 1000x magnification)

Table 14: Average prosities of the 1st set.

Sample	Cooling	Average porosity	Stddev
1a	130 mm, air, 6 bar, nozzle	9,0 %	0,6 %
1b	130 mm, air, 6 bar, nozzle + BC	10,5 %	0,2 %
2g	130 mm, ice, 4 bar, 40 kg/h + BC	15,0 %	0,3 %
2h	130 mm, ice, 4 bar, 40 kg/h + preheat	14,9 %	0,5 %
2i	130 mm, ice, 4 bar, 40 kg/h + pretreatment	15,9 %	0,3 %
2e	130 mm, ice, 4 bar, 40 kg/h	15,0 %	1,4 %
2b	130 mm, ice, 6 bar, 30 kg/h	15,0 %	0,0 %
2a	130 mm, ice, 6 bar, 40 kg/h	13,2 %	0,1 %
2d	130 mm, ice, 6 bar, 40 kg/h, 1,5 mm pellet	16,7 %	0,9 %
2c	130 mm, ice, 6 bar, 60 kg/h	15,4 %	0,0 %
2f	130 mm, ice, 4 bar, 40 kg/h, reversed	12,4 %	0,7 %

In the second spraying set, the cooling method and the spraying distance had the most effect on the microstructure. The reference sample 0 with the spread out air cooling (Figure 43) appears slightly more cohesive than sample 1c (Figure 44) with the nozzle applied air cooling, sample 0 also had the second lowest measured porosity (6,7 %) in this set (Table 15). Dry ice blasted samples with the same spraying distance appear relatively identical in microstructure.

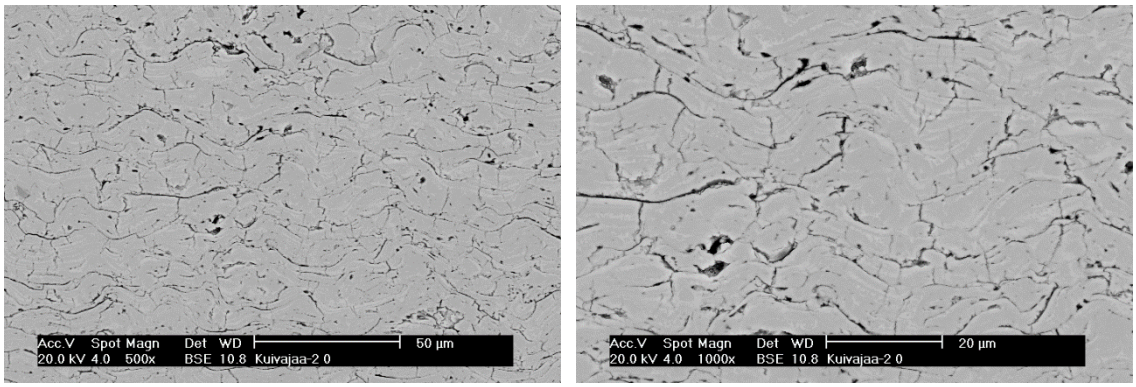

Figure 43: Sample 0: 110 mm, air, 6 bar, spread out cooling (500x and 1000x magnification)

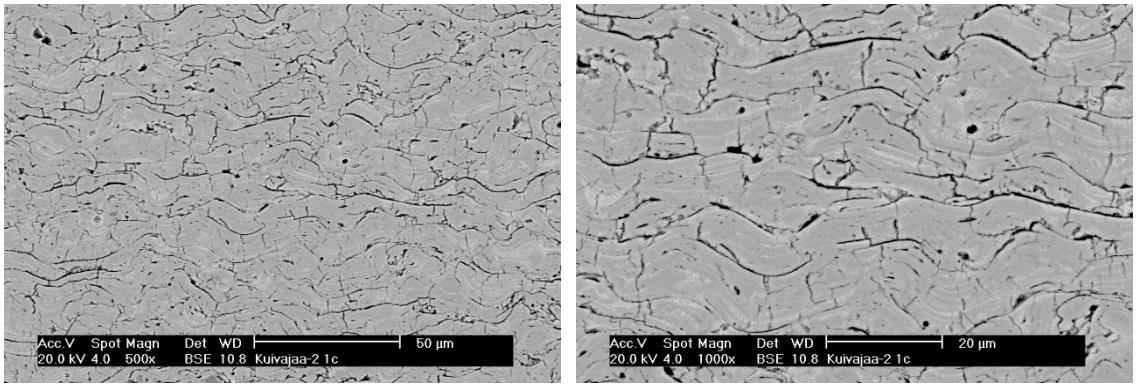

Figure 44: Sample 1c: 110 mm, air, 6 bar, nozzle (500x and 1000x magnification)

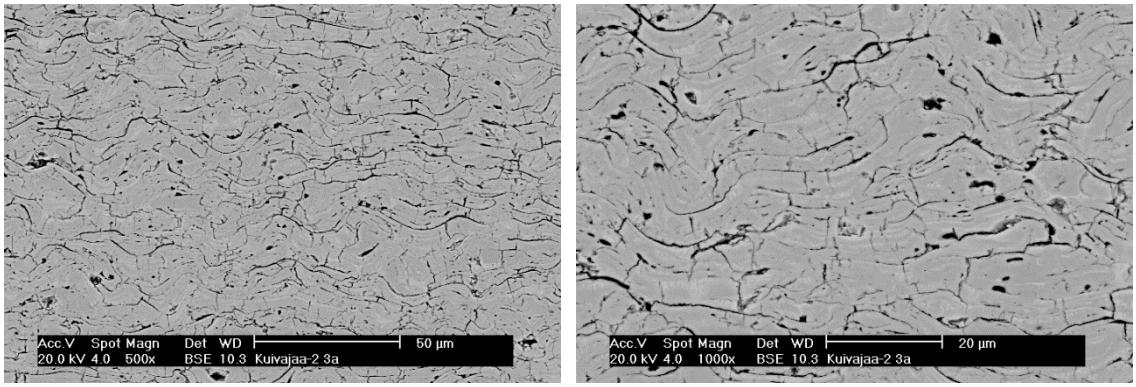

Figure 45: Sample 3a: 130 mm, ice, 4 bar, 40 kg/h (500x and 1000x magnification)

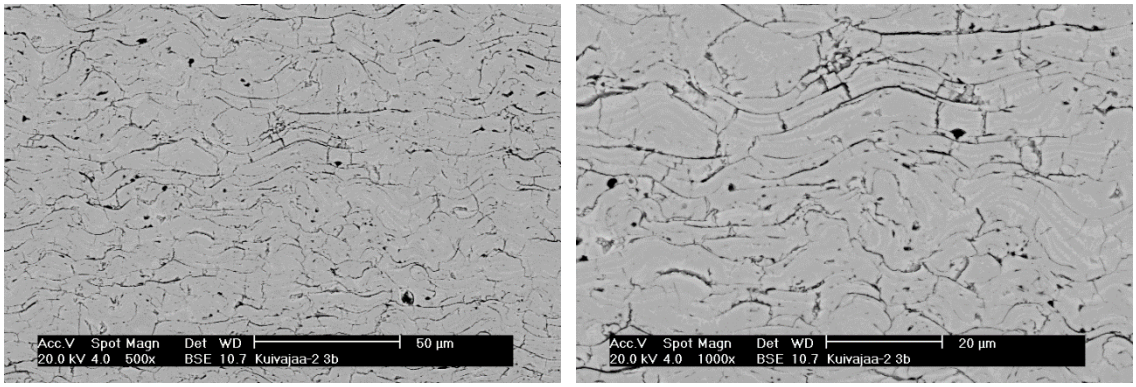

Figure 46: Sample 3b: 110 mm, ice, 4 bar, 40 kg/h (500x and 1000x magnification)

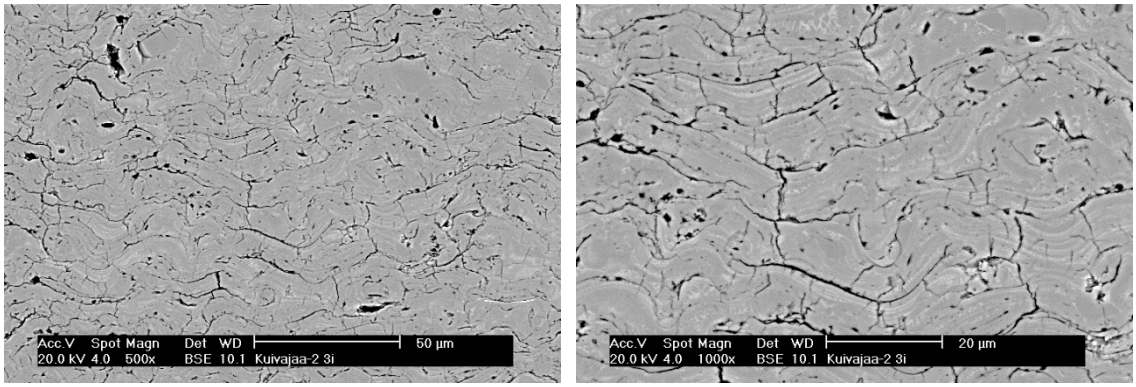

Figure 47: Sample 3i: 70 mm, ice, 4 bar, 40 kg/h (500x and 1000x magnification)

Table 15: Average porosities of the 2nd set.

Sample	Cooling	Average porosity	Stddev
3i	70 mm, ice, 4 bar, 40 kg/h	8,7 %	0,2 %
3h	90 mm, ice, 3 bar, 40 kg/h	7,5 %	0,1 %
3f	90 mm, ice, 4 bar, 40 kg/h	9,4 %	1,1 %
3j	90 mm, ice, 6 bar, 40 kg/h	9,5 %	1,2 %
0	110 mm, air, 6 bar, spread out cooling	6,7 %	0,0 %
1c	110 mm, air, 6 bar, nozzle	8,1 %	0,1 %
3d	110 mm, ice, 3 bar, 40 kg/h	7,8 %	0,2 %
3e	110 mm, ice, 3 bar, 60 kg/h	8,2 %	0,1 %
3b	110 mm, ice, 4 bar, 40 kg/h	6,1 %	0,5 %
3c	110 mm, ice, 4 bar, 40 kg/h, 1,5 mm	8,2 %	0,2 %
3k	110 mm, ice, 6 bar, 40 kg/h	8,7 %	0,1 %
3a	130 mm, ice, 4 bar, 40 kg/h	9,2 %	0,1 %
3g	90 mm, ice, 4 bar, 40 kg/h, reversed	8,2 %	0,2 %

Comparing samples sprayed from 130 mm (3a, Figure 45) and 110 mm (3b, Figure 46) it appears that the longer spraying distance decreases bonding between splats as can be seen in the images and in the porosity percentages (9,24 % vs. 6,08 %). Meanwhile there is little difference between samples sprayed from 110 mm and 90 mm. The sample sprayed from 70 mm (3i, Figure 47) however has a slightly more irregular structure with larger well-bonded areas as well as some grainy unmelted regions.

The samples of the third and final spraying set exhibit quite similar structures as the samples from the previous sets with porosity numbers also on the same level. Once again, the air-cooled sample (0a, Figure 48) appears the most cohesive with the least pronounced splat boundaries and a porosity percentage in the lower range, though sample 4e (Figure 49) was not much more porous either (Table 16).

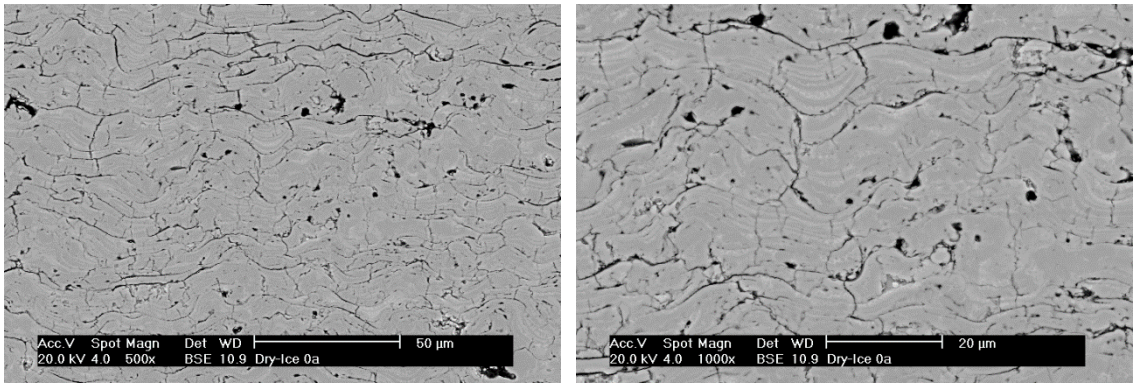

Figure 48: Sample 0a: 110 mm, air, 6 bar, spread out cooling, 60 m/min (500x and 1000x magnification)

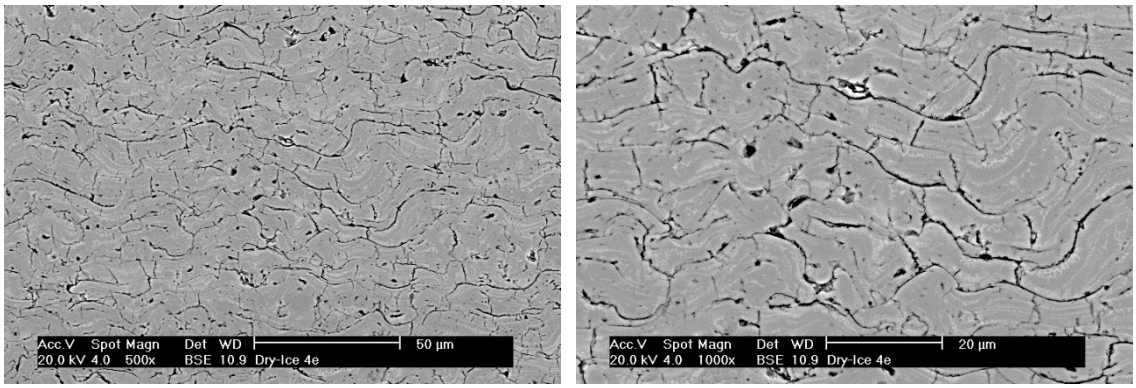

Figure 49: Sample 4e: 110 mm, ice, 2 bar, 20 kg/h, 60 m/min (500x and 1000x magnification)

Table 16: Average porosities of the 3rd set

Sample	Cooling	Average porosity	Stddev
0a	110 mm, air, 6 bar, spread out cooling, 60 m/min	7,1 %	0,1 %
4e	110 mm, ice, 2 bar, 20 kg/h, 60 m/min	8,6 %	0,4 %
4c	110 mm, ice, 2 bar, 20 kg/h, 90 m/min	8,6 %	0,2 %
4b	110 mm, ice, 4 bar, 20 kg/h, 90 m/min	10,0 %	0,0 %
4d	110 mm, ice, 4 bar, 40 kg/h, 60 m/min	9,0 %	0,2 %
4a	110 mm, ice, 4 bar, 40 kg/h, 90 m/min	9,6 %	0,0 %

With the dry ice blasted samples, the same trend is repeated with lower blasting pressures producing coatings that appear cohesive. Samples with identical blasting parameters but different surface speeds do not show any great differences in the images nor in the porosity results.

7.4 Thickness & surface roughness

Coating thickness and surface roughness measurements are presented in Tables 17-19. In the first set a bit higher deposition efficiency was achieved with 4 bar dry ice and 6 bar air cooling, while a decrease was observed with 6 bar dry ice treatment. Highest deposition efficiency of 7,7 µm/pass was realized in the second set at the 70 mm spraying distance (3i). The deposition efficiency observed at 90 mm and 110 mm seems to be on the same level above 6 µm/pass, but deposition efficiency under 6 µm/pass was observed in a few samples indicating that a smaller pellet size (3c), a longer spraying distance of 130 mm (3a), a higher blasting pressure (3k) or a reversed drum rotation (3g) are somewhat detrimental. The higher surface speed (90 m/min) samples of the third set have similar deposition efficiency levels as earlier samples. In the other third set samples the slower surface speed (60 m/min) naturally produces thicker coatings per pass.

Table 17: Coating thickness and surface roughness values of 1st set samples.

Sample	Cooling	Passes	Thickness [µm]	Thickness/ pass [µm]	Ra [µm]	Ry [µm]	Rz [µm]
1a	130 mm, air, 6 bar, nozzle	74	421	5,7	3,3	24,6	21,1
1b	130 mm, air, 6 bar, nozzle + BC	80	439	5,5	3,7	28,1	22,0
2g	130 mm, dry ice, 4 bar, 40 kg/h + BC	80	424	5,3	3,5	26,4	22,3
2h	130 mm, dry ice, 4 bar, 40 kg/h + preheating	80	390	4,9	3,7	25,6	22,1
2i	130 mm, dry ice, 4 bar, 40 kg/h + pretreatment	80	402	5,0	3,4	25,4	21,1
2e	130 mm, dry ice, 4 bar, 40 kg/h	80	396	5,0	3,4	26,5	21,7
2b	130 mm, dry ice, 6 bar, 30 kg/h	80	352	4,4	3,4	26,8	21,8
2a	130mm, dry ice, 6 bar, 40 kg/h	80	312	3,9	3,2	23,8	20,0
2d	130 mm, dry ice, 6 bar, 40 kg/h, 1,5 mm pellet	51	195	3,8	3,2	24,4	20,1
2c	130 mm, dry ice, 6 bar, 60 kg/h	82	344	4,2	3,6	25,0	20,6
2f	130 mm, dry ice, 4 bar, 40 kg/h, reversed	80	406	5,1	3,2	24,4	21,0

Table 18: Coating thickness and surface roughness values of 2nd set samples.

Sample	Cooling	Passes	Thickness [µm]	Thickness/ pass [µm]	Ra [µm]	Ry [µm]	Rz [µm]
3i	70 mm, dry ice, 4 bar, 40 kg/h	60	459	7,7	27,8	155,1	155,1
3h	90 mm, dry ice, 3 bar, 40 kg/h	60	389	6,5	4,9	32,8	28,0
3f	90 mm, dry ice, 4 bar, 40 kg/h	60	404	6,7	4,7	34,5	27,8
3j	90 mm, dry ice, 6 bar, 40 kg/h	60	377	6,3	3,8	28,7	23,9
0	110 mm, air, 6 bar, spread out cooling	60	401	6,7	3,7	26,1	22,3
1c	110 mm, air, 6 bar, nozzle	60	387	6,4	3,6	25,4	22,2
3d	110 mm, dry ice, 3 bar, 40 kg/h	60	390	6,5	3,7	27,0	23,2
3e	110 mm, dry ice, 3 bar, 60 kg/h	60	392	6,5	3,6	28,2	22,4
3b	110 mm, dry ice, 4 bar, 40 kg/h	60	366	6,1	3,5	24,8	21,4
3c	110 mm, dry ice, 4 bar, 40 kg/h, 1,5 mm	60	320	5,3	3,6	26,3	22,1
3k	110 mm, dry ice, 6 bar, 40 kg/h	60	333	5,6	3,4	24,2	20,8
3a	130 mm, dry ice, 4 bar, 40 kg/h	61	351	5,7	3,3	23,9	20,7
3g	90 mm, dry ice, 4 bar, 40 kg/h, reversed	60	329	5,5	4,2	28,9	24,3

Table 19: Coating thickness and surface roughness values of 3rd set samples.

Sample	Cooling	Passes	Thickness [µm]	Thickness/ pass [µm]	Ra [µm]	Ry [µm]	Rz [µm]
0a	110 mm, air, 6 bar, spread out cooling, 60 m/min	30	288	9,6	4,7	36,5	33,0
4e	110 mm, ice, 2 bar, 20 kg/h, 60 m/min	30	323	10,8	4,8	39,0	32,9
4c	110 mm, ice, 2 bar, 20 kg/h, 90 m/min	40	262	6,5	4,6	36,6	32,5
4b	110 mm, ice, 4 bar, 20 kg/h, 90 m/min	40	213	5,3	4,3	33,6	29,8
4d	110 mm, ice, 4 bar, 40 kg/h, 60 m/min	30	274	9,1	4,3	32,1	29,9
4a	110 mm, ice, 4 bar, 40 kg/h, 90 m/min	40	214	5,4	4,2	33,0	28,9

The first set samples had a uniform surface quality with all R_a, R_y and R_z having only slight variation. The second set exhibited some differences in surface quality, the sample sprayed at 70 mm (3i) having a very rough bumpy texture with the highest R_a value of 27,8 µm. Most samples had an R_a value below 4 µm but samples sprayed at 90 mm with lighter cooling had slightly higher values at 4,9 µm and 4,7 µm. The third set had slightly higher surface roughness values between 4 µm to 5 µm with lower values favouring the more heavily dry ice blasted samples.

7.5 Hardness

Even though the cohesion between splats appeared weak in the SEM images, high hardnesses were achieved. Most samples from the first set were in the range of 1100-1200 HV with a couple samples going above 1300 HV. The highest hardness of 1385 HV was achieved with dry ice blasting at a pressure of 4 bars. The hardness test results are presented in Figure 50, ordered primarily by auxiliary cooling pressure.

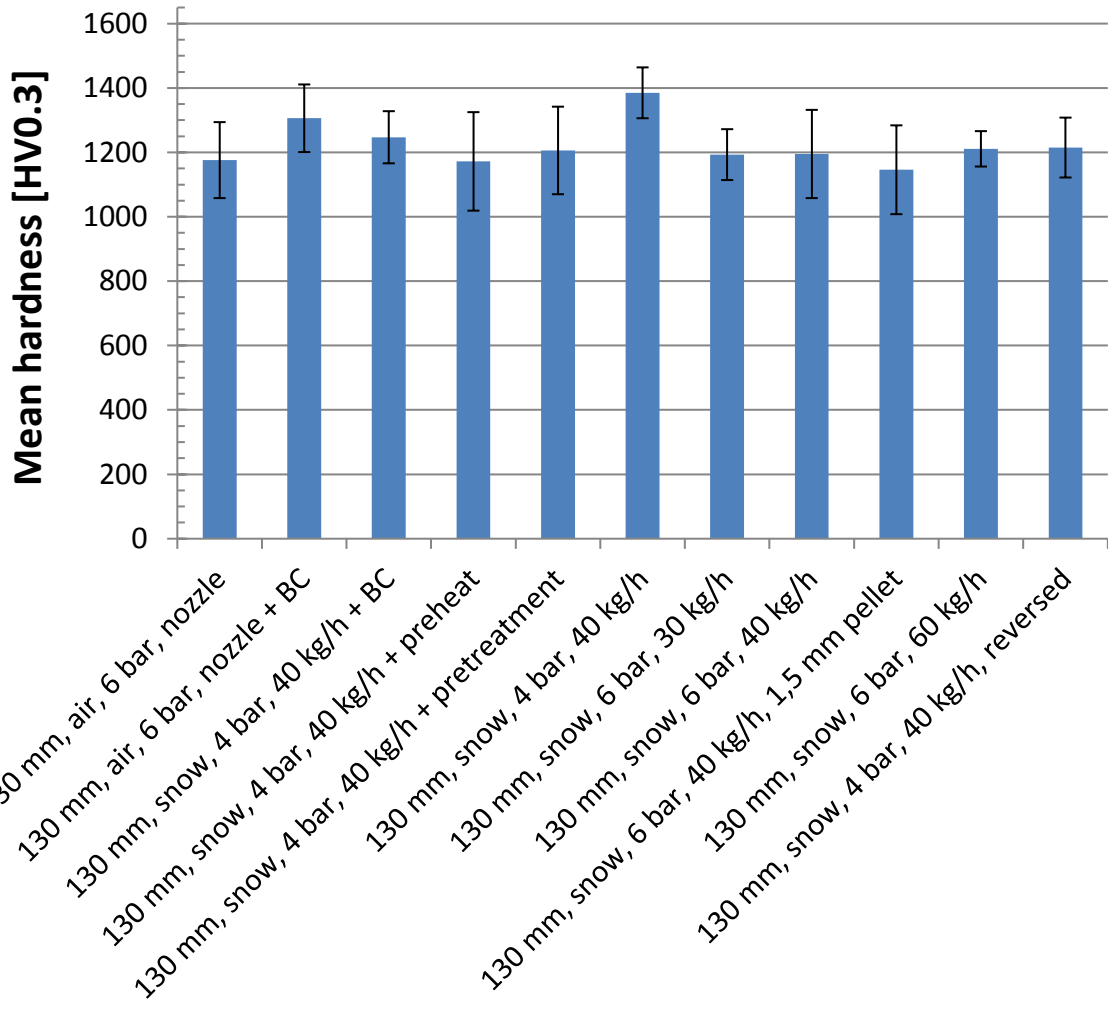

Figure 50: Cross-section hardnesses, 1st spraying set

On average, the hardnesses of the second set were higher than the first, although so was the standard deviation in the results (Figure 51). The highest hardness of 1469 HV was measured from the sample sprayed at 70 mm. In general, samples sprayed at 70 mm and 90 mm had slightly higher hardnesses around 1400 HV.

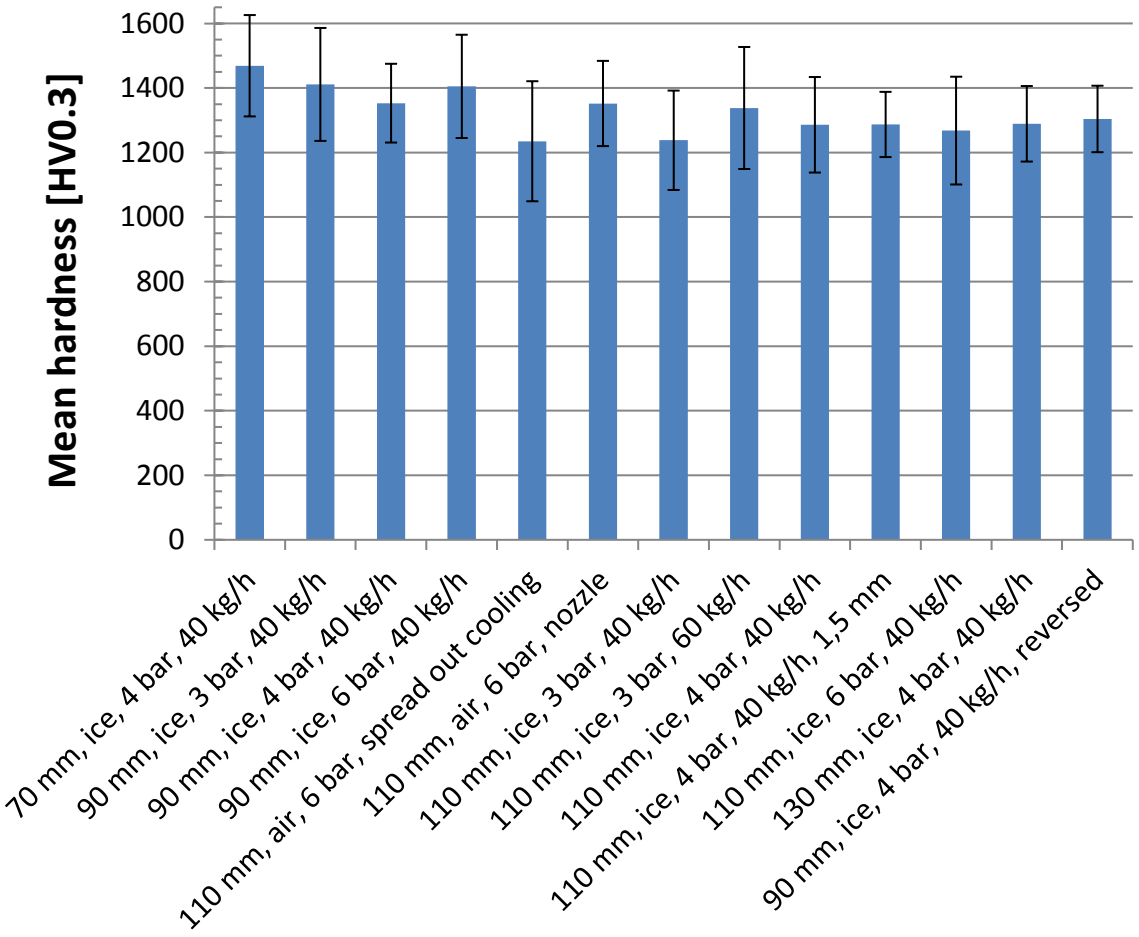

Figure 51: Cross-section hardnesses, 2nd spraying set

The third set samples maintained the same hardness levels (1200-1400 HV) as the previous set; it also followed a similar trend as the second set linking hotter processes to higher hardnesses (Figure 52). The slower surface speed may indeed be favourable as the air-cooled sample was 100 HV harder than the equivalent sample made with faster surface speed in the previous set. In addition, the slow surface speed 2 bar blasted sample had the highest average hardness (1482 HV) out of all the samples.

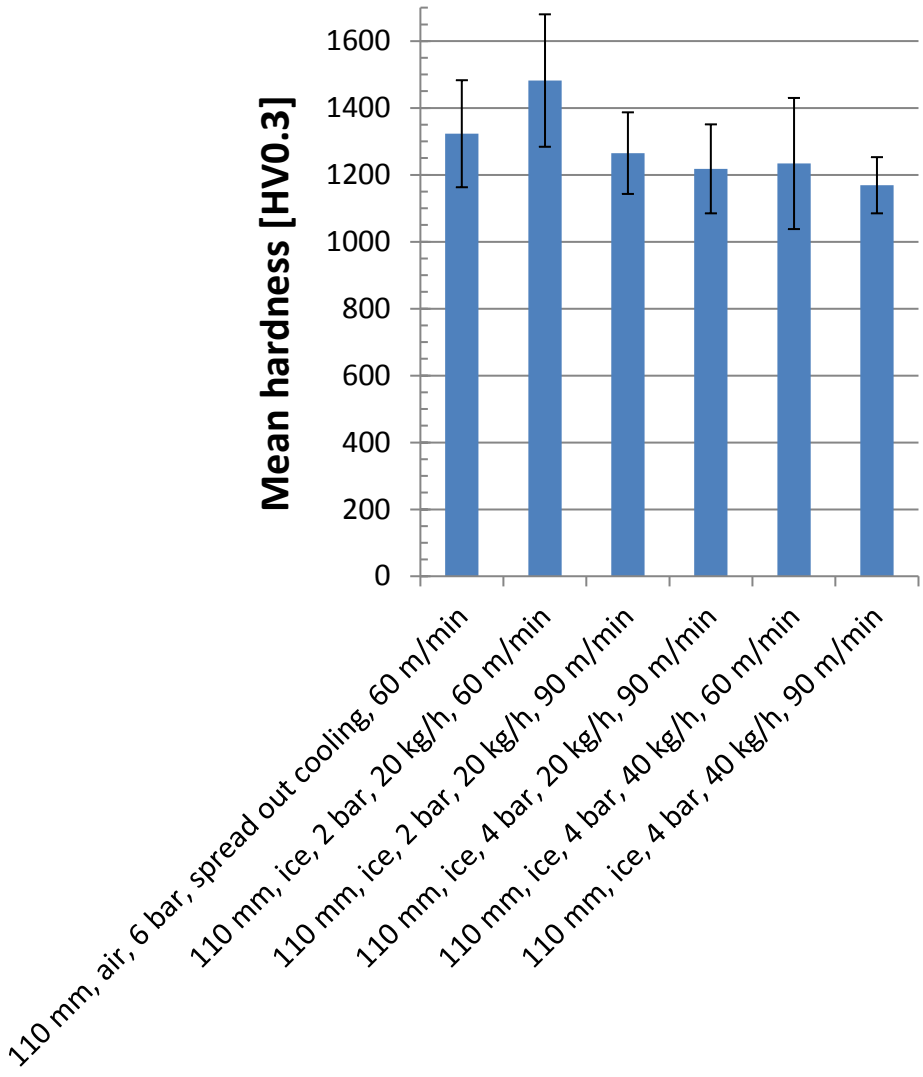

Figure 52: Cross-section hardnesses, 3rd spraying set

In addition to the cross-section hardness discussed above, surface hardness was also measured from the first (Figure 53) and second (Figure 54) set samples with varying loads from 25 gf to 1000 gf. In both sets the measured hardness values grouped up relatively tight. Overall, first set had slightly lower hardness than the second. Just as with the hardness values measured from the cross-sections, the connection between parameters and hardness is not very clear.

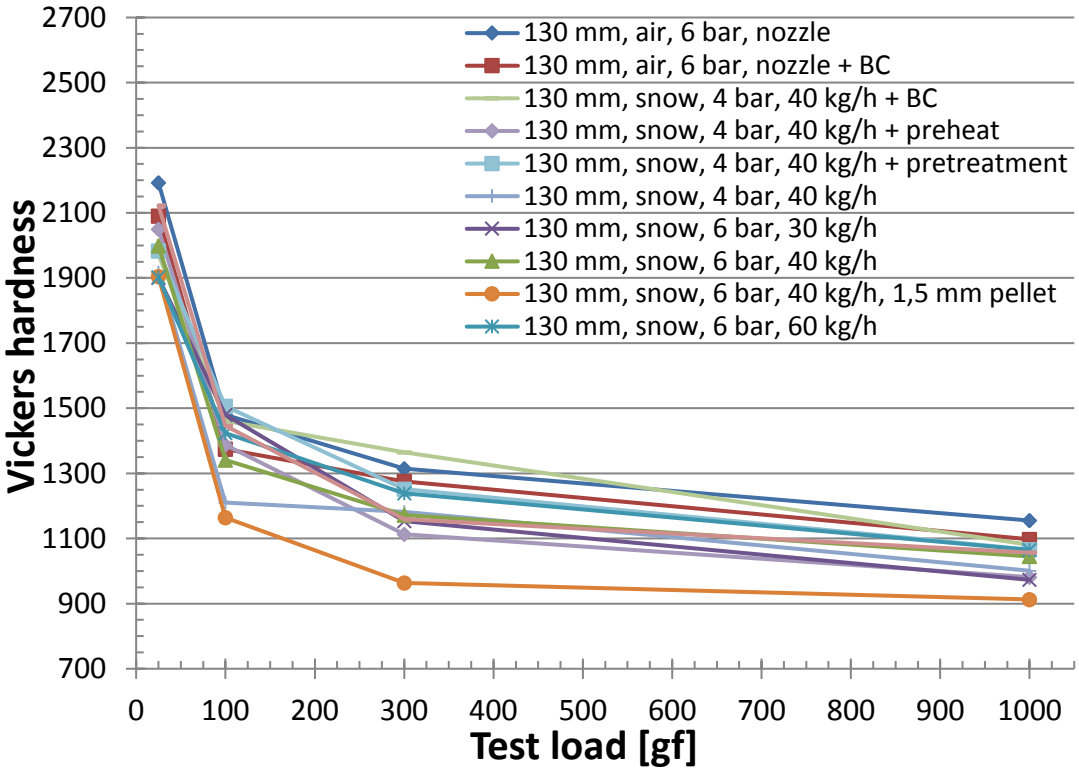

Figure 53: Surface hardness, measured with varying loads, 1st spraying set

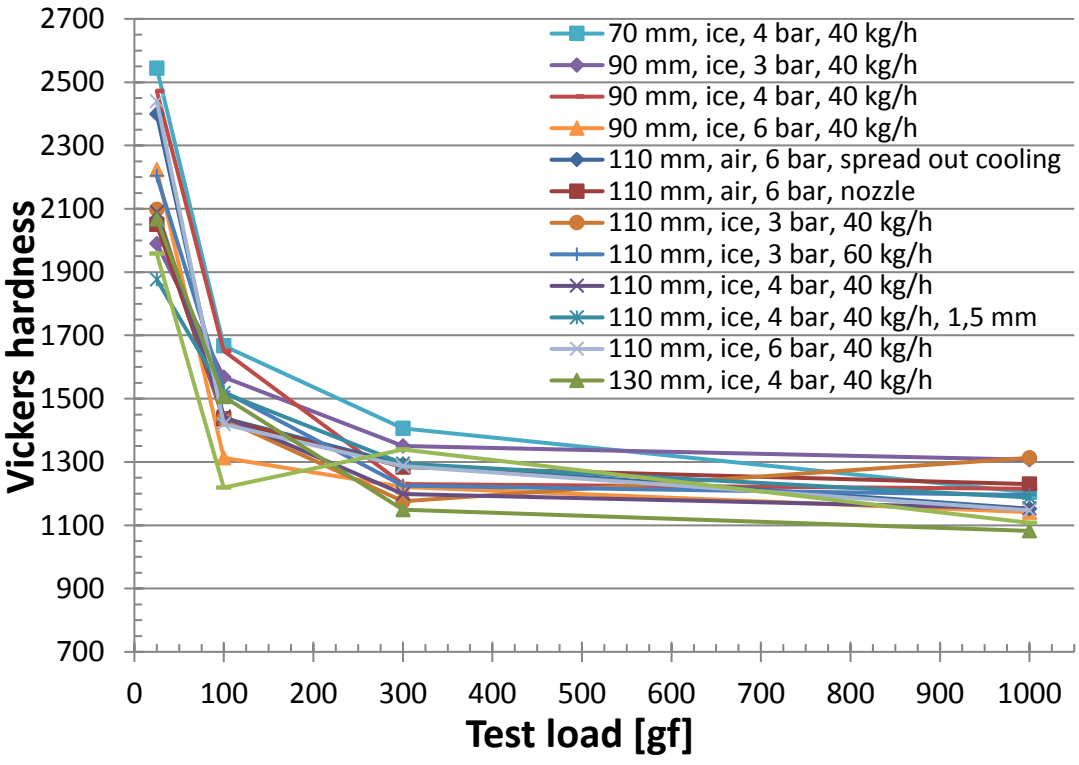

Figure 54: Surface hardness, measured with varying loads, 2nd spraying set

The smaller the load is the smaller the measured area is. In a thermal sprayed coating consisting of splats, the small indentations are able to fit inside single splats therefore measuring the hardness of the microstructure. With larger indents, cracks and splat interfaces start having an effect on the hardness reading providing a hardness reading closer to the bulk value. The curves shown above clearly indicate that the microstructures that form are very hard but the crack networks and poor splat cohesion weaken the overall structure greatly in all of the samples.

7.6 Abrasion resistance

In the first set, the air-cooled samples had the lowest wear, which is to be expected given the long spraying distance. Out of the dry ice blasted samples the lower 4 bar pressure yielded the least wear (Figure 55). The slightly thinner coating made with 1,5 mm pellets wore out during testing and is represented by a striped column.

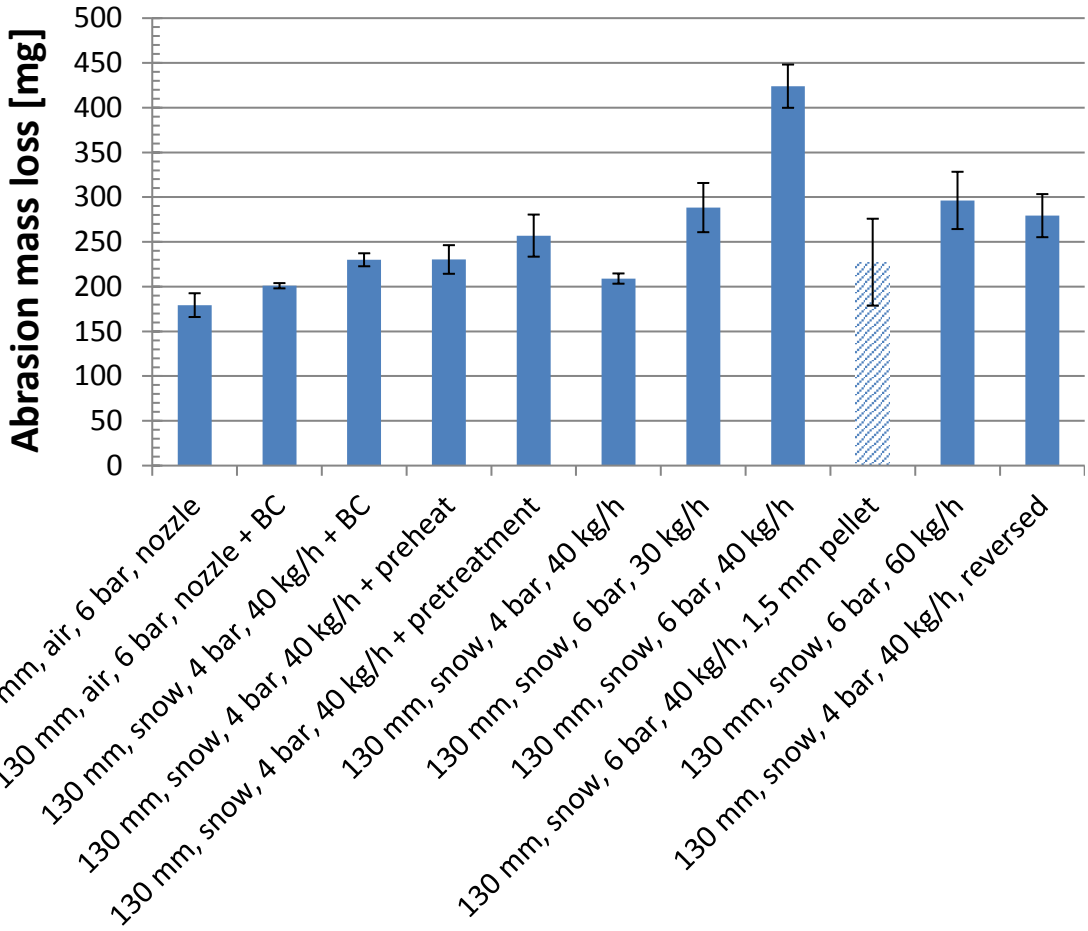

Figure 55: Abrasion test results, 1st spraying set, worn out sample represented by striped column.

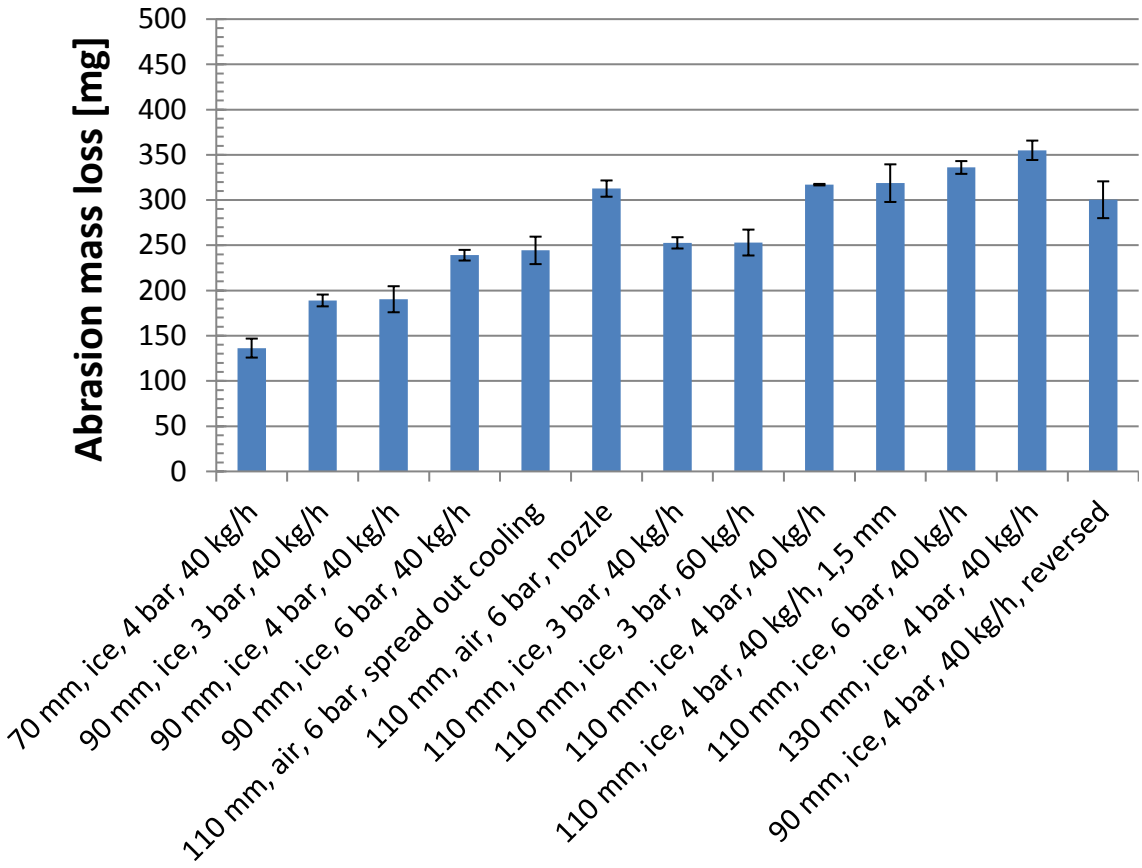

Figure 56: Abrasion test results, 2nd spraying set.

In the second set (Figure 56) there appears to be a relatively good correlation between wear resistance, spraying distance and cooling intensity. Lower spraying distances produce coatings that are more wear resistant and with the same spraying distance lower cooling pressure seems to be better or at least have no negative effect. In both sets the reversed rotation direction, meaning that the cooling nozzle comes right after spray deposition, seems to decrease wear resistance compared to samples sprayed with the normal rotation direction with the same parameters.

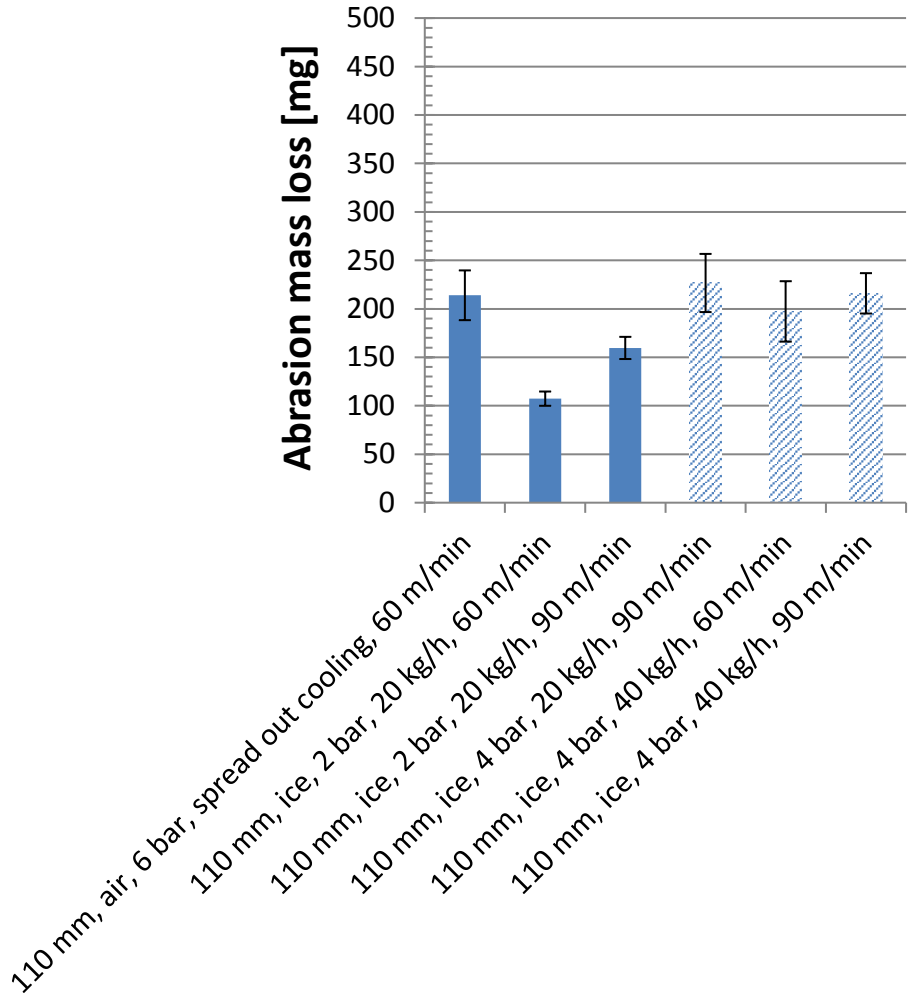

Figure 57: Abrasion test results, 3rd spraying set, worn out samples represented by striped columns.

As with the first set, the samples that wore out are represented by striped columns, compared to the second set the wear masses of the third set (Figure 57) are roughly on the same levels. As with the hardness results, the slower surface speed of 60 m/min comes across as more wear resistant out of the air-cooled samples from the second and third set with different surface speeds. Also the lowest mass loss of 107 mg amongst all samples was achieved with the 60 m/min surface speed and 2 bar, 20 kg/h dry ice blasting, also the same blasting parameters with 90 m/min resulted in the overall third best coating.

7.7 Erosion resistance

In erosion wear, it is typical for ceramic coatings to wear most with a straight particle impact angle (90˚) than with a lower inclination [97] as seen in the results below. Overall, the erosion results (Figures 58 and 59) are very similar to the abrasion results, there is a slight dependency between erosion resistance, cooling intensity and spraying distance, which is clearer with the second set samples.

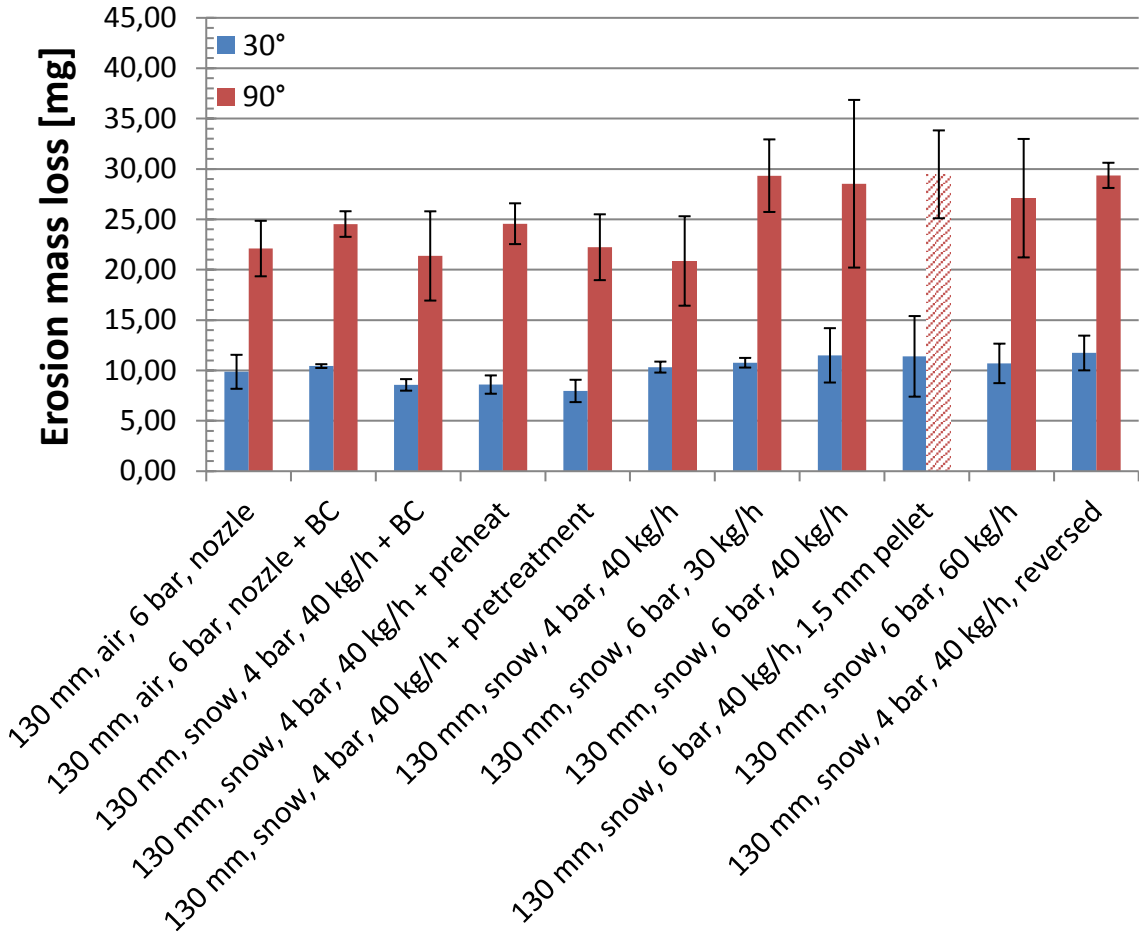

Figure 58: Erosion test results, 1st spraying set, worn out sample represented by striped column.

Overall, the differences in wear at 30˚ angle are quite minute and very little comparisons can be made based on them. The 90˚ results however divide the set somewhat into two groups. Air-cooled and 4 bar dry ice blasted samples (excluding the reversed) wore less than the 6 bar blasted samples and just like with the abrasion test the thinner 1.5 mm pellet blasted sample wore through as represented by the striped column.

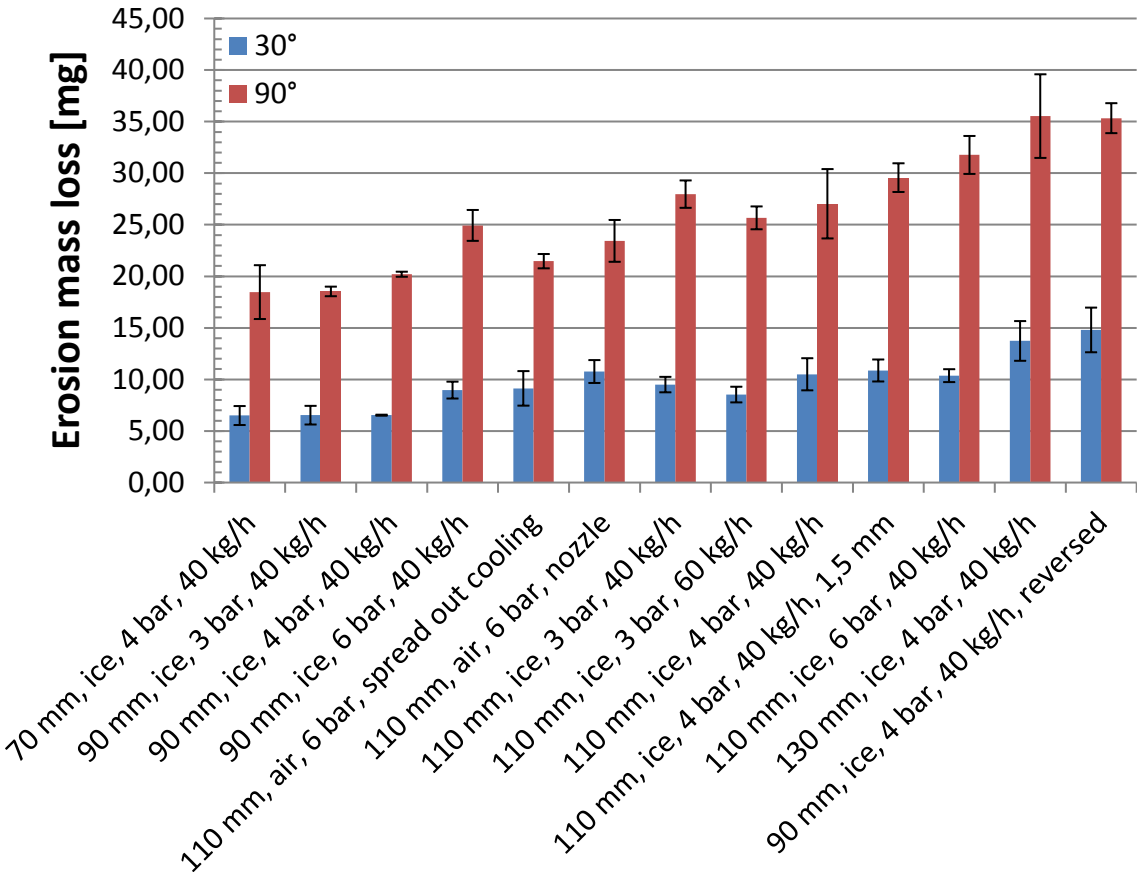

Figure 59: Erosion test results, 2nd spraying set.

Highest wear resistance in the second set in both 30˚ and 90˚ angles was recorded in samples sprayed at 70 mm and 90 mm, with 3 or 4 bar dry ice blasting, an increase in either the distance or the blasting pressure weakened the coating which can be seen throughout the series. Especially detrimental was the reversed rotation direction.

7.8 Cavitation resistance

As with the abrasion test, the best samples of the first set were the air-cooled ones with the 4 bar dry ice blasted sample coming next. The 1,5 mm pellet blasted sample wore out within the first 30 minutes of the test and is represented by a striped column. Otherwise, there is a slight trend favouring lightly cooled samples as with the other wear tests (Figure 60).

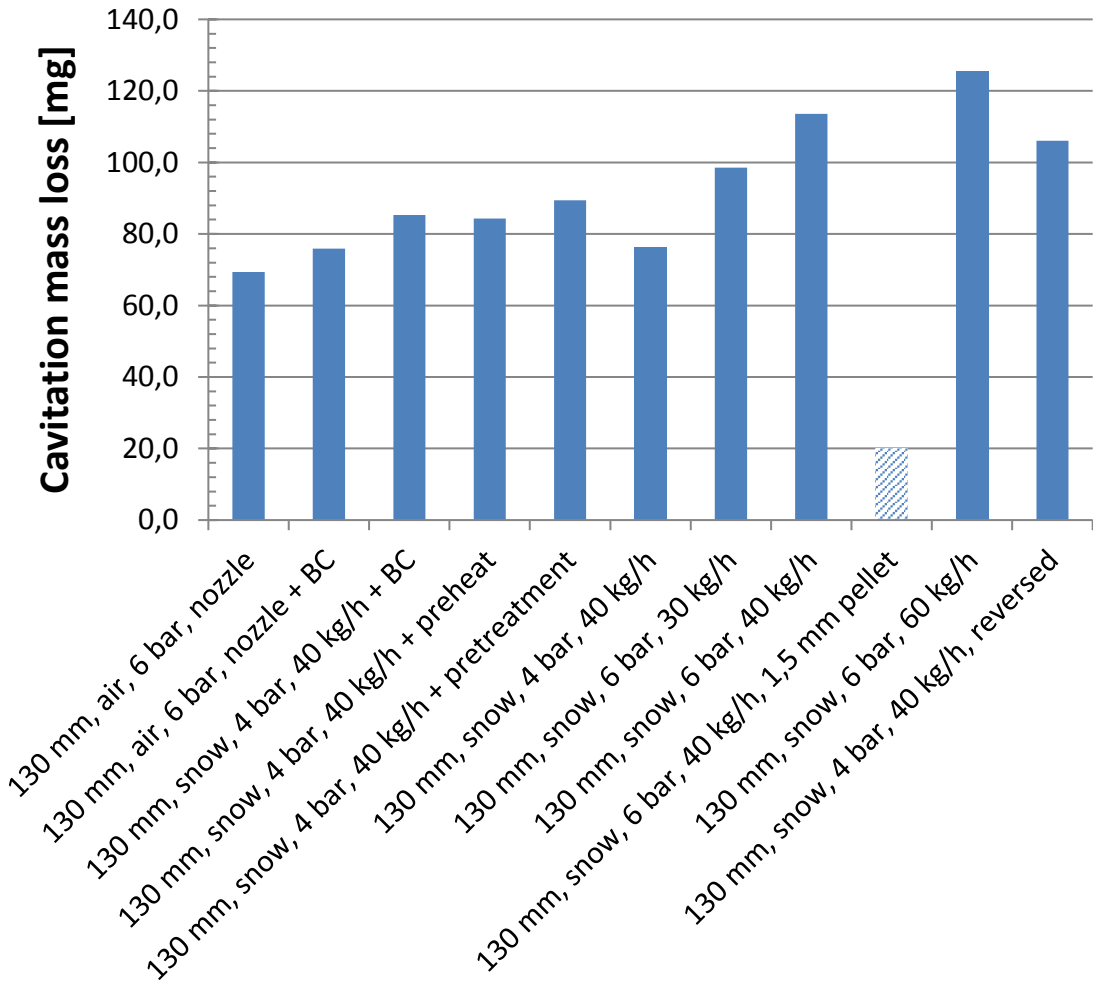

Figure 60: Cavitation test results, 1st spraying set, worn out sample represented by striped column.

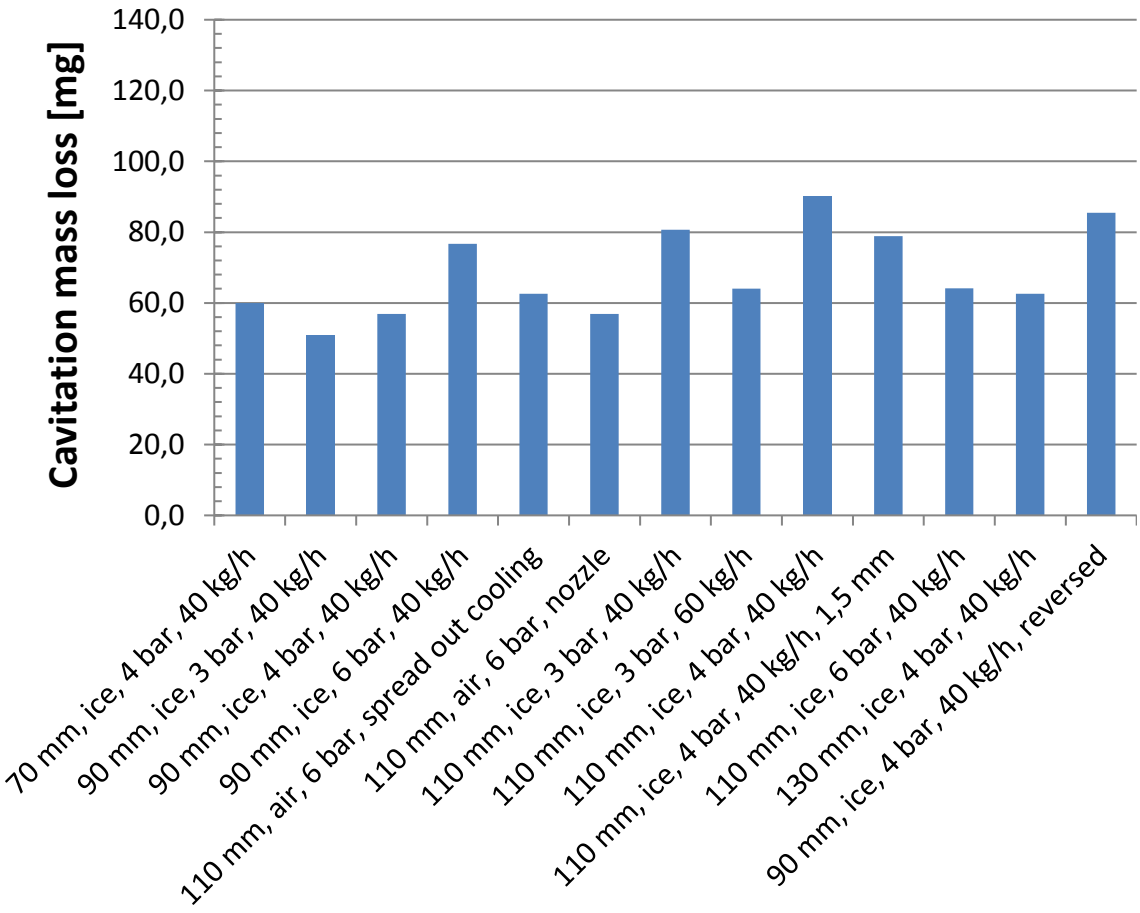

Figure 61: Cavitation test results, 2nd spraying set.

In the second set samples (Figure 61) the data is quite scattered, the samples most wear resistant in earlier tests endured the cavitation test relatively well but in addition to those a group of other samples reached similar values. It can actually be seen that the values are divided into two separate groupings: total mass loss around 60 mg and around 80 mg. Both groups are quite irregular and include samples that were sprayed at close and long distances and cooled with low and high pressures.

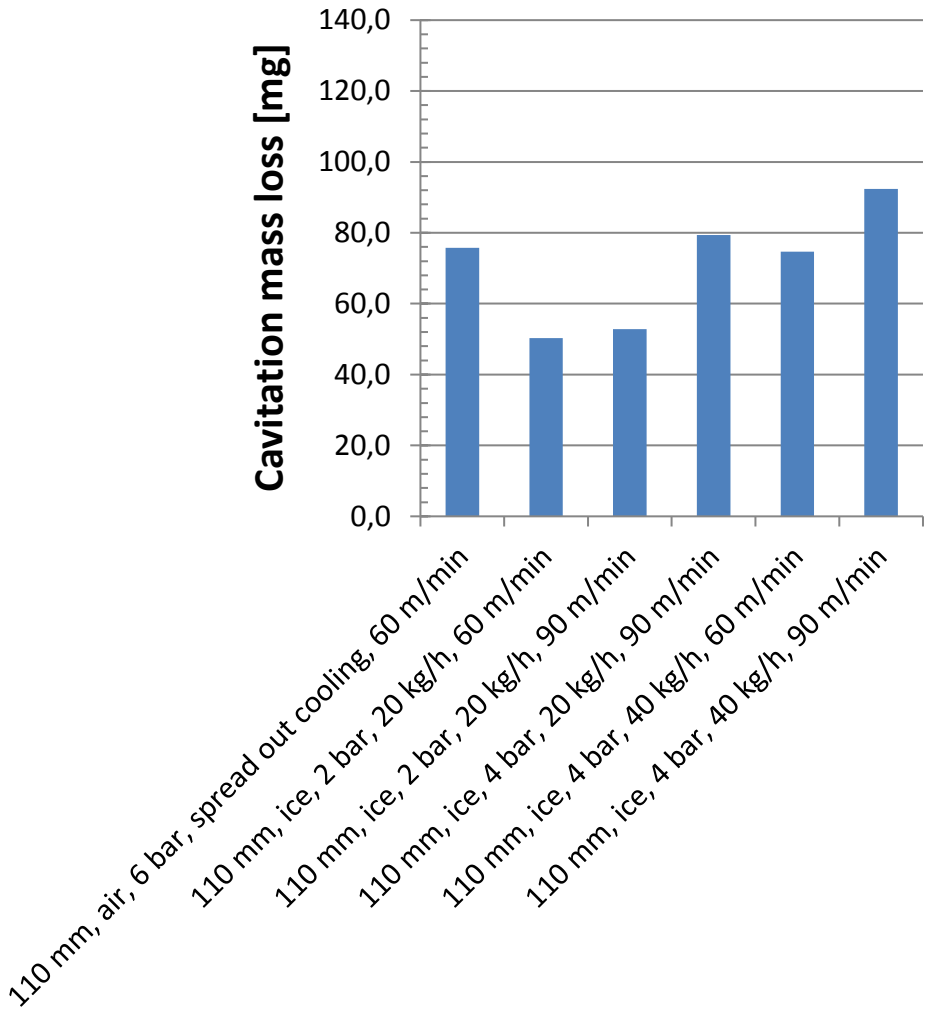

Figure 62: Cavitation test results, 3rd spraying set.

The cavitation wear ranking of the third set samples (Figure 62) mimics the results gained from the abrasion test with the 2 bar, 20 kg/h blasted sample with 60 m/min surface speed having the least wear out of all samples with a mass loss of 50,3 mg. Although, the second set sample sprayed at 90 mm with 3 bar blasting reached nearly the same value at 50,9 mg.

7.9 Tensile adhesion strength

On the contrary to the original studies by Dong et al. significant increases in coating adhesion were not realized in our testing with dry ice processing. The results from the first (Figure 63) and second (Figure 64) sets are presented below. Highest adhesion values were achieved with the application of bond coats, next in line were coatings with preheating and pretreatment, but surprisingly the preheating performed better than the pretreatment.

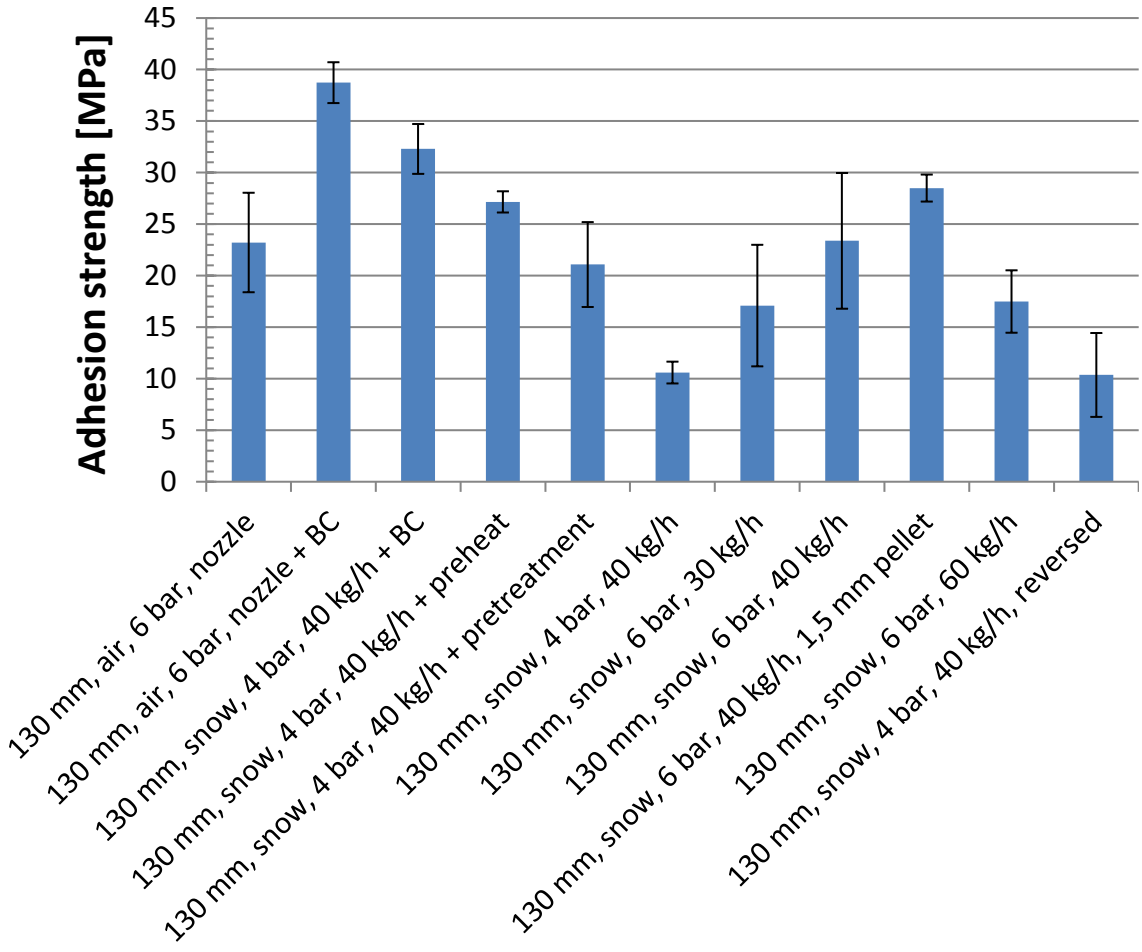

Figure 63: Adhesion test results, 1st spraying set.

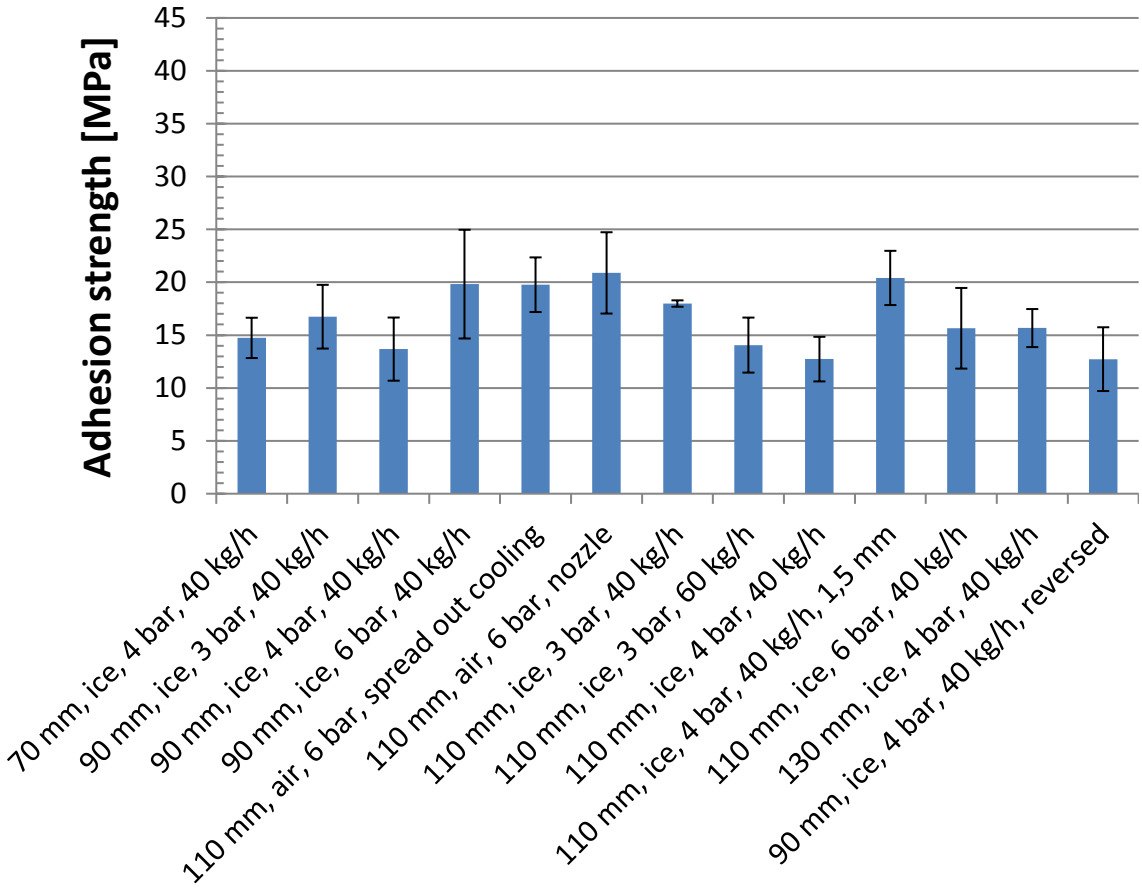

Figure 64: Adhesion test results, 2nd spraying set.

In the second set there were no pretreatments used as the focus of the set was shifted towards achieving good structure. Samples exhibited low mixed values between 10 and 25 MPa with no clear relation to parameter variation. The high adhesion measured from the 130 mm, 1,5 mm pellet sample could be attributed to the thinner coating and therefore is not suited for direct comparison with the others. The air-cooled samples had bit higher adhesion but overall the results are even lower than some non-pretreated samples from the first set.

7.10 Gas permeability

The gas permeability test results are presented in Figure 65; tests were only done for the second set samples. The lowest values were obtained from air-cooled samples; however the difference is quite minor. The permeability coefficient represents the area of through pores in 1 m^2 of coating.

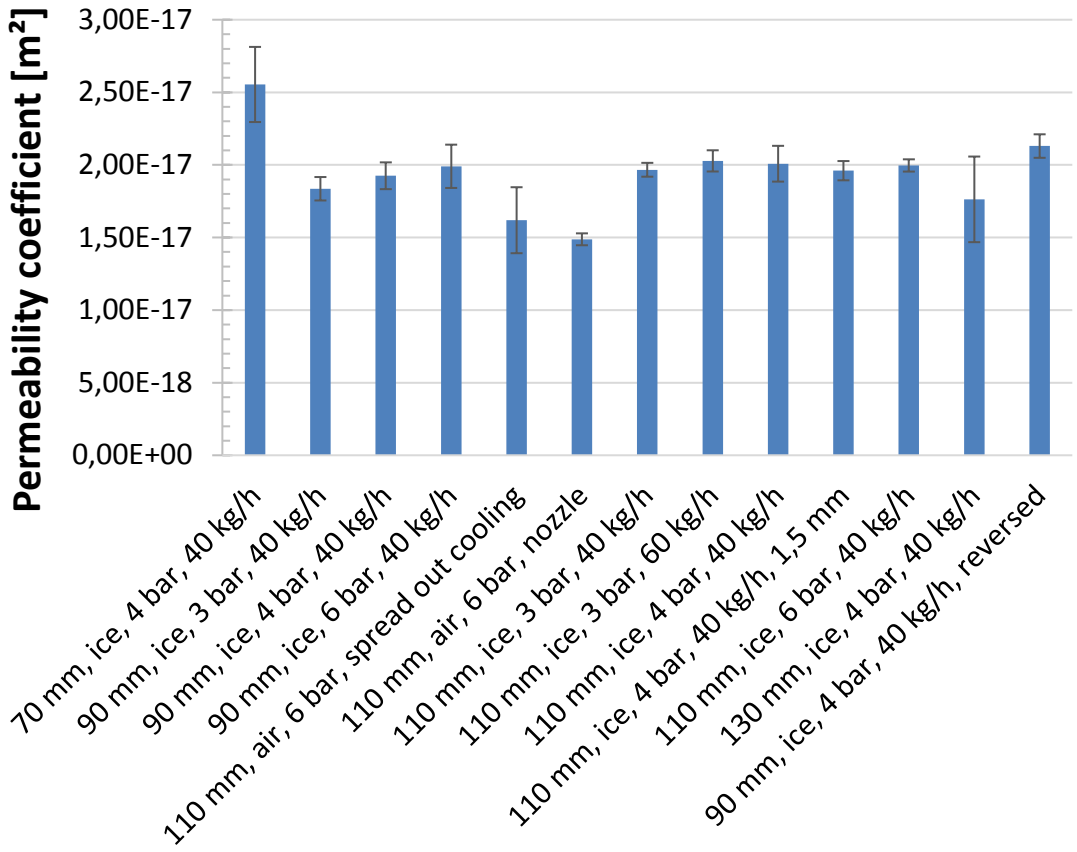

Figure 65: Gas permeability test results, 2nd spraying set only.

One explanation for the lower gas permeability of the air-cooled samples could be the fine chromia dust. The air-cooled samples were the only ones with a noticeable layer of chromia dust on them after spraying, it is possible that the same dust is trapped between the lamellae and was inhibiting the gas flow within.

The single peak value of the 70 mm sprayed sample resulted from an inadequate seal caused by the very rough as sprayed surface. Apart from the highest and lowest values, the rest of the dry ice blasted samples are very close to one another regardless of sample parameters.

8. DISCUSSION

For most cooling purposes, a concentrated stream of pressurized air seems to be sufficient and easier to apply than dry ice blasting. As seen in Figure 37 (p. 59), a 6 bar concentrated pressurized air stream already cools more than dry ice at 3 bars and 40 kg/h. In an ideal situation, auxiliary cooling – whether it is dry ice, liquid nitrogen or compressed air – should be mainly considered for a process that is already relying on cooling breaks to prevent thermal stresses, coating or substrate damage. Otherwise, the spraying parameters may need adjustment to accommodate the cooling system before appropriate coating quality is achieved. For this reason temperature monitoring is highly recommended.

Even though in all of the dry ice blasted samples, the as-sprayed surfaces were very clean compared to air-cooled samples, the particle sizes with the first blaster may have still been inadequate. As stated in earlier segments, the cleaning effect of dry ice blasting works through three mechanisms: kinetic impact of particles, thermal shock and rapid sublimation of particles. Especially the kinetic effect is affected by the particle size and velocity, hence for maximum cleaning larger intact particles would be preferred, instead of a fine stream of snow like dry ice dust which seemed to be the case with the first blaster we used. Even if the cleaning effect is lessened due to particle size, the cold particle stream will only cool down the substrate and coating, occasionally too much.

The choice of dry ice blaster makes a clear difference as models from different manufacturers may differ significantly as the HiWatch results showed. Possibly the greatest difference between the commercial blasters used here and the blaster used by Dong et al. [70] lies in the nozzle design. Most commercial blasters today use a single hose system that transports the pellets at full pressure from the tank through a long hose to the nozzle. This will result in more fragmented and faster pellets compared to feeding the pellets directly into the nozzle as Dong et al. did.

In the first set of samples, the splat boundaries were very pronounced indicating a poor splat to splat bonding. This was attributed to the longer spraying distance of 130 mm as well as the reduction of the overall substrate temperature by the auxiliary cooling. The air-cooled samples had slightly tighter boundaries than the dry ice cooled samples indicating that the overall process was indeed too cold especially with the dry ice blasted samples. Although the air-cooled samples were not up to usual standards either. In addition to the overall low process temperature, excessive thermal cycling - as indicated by the temperature curves - could have also been responsible for some of the low quality.

In the second set, the spraying distance was adjusted shorter and already some improvement was noted at the commonly used 110 mm distance, but further improvement happened with spraying distances lower than what would normally be possible. Due to added cooling, the adverse effects caused by substrate overheating were avoided. An alternative approach would have been adjusting the plasma parameters hotter but this could have been challenging due to vaporization of chromia at high temperatures. In the third set, the surface speed was lowered resulting in slightly higher substrate temperatures, which in the end proved to be a better approach.

In the first and second sets, practically no benefit was achieved with dry ice blasting alone, in both sets the air-cooled samples performed the best or were at least on par with the best dry ice blasted samples sprayed at the same distance. Samples sprayed at 70 mm and 90 mm may have benefitted from the dry ice treatment primarily due to the added cooling, which balanced out the excess heat. A shorter spraying distance allows the particles to have a higher velocity and temperature (see Figure 4, p. 11) on impact, which should create well bonded splats but will also introduce more heat which could have been detrimental without the dry ice blasting.

However, changing the blaster seemed to make a great difference, as the 2 bar, 20 kg/h blasted samples with 60 m/min and 90 m/min had significantly higher wear resistance in both abrasion and cavitation than most samples. Even though the dry ice still maintained a relatively low substrate temperature, the larger dry ice particles and their kinetic energy seemed to have either cleaned the surface of dust or compacted the solidifying splats, just as speculated in previous studies [70]. On the contrary, to the previous study where the air pressure was 6 bars and the dry ice feed was roughly 40 kg/h, only very light dry ice blasting was actually required in our case to produce the desired results.

Dry ice processing does not seem to improve an already adequate surface quality of a coating but it may still reduce surface defects with problematic coating processes or materials. Every dry ice blasted sample regardless of parameters did however present with a very clean dust free surface right after spraying whereas the air-cooled samples were covered with green chromia dust. As long as the dry ice blasting is kept moderate, it should not reduce deposition efficiency but with intense dry ice blasting the deposition efficiency will drop, usually along with coating quality.

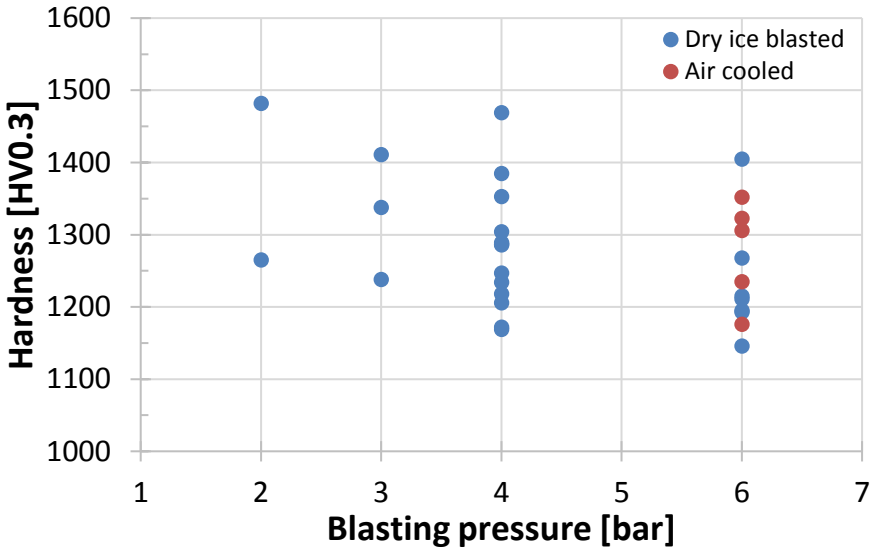

Figure 66: Cross-section hardness and blasting pressure xy-scatter chart.

It is challenging to find clear correlations on the effect of different cooling parameters on hardness as the standard deviations are quite significant. At a glance, higher hardnesses do however tend to result from hotter processes with light cooling (Figure 66), short spraying distance, and/or slower surface speed. On the other hand, hardness itself appears to have some impact on both abrasion and cavitation wear (Figure 67), the correlation being slightly better between cavitation wear and hardness.

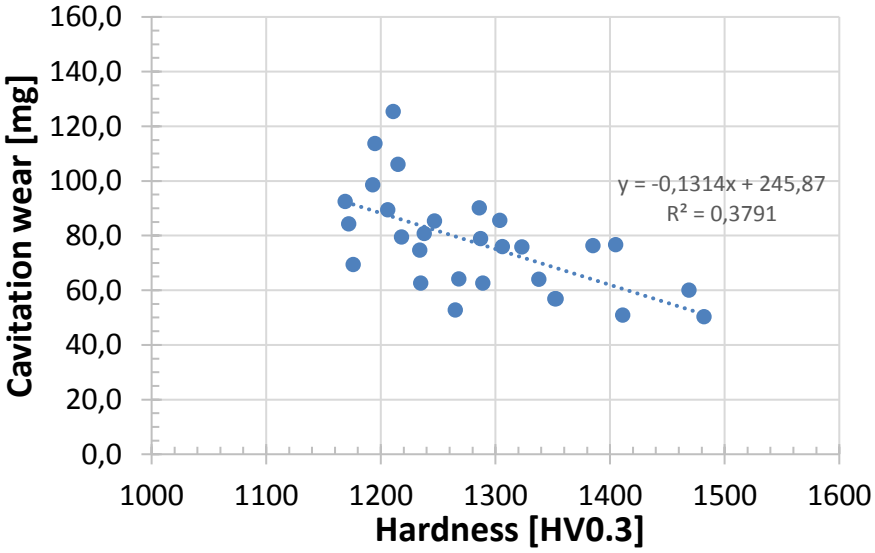

Figure 67: Cavitation wear and cross-section xy-scatter chart.

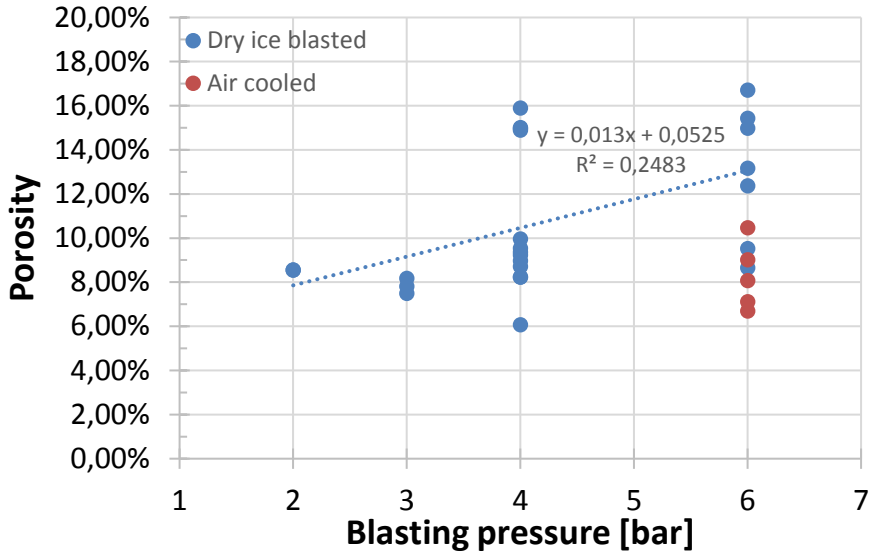

Figure 68: Porosity and blasting pressure xy-scatter chart.

The same applies to measured porosity. The data suggests some links between the blasting pressure and the measured porosity, higher pressure leading to more porosity in the coating (Figure 68). High porosity does not seem to play a large role in increasing abrasion wear but its effect on cavitation wear is slight (Figure 69).

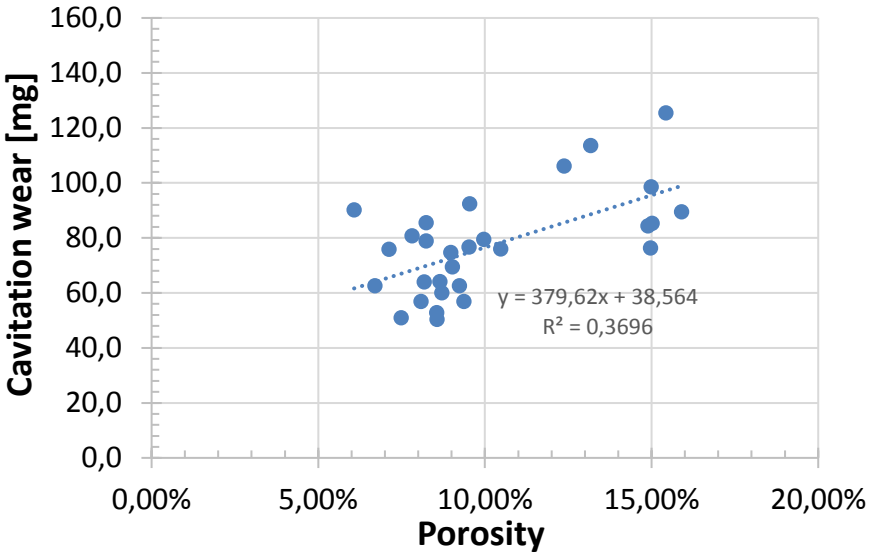

Figure 69: Cavitation and porosity xy-scatter chart.

The relationships with blasting parameters and coating quality might be more related to balancing the sample temperature and reducing fluctuations by matching the spraying parameters with the cooling parameters. Even though the individual splats are very hard, loose splat boundaries weakened by thermal cycling weaken the entire coating.

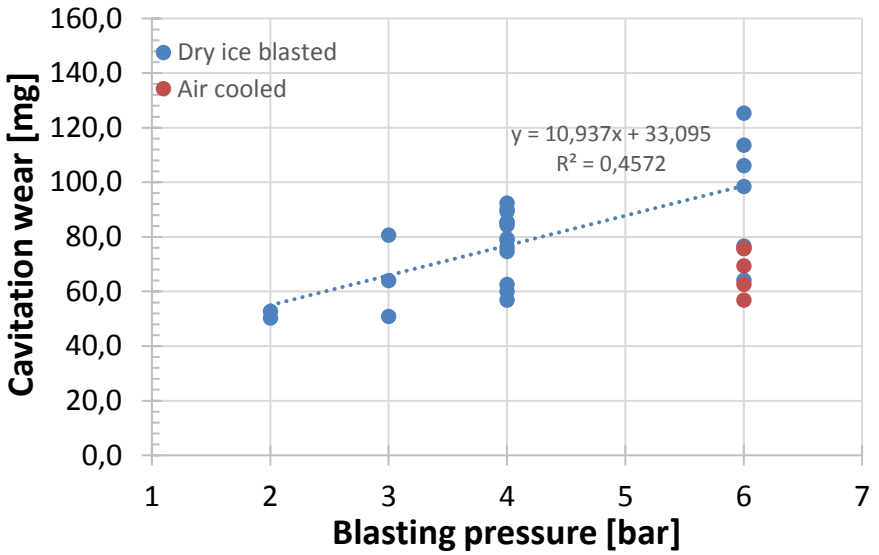

Figure 70: Cavitation and blasting pressure xy-scatter chart.

Comparing the blasting parameters to the wear results works slightly better than comparing them to hardness and porosity (Figure 70). High blasting pressures do lead to more wear in both abrasion and cavitation tests. All the erosion results on the other hand are too scattered and there are practically no visible links to coating properties or cooling parameters.

9. CONCLUSIONS

The earlier research conducted by Dong et al. [70] presented dry ice blasting as a simple and nearly foolproof auxiliary system for improving thermal sprayed coating quality. In our testing however, the implementation of dry ice blasting was found to be surprisingly challenging. Typically, a well-established thermal spray process is optimized for certain feedstock, spray gun and substrate. In some cases, this is a delicate balance especially with the particle and substrate temperature. Introducing any type of auxiliary cooling to an already balanced process may have unexpected results, as was learned during this study.

Initial experiments indicated that dry ice blasting primarily only affects the temperature of the process cooling it greatly. After several parameter combinations and gradual adjustments, actual benefits, possibly arising from the cleaning effect, were eventually realized. Although air cooled samples appeared more dense, lightly dry ice blasted samples exhibited hardnesses as high as 1482 HV compared to the highest value of 1176 HV for the air cooled samples. The respective lowest mass losses for air-cooled and dry ice blasted samples were 179 mg and 107 mg in abrasion and 56,9 mg and 50,3 mg in cavitation wear tests.

The benefits of auxiliary dry ice blasting do seem to exist but their positive effect on coating quality is not as significant as expected. Plasma spraying is already a complex process with a myriad of parameters to adjust, adding an auxiliary system creates even more degrees of freedom making the overall process much more complicated to optimize. Even when optimized correctly it is unclear whether the process would be worth the additional costs in relation to the quality improvement achieved. In cases where spraying parameter or powder composition adjustments or alternative thermal spraying technologies do not help, auxiliary systems may provide additional routes of improvement.

With constant development of HVOF spray guns, HVOF spraying of chromium oxide and other ceramics is gradually becoming easier and more common. The best coatings attained with APS and auxiliary dry ice blasting are still far from the quality levels attainable with HVOF spraying of chromium oxide. HVOF coating processes do however tend to suffer from overheating and the resulting quality issues, so there are good possibilities for the implementation of auxiliary dry ice blasting in HVOF coating processes.

REFERENCES

[1] R.C.J. Tucker, ASM Handbook, Volume 05A - Thermal Spray Technology, ASM International, Materials Park, 2013, 412 p.

[2] P.L. Fauchais, J.V.R. Heberlein, M. Boulos, Thermal Spray Fundamentals - From Powder to Part, Springer, New York, 2014, 1566 p.

[3] H. Mathesius, W. Krömmer, Practice of thermal spraying: guidance for technical personnel, English Edition ed. DVS Media GmbH, Düsseldorf, 2014, 168 p.

[4] L. Pawlowski, The Science and Engineering of Thermal Spray Coatings, 2nd Edition ed. John Wiley & Sons, Chichester, 2008, 626 p.

[5] R.S. Lima, B.R. Marple, Optimized HVOF Titania Coatings, Journal of Thermal Spray Technology, Vol. 12, No. 3, 2003, pp. 360-369.

[6] G. Bolelli, L. Lusvarghi, T. Manfredini, F. Pighetti Mantini, E. Turunen, T. Varis, S. Hannula, Comparison between plasma-and HVOF-sprayed ceramic coatings. Part I: Microstructure and mechanical properties, International Journal of Surface Science and Engineering, Vol. 1, No. 1, 2007, pp. 38-61.

[7] G. Bolelli, L. Lusvarghi, T. Manfredini, F. Pighetti Mantini, E. Turunen, T. Varis, S. Hannula, Comparison between plasma-and HVOF-sprayed ceramic coatings. Part II: Tribological behaviour, International Journal of Surface Science and Engineering, Vol. 1, No. 1, 2007, pp. 62-79.

[8] P. Vuoristo, K. Niemi, V. Matikainen, L. Hyvärinen, H. Koivuluoto, L.-. Berger, S. Scheitz, I. Shakhverdova, Structure and Properties of HVOF and Plasma Sprayed Ceramic Alumina-Chromia Coatings Deposited from Fused and Crushed Powders, Proceedings of the International Thermal Spray Conference: Thermal Spray 2013 - ITSC 2013: Innovative Coatings Solutions for the Global Economy, Busan, Republic of Korea, May 13-15, 2013, ASM International, Materials Park, pp. 465-470.

[9] P. Vuoristo, Plasmaruiskutetuista oksidipinnoitteista (in Finnish), 29, Tampere University of Technology, Tampere, 1985.

[10] L.C. Erickson, H.M. Hawthorne, T. Troczynski, Correlations between microstructural parameters, micromechanical properties and wear resistance of plasma sprayed ceramic coatings, Wear, Vol. 250, No. 1–12, 2001, pp. 569-575.

[11] G. Bolelli, L. Lusvarghi, T. Varis, E. Turunen, M. Leoni, P. Scardi, C.L. Azanza-Ricardo, M. Barletta, Residual stresses in HVOF-sprayed ceramic coatings, Surface and Coatings Technology, Vol. 202, No. 19, 2008, pp. 4810-4819.

[12] P. Chráska, J. Dubsky, K. Neufuss, J. Písacka, Alumina-base plasma-sprayed materials Part I: Phase stability of alumina and alumina-chromia, Journal of Thermal Spray Technology, Vol. 6, No. 3, 1997, pp. 320-326.

[13] K. Yang, X. Zhou, H. Zhao, S. Tao, Microstructure and mechanical properties of Al_2O_3–Cr_2O_3 composite coatings produced by atmospheric plasma spraying, Surface and Coatings Technology, Vol. 206, No. 6, 2011, pp. 1362-1371.

[14] R.S. Lima, B.R. Marple, From APS to HVOF spraying of conventional and nanostructured titania feedstock powders: A study on the enhancement of the mechanical properties, Surface and Coatings Technology, Vol. 200, No. 11, 2006, pp. 3428-3437.

[15] Anilox Rolls, Recograph International, web page. Available (accessed 06.16.2016): http://www.recograph.com/product/anilox-rolls/.

[16] Thermal Spray Materials Guide, April ed., Oerlikon Metco, 2015.

[17] H. Eschnauer, Hard material powders and hard alloy powders for plasma surface coating, Thin Solid Films, Vol. 73, No. 1, 1980, pp. 1-17.

[18] I. Lyo, H. Ahn, D. Lim, Microstructure and tribological properties of plasma-sprayed chromium oxide–molybdenum oxide composite coatings, Surface and Coatings Technology, Vol. 163–164, 2003, pp. 413-421.

[19] J.H. Ouyang, S. Sasaki, Effects of different additives on microstructure and high-temperature tribological properties of plasma-sprayed Cr_2O_3 ceramic coatings, Wear, Vol. 249, No. 1–2, 2001, pp. 56-66.

[20] A. Cellard, V. Garnier, G. Fantozzi, G. Baret, P. Fort, Wear resistance of chromium oxide nanostructured coatings, Ceramics International, Vol. 35, No. 2, 2009, pp. 913-916.

[21] V.P. Singh, A. Sil, R. Jayaganthan, Tribological behavior of plasma sprayed Cr_2O_3–3%TiO_2 coatings, Wear, Vol. 272, No. 1, 2011, pp. 149.

[22] G. Bolelli, V. Cannillo, L. Lusvarghi, T. Manfredini, Wear behaviour of thermally sprayed ceramic oxide coatings, Wear, Vol. 261, No. 11–12, 2006, pp. 1298-1315.

[23] H. Ahn, O. Kwon, Tribological behaviour of plasma-sprayed chromium oxide coating, Wear, Vol. 225–229, Part 2, 1999, pp. 814-824.

[24] Y. Xie, H.M. Hawthorne, The damage mechanisms of several plasma-sprayed ceramic coatings in controlled scratching, Wear, Vol. 233–235, 1999, pp. 293-305.

[25] E. Turunen, A. Hirvonen, T. Varis, T. Fält, S. Hannula, T. Sekino, K. Niihara, Application of HVOF Techniques for Spraying of Ceramic Coatings, The AZo Journal of Materials Online, Vol. 3, 2007, Available (accessed 06.16.2016): http://www.azom.com/article.aspx?ArticleID=4034.

[26] R. Schwetzke, H. Kreye, Cavitation Erosion of HVOF Coatings, Thermal Spray: Practical Solutions for Engineering Problems: Proceedings of the 9th National Thermal Spray Conference, Cincinnati, Ohio, USA, October 7-11, 1996, ASM International, Materials Park, pp. 153-158.

[27] L. Berger, C.C. Stahr, F. Toma, S. Saaro, M. Herrmann, D. Deska, G. Michael, S. Thiele, Corrosion of Thermally Sprayed Oxide Ceramic Coatings, Thermal Spray Bulletin, Vol. 61, No. 1, 2009, Available (accessed 06.16.2016): http://www.thermal-spray-bulletin.info/article/korrosion-thermisch-gespritzter-oxidkeramischerschichten/.

[28] C.L. Li, H.X. Zhao, M. Matsumura, T. Takahashi, M. Asahara, H. Yamaguchi, The effect of NiCr intermediate layer on corrosion behavior of Cr_2O_3 ceramic coated materials, Surface and Coatings Technology, Vol. 124, No. 1, 2000, pp. 53-60.

[29] E.M. Leivo, M.S. Vippola, P.P.A. Sorsa, P.M.J. Vuoristo, T.A. Mäntylä, Wear and corrosion properties of plasma sprayed AI_2O_3 and Cr_2O_3 coatings sealed by aluminum phosphates, Journal of Thermal Spray Technology, Vol. 6, No. 2, 1997, pp. 205-210.

[30] W. Kaczmar, J. Nadwyczawski, Properties of plasma sprayed layers of Cr_2O_3 powder, 10th International Thermal Spraying Conference - Poster Show Reports, Essen, Germany, May 2-6, 1983, German Welding Society, Essen.

[31] W. Funk, F. Goebe, Bond strength optimization of plasma-sprayed Cr_2O_3 layers by factorial two-level experiments, Thin Solid Films, Vol. 128, No. 1, 1985, pp. 45-55.

[32] S. Sampath, X. Jiang, Splat formation and microstructure development during plasma spraying: deposition temperature effects, Materials Science and Engineering: A, Vol. 304–306, 2001, pp. 144-150.

[33] T. Morishita, Coatings by 250 kW Plasma Jet Spray System, Proceedings: 2nd Plasma-Technik-Symposium, Lucerne, Switzerland, June 5-7, 1991, Plasma-Technik, Lucerne, pp. 137-141.

[34] E. Lugscheider, H. Jungklaus, G. Schwier, H. Mathesius, P. Heinrich, High Power Plasma Spraying of Oxide Ceramics, Advances in Thermal Spray Science and Technology: Proceedings of the 8th National Thermal Spray Conference, Houston, Texas, USA, September 11-15, 1995, ASM International, Materials Park, pp. 333-337.

[35] G. Irons, D. Poirier, A. Roy, The Application of High Power, High Velocity Plasma Coatings on Rolls for the Paper and Printing Industries, Proceedings of ITSC '95 (International Thermal Spray Conference '95), Kobe, Japan, May 22-26, 1995, High Temperature Society of Japan, Osaka, pp. 205-209.

[36] M. Cole, G. Creffield, The Utilization of Acetylene and Acetylene Based Gas Mixtures for the HVOF Coating of Chromium Oxide, Thermal Spray: Practical Solutions for Engineering Problems: Proceedings of the 9th National Thermal Spray Conference, Cincinnati, Ohio, USA, October 7-11, 1996, ASM International, Materials Park, pp. 129-133.

[37] D.J. Varacalle Jr., G.C. Wilson, D.E. Crawmer, Studies of the Air Plasma Spraying of Chromium Oxide Powder, Advances in Thermal Spray Science and Technology: Proceedings of the 8th National Thermal Spray Conference, Houston, Texas, USA, September 11-15, 1995, ASM International, Materials Park, pp. 365-372.

[38] T. Varis, J. Knuuttila, T. Suhonen, U. Kanerva, J. Silvonen, J. Leivo, E. Turunen, Improving the properties of HVOF- sprayed Cr_2O_3 by nanocomposite powders, Thermal Spray 2008: Crossing Borders: Proceedings of the International Thermal Spray Conference, Maastricht, The Netherlands, June 2-4, 2008, Springer, New York, pp. 440-443.

[39] V. Hurevich, I. Smurov, L. Pawlowski, Theoretical study of the powder behavior of porous particles in a flame during plasma spraying, Surface and Coatings Technology, Vol. 151–152, 2002, pp. 370-376.

[40] A. Vardelle, M. Vardelle, H. Zhang, N.J. Themelis, K. Gross, Volatilization of metal powders in plasma sprays, Journal of Thermal Spray Technology, Vol. 11, No. 2, 2002, pp. 244-252.

[41] K.A. Gross, P. Fauchals, M. Vardelle, J. Tikkanen, J. Keskinen, Vaporization and Ultra-Fine Particle Generation During the Plasma Spraying Process, Thermal

Spray 1997: A United Forum for Scientific and Technological Advances: Proceedings of the 1st United Thermal Spray Conference, Indianapolis, Indiana, USA, September 15-18, 1997, ASM International, Materials Park, pp. 543-548.

[42] A. Haddadi, A. Grimaud, A. Denoirjean, F. Nardou, P. Fauchais, Crystalline Growth within Alumina and Zirconia Coatings with Coating Temperature Control During Spraying, Thermal Spray: Practical Solutions for Engineering Problems: Proceedings of the 9th National Thermal Spray Conference, Cincinnati, Ohio, USA, October 7-11, 1996, ASM International, Materials Park, pp. 615-622.

[43] D. Caplan, M. Cohen, The Volatilization of Chromium Oxide, Journal of the Electrochemical Society, Vol. 108, No. 5, 1961, pp. 438-442.

[44] B. Ebbinghaus, Thermodynamics of gas phase chromium species: The chromium oxides, the chromium oxyhydroxides, and volatility calculations in waste incineration processes, Combustion and Flame, Vol. 93, No. 1, 1993, pp. 119-137.

[45] C.Y. Wu, P. Biswas, An Equilibrium Analysis to Determine the Speciation of Metals in an Incinerator, Combustion and Flame, Vol. 93, No. 1, 1993, pp. 31-40.

[46] O.E. Kashireninov, A. Fontijn, Modeling of Chromium Combustion in Incineration: Thermochemistry of Cr-C-H-Cl Combustion in Air and Selection of Key Reactions, Combustion and Flame, Vol. 113, No. 4, 1998, pp. 498-506.

[47] C. Gindorf, L. Singheiser, K. Hilpert, Vaporisation of chromia in humid air, Journal of Physics and Chemistry of Solids, Vol. 66, No. 2–4, 2005, pp. 384-387.

[48] N. Jacobson, D. Myers, E. Opila, E. Copland, Interactions of water vapor with oxides at elevated temperatures, Journal of Physics and Chemistry of Solids, Vol. 66, No. 2–4, 2005, pp. 471-478.

[49] E.J. Opila, D.L. Myers, N.S. Jacobson, I.M.B. Nielsen, D.F. Johnson, J.K. Olminsky, M.D. Allendorf, Theoretical and Experimental Investigation of the Thermochemistry of $CrO_2(OH)_2(g)$, The Journal of Physical Chemistry A, Vol. 111, No. 10, 2007, pp. 1971-1980.

[50] S.H. Yu, H. Wallar, CHROMIA SPRAY POWDERS, US 7,012,037 B2, 10/118,133, 8.4.2002, (14.03.2006), 5 p.

[51] F. Serita, K. Homma, K. Fukuda, K. Sawatari, Y. Suzuki, T. Toya, Development of an Inhalation System of High Melting Point Metal Fumes and Its Use for Exposure of Rats to Chromium and Nickel Fumes, Industrial Health, Vol. 28, No. 4, 1990, pp. 185-197.

[52] K. Sawatari, F. Serita, Determination of chromium speciation in fumes prepared by a plasma metal sprayer as a model of actual welding fumes, Industrial Health, Vol. 24, No. 1, 1986, pp. 51-61.

[53] Appendix C - Methodology for Estimating Hexavalent Chromium emissions from Thermal Spraying. Airborne Toxic Control Measure to Reduce Emissions of Hexavalent Chromium and Nickel from Thermal Spraying, Title 17, California Code of Regulations, Section 93101.5. California Air Resources Board, Sacramento, 2005.

[54] C. Coddet, On the use of auxiliary systems during thermal spraying, Surface and Coatings Technology, Vol. 201, No. 5, 2006, pp. 1969-1974.

[55] J. Dhers, N. Goubot, T. David, J. Baudoin, Cryogenic Cooling in High Power Plasma Spraying, Thermal Spray 2001: New Surfaces for a New Millenium: Proceedings of the International Thermal Spray Conference, Singapore, 28-30 May, 2001, ASM International, Materials Park, pp. 533-538.

[56] Y.A. Cengel, M.A. Boles, Thermodynamics: An Engineering Approach, 7th edition in SI units ed. McGraw-Hill, Boston, 2011, 978 p.

[57] BIOGON® C kuivajää -tuotetiedote (in Finnish), AGA, web page. Available (accessed 21.06.2016): http://www.aga.fi/internet.lg.lg.fin/fi/images/AGA_BIOGON_dry_ice_datasheet_FI634_168273.pdf.

[58] S. Dong, B. Song, B. Hansz, H. Liao, C. Coddet, Modelling of dry ice blasting and its application in thermal spray, 2012, 16(1), 61-66. Materials Research Innovations, Vol. 16, No. 1, 2012, pp. 61-66.

[59] W. Krömmer, The Importance of Temperature Management in Thermal Spraying and the Respective Advantages of CO_2 for Cooling, ITSC 2015 - Proceedings of the International Thermal Spray Conference, Long Beach, California, USA, May 11-14, 2015, ASM International, Materials Park, pp. 713-717.

[60] E. Uhlmann, R. Hollan, A. El Mernissi, Dry Ice Blasting - Energy-Efficiency and New Fields of Application, Engineering Against Fracture: Proceedings of the 1st Conference, Patras, Greece, May 28-30, 2008, Springer Netherlands, Dordrecht, pp. 399-409.

[61] D.M. Brewis, G.W. Critchlow, C.A. Curtis, Cryoblasting as a pretreatment to enhance adhesion to aluminium alloys: an initial study, International Journal of Adhesion and Adhesives, Vol. 19, No. 4, 1999, pp. 253-256.

[62] G. Spur, E. Uhlmann, F. Elbing, Dry-ice blasting for cleaning: process, optimization and application, Wear, Vol. 233–235, 1999, pp. 402-411.

[63] C. Giolli, B. Allegrini, T. Duda, L. Engl, A. Giorgetti, A. Groppetti, A. Lanzi, S. Pini, M. Spagnoli, A. Scrivani, TBC Dry Ice Stripping, Thermal Spray 2010: Global Solutions for Future Application, Proceedings of the International Thermal Spray Conference, Singapore, May 3-5, 2010, DVS Media GmbH, Dusseldorf, pp. 690-694.

[64] S. Dong, B. Song, B. Hansz, H. Liao, C. Coddet, Improvement of adhesion of plasma-sprayed Al_2O_3 coatings by using dry-ice blasting, Materials Letters, Vol. 66, No. 1, 2012, pp. 289-291.

[65] S. Dong, B. Song, B. Hansz, H. Liao, C. Coddet, Improvement in the properties of plasma-sprayed metallic, alloy and ceramic coatings using dry-ice blasting, Applied Surface Science, Vol. 257, No. 24, 2011, pp. 10828-10833.

[66] S. Dong, B. Song, B. Hansz, H. Liao, C. Coddet, Improvement in the microstructure and property of plasma sprayed metallic, alloy and ceramic coatings by pre-/during-treatment of dry-ice blasting, Surface and Coatings Technology, Vol. 220, 2013, pp. 199-203.

[67] S. Dong, B. Song, H. Liao, C. Coddet, Effects of Substrate Treated by Dry-Ice Blasting on the Formation of CoNiCrAlY Splats, Thermal Spray 2012: Proceedings of the International Thermal Spray Conference, Houston, Texas, USA, May 21-24, 2012, ASM International, Materials Park, pp. 646-650.

[68] B. Song, S. Dong, H. Liao, C. Coddet, Property Improvement of Plasma-Sprayed FeAl Coating by Dry-Ice Blasting, Thermal Spray 2012: Proceedings of the International Thermal Spray Conference, Houston, Texas, USA, May 21-24, 2012, ASM International, Materials Park, pp. 651-656.

[69] S. Dong, B. Song, B. Hansz, H. Liao, C. Coddet, Study on the Mechanism of Adhesion Improvement Using Dry-Ice Blasting for Plasma-Sprayed Al_2O_3 Coatings, Journal of Thermal Spray Technology, Vol. 22, No. 2, 2013, pp. 213-220.

[70] S. Dong, B. Song, B. Hansz, H. Liao, C. Coddet, Microstructure and properties of Cr_2O_3 coating deposited by plasma spraying and dry-ice blasting, Surface and Coatings Technology, Vol. 225, 2013, pp. 58-65.

[71] S. Dong, B. Song, G. Zhou, C. Li, B. Hansz, H. Liao, C. Coddet, Preparation of Aluminum Coatings by Atmospheric Plasma Spraying and Dry-Ice Blasting and

Their Corrosion Behavior, Journal of Thermal Spray Technology, Vol. 22, No. 7, 2013, pp. 1222-1229.

[72] S. Dong, B. Song, B. Hansz, H. Liao, C. Coddet, Parameter Optimization of Dry-Ice Blasting during Plasma Spraying Process by Characterizing CoNiCrAlY Coatings, Thermal Spray 2013: Proceedings of the International Thermal Spray Conference, Busan, South Korea, May 13-15, 2013, ASM International, Materials Park, pp. 672-676.

[73] S. Dong, B. Song, G. Zhou, B. Hansz, H. Liao, C. Coddet, Multi-layered thermal barrier coatings fabricated by plasma-spraying and dry-ice blasting: Microstructure characterization and prolonged lifetime, Surface and Coatings Technology, Vol. 236, 2013, pp. 557-567.

[74] B. Song, S. Dong, B. Hansz, H. Liao, C. Coddet, Suppression effect of decarburization by dry-ice blasting on plasma-sprayed steel coatings: Structure, wear performance and magnetic properties, Surface and Coatings Technology, Vol. 253, 2014, pp. 44-51.

[75] S. Dong, B. Song, H. Liao, C. Coddet, Deposition of NiCrBSi coatings by atmospheric plasma spraying and dry-ice blasting: Microstructure and wear resistance, Surface and Coatings Technology, Vol. 268, 2015, pp. 36-45.

[76] D. Schinzler, Back to the Basics: The Fundamentals of Dry Ice Blasting, Continental Carbonic Products, Inc., web page. Available (accessed 29.6.2016): https://www.continentalcarbonic.com/blog/back-basics-fundamentals-dry-ice-blasting/.

[77] LINSPRAY® CO_2 cooling -brochure, Linde North America, Inc, web page. Available (accessed 29.6.2016): http://www.lindeus.com/internet.lg.lg.usa/en/images/linspray-CO2-cooling138_23307.pdf.

[78] CRYOCLEAN® SNOW -brochure, Linde North America, Inc, web page. Available (accessed 29.6.2016): http://www.lindeus.com/internet.lg.lg.usa/en/images/CRYOCLEAN-Snow-Dry-Ice-Blasting-2-1-2013138_86132.pdf.

[79] CO2-Snow Jet Cleaning, advanced clean production GmbH, web page. Available (accessed 29.6.2016): http://www.acp-micron.com/5699_CO2-Schneestrahl-Reinigung.html?lang=1.

[80] IceMaster, mycon GmbH, web page. Available (accessed 29.6.2016): http://www.mycon.info/en/products/icemaster.

[81] M. Magnani, P.H. Suegama, N. Espallargas, S. Dosta, C.S. Fugivara, J.M. Guilemany, A.V. Benedetti, Influence of HVOF parameters on the corrosion and wear resistance of WC-Co coatings sprayed on AA7050 T7, Surface and Coatings Technology, Vol. 202, No. 19, 2008, pp. 4746-4757.

[82] H. Bhat, H. Herman, Plasma-spray-quenched martensitic stainless steel coatings, Thin Solid Films, Vol. 95, No. 3, 1982, pp. 227-235.

[83] Z. Zurecki, R. Ghosh, T. Mebrahtu, M.J. Thayer, S.R. Stringer, Automated Substrate Cooling System for HVOF Coating Operations, Thermal Spray 2008: Crossing Borders: Proceedings of the International Thermal Spray Conference, Maastricht, The Netherlands, June 2-4, 2008, Springer, New York, pp. 206-211.

[84] M. Akuh, L. Mercando, Z. Zurecki, Cryo-Gas Cooling Method and System for Thermal Spray Coatings, Thermal Spray 2011: Proceedings of the International Thermal Spray Conference, Hamburg, Germany, September 27-29, 2011, DVS Media GmbH, Dusseldorf, pp. 1411-1418.

[85] R. Kapp, Chromium Hexavalent Compounds, in: P. Wexler (ed.), Encyclopedia of Toxicology, Second Edition, Elsevier, New York, 2005, pp. 602-606.

[86] J. Abelson, NIOSH Recommendations for Hexavalent Chromium – 2013 Update, Donaldson Company, Inc., web page. Available (accessed 29.6.2016): http://www2.donaldson.com/torit/en-us/pages/technicalinformation/niosh-recommendations-for-hexavalent-chromium-2013-update.aspx.

[87] A. Heilig, Chromium, in: P. Wexler (ed.), Encyclopedia of Toxicology, Second Edition, Elsevier, New York, 2005, pp. 600-602.

[88] OSHA Hexavalent Chromium Regulation, Advanced Materials & Processes, Vol. 164, Iss. 8, 2006, pp. 12-25.

[89] HTP-arvot 2014. Haitallisiksi tunnetut pitoisuudet (in Finnish), Sosiaali- ja terveysministeriö, Helsinki, 2014.

[90] DIRECTIVE 2011/65/EU OF THE EUROPEAN PARLIAMENT AND OF THE COUNCIL of 8 June 2011 on the restriction of the use of certain hazardous substances in electrical and electronic equipment, European Commission, Brussels, 2011.

[91] Electric dry ice blasting machine IC 110-E, ICS Ice Cleaning Systems GmbH, web page. Available (accessed 9/14): http://www.ics-dryice.de/en/products/dry-ice-blasting-machines/electric/ic-110-e.

[92] ASTM C633-13, Standard Test Method for Adhesion or Cohesion Strength of Thermal Spray Coatings, ASTM International, West Conshohocken, PA, 2013, 8 p.

[93] ASTM G65-16, Standard Test Method for Measuring Abrasion Using the Dry Sand/Rubber Wheel Apparatus, ASTM International, West Conshohocken, PA, 2016, 14 p.

[94] ASTM G32-16, Standard Test Method for Cavitation Erosion Using Vibratory Apparatus, ASTM International, West Conshohocken, PA, 2016, 20 p.

[95] MANUAL FOR KG20 KG6 KG6 BASIC, IceTech A/S, web page. Available (accessed 1/26): https://www.continentalcarbonic.com/cmss_files/attachmentlibrary/KG620Manual1-28-10.pdf.

[96] K. Wittmann-Ténèze, N. Caron, S. Alexandre, Gas Permeability of Porous Plasma-Sprayed Coatings, Journal of Thermal Spray Technology, Vol. 17, No. 5, 2008, pp. 902-907.

[97] Erosion Resistance of Powder Materials and Coatings, in: I. Kleis, P. Kulu (ed.), Solid Particle Erosion: Occurrence, Prediction and Control, Springer London, London, 2008, pp. 129-168.

APPENDIX A: SEM IMAGES

500x and 1000x SEM images of all the sample cross sections are included in this appendix.

1st spraying set:

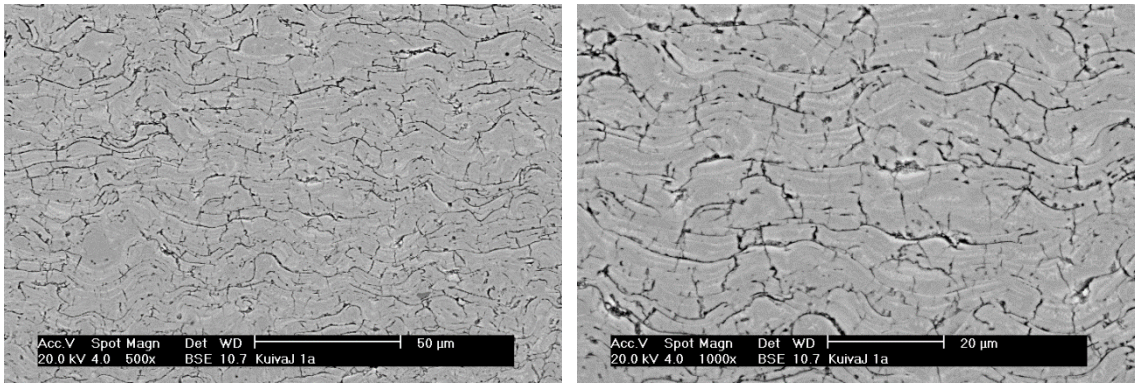

Figure 71: Sample 1a: 130 mm, air, 6 bar, nozzle

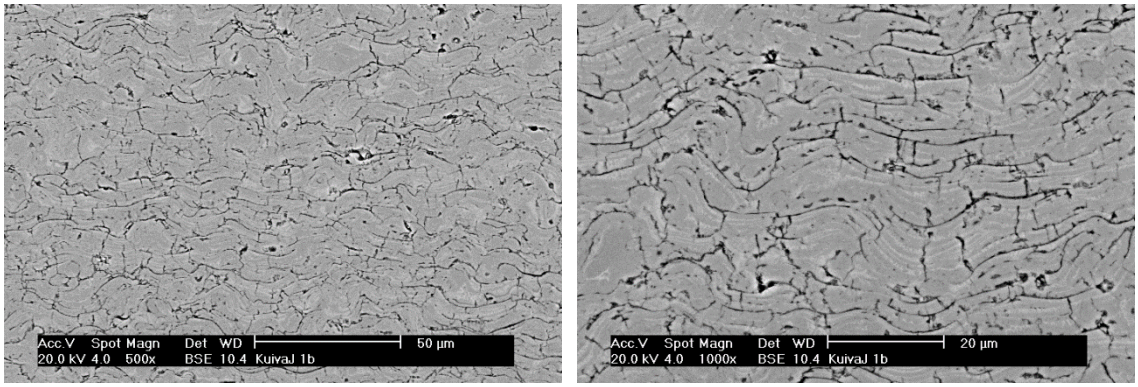

Figure 72: Sample 1b: 130 mm, air, 6 bar, nozzle + BC

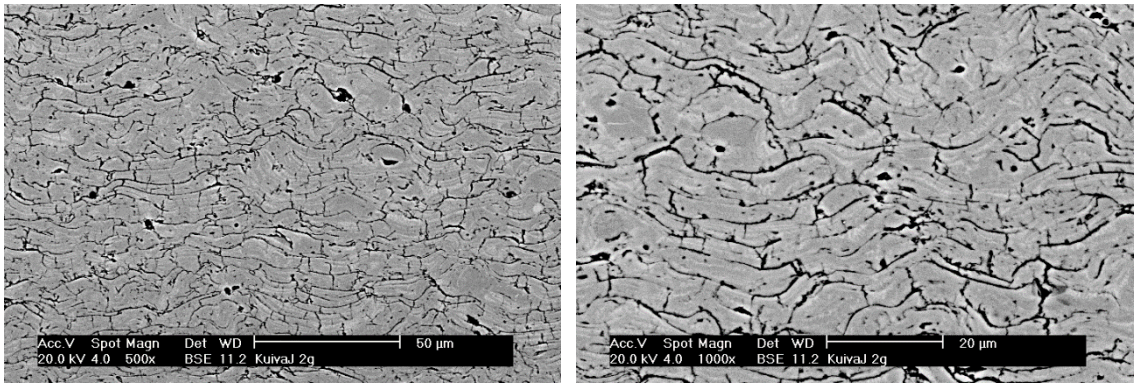

Figure 73: Sample 2g: 130 mm, snow, 4 bar, 40 kg/h + BC

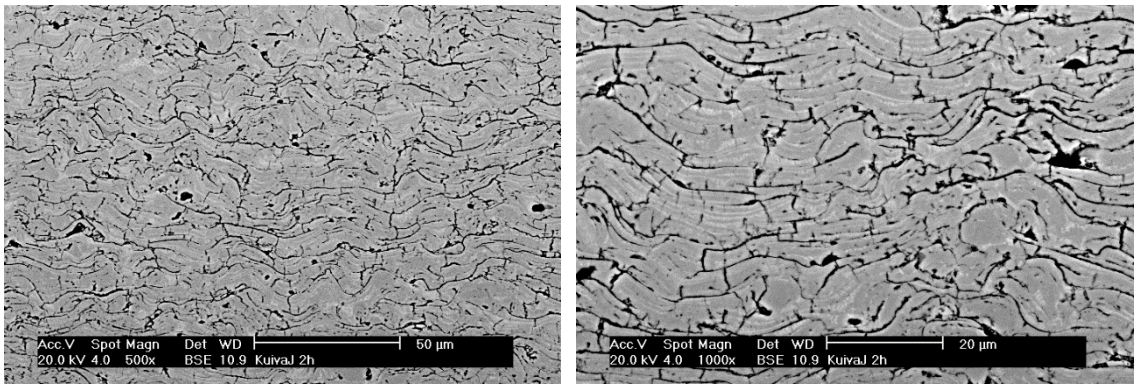

Figure 74: Sample 2h: 130 mm, snow, 4 bar, 40 kg/h + preheat

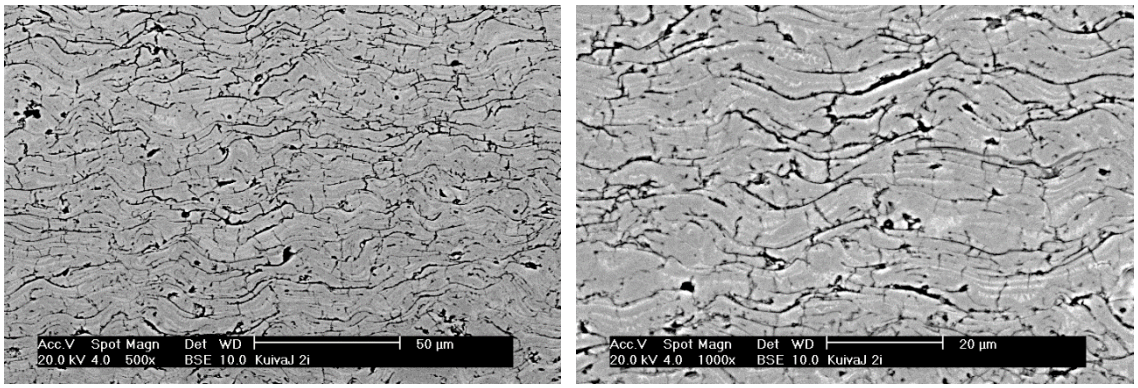

Figure 75: Sample 2i: 130 mm, snow, 4 bar, 40 kg/h + pretreatment

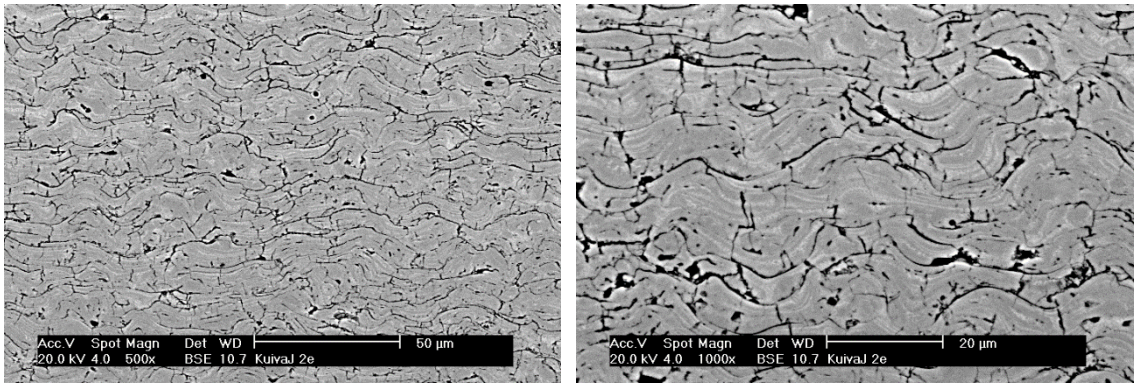

Figure 76: Sample 2e: 130 mm, snow, 4 bar, 40 kg/h

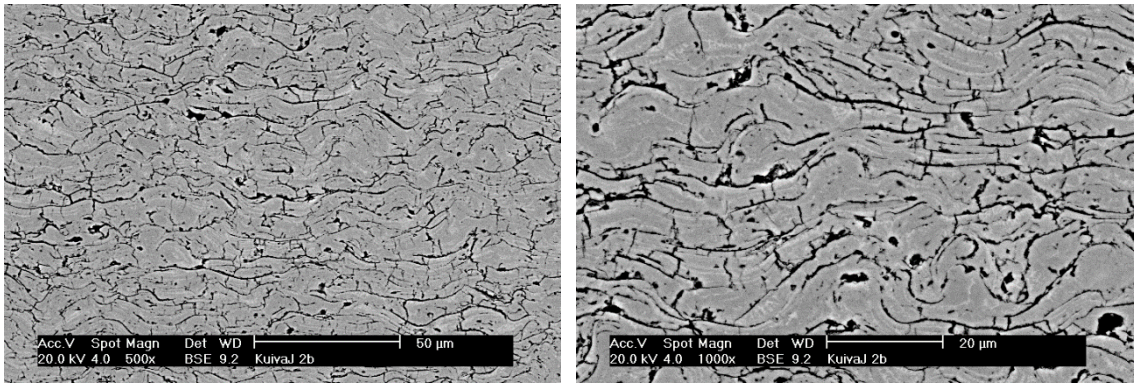

Figure 77: Sample 2b: 130 mm, snow, 6 bar, 30 kg/h

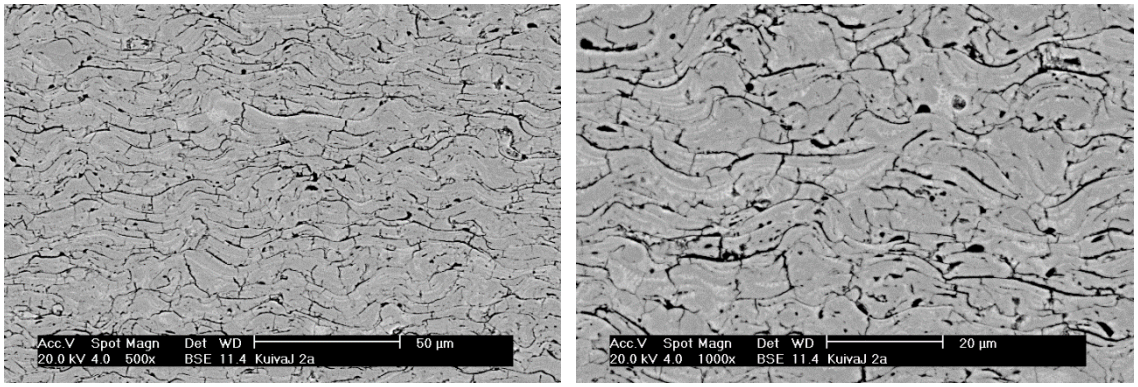

Figure 78: Sample 2a: 130 mm, snow, 6 bar, 40 kg/h

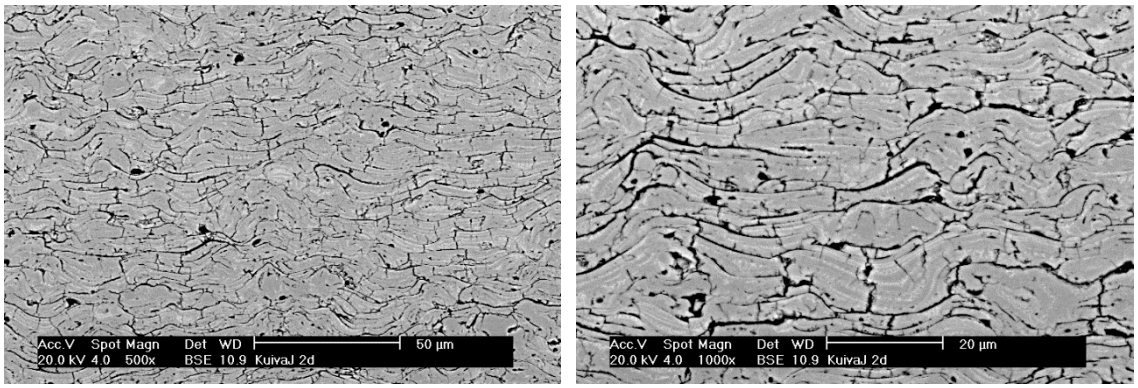

Figure 79: Sample 2d: 130 mm, snow, 6 bar, 40 kg/h, 1,5 mm pellet

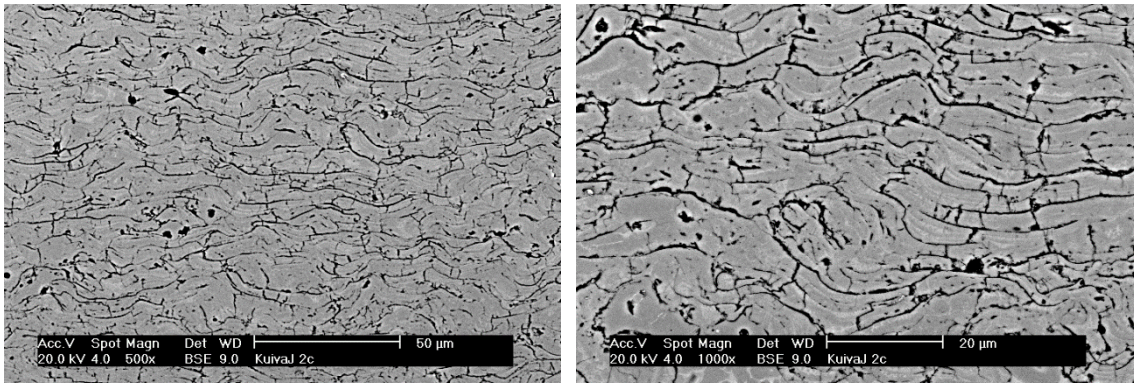

Figure 80: Sample 2c: 130 mm, snow, 6 bar, 60 kg/h

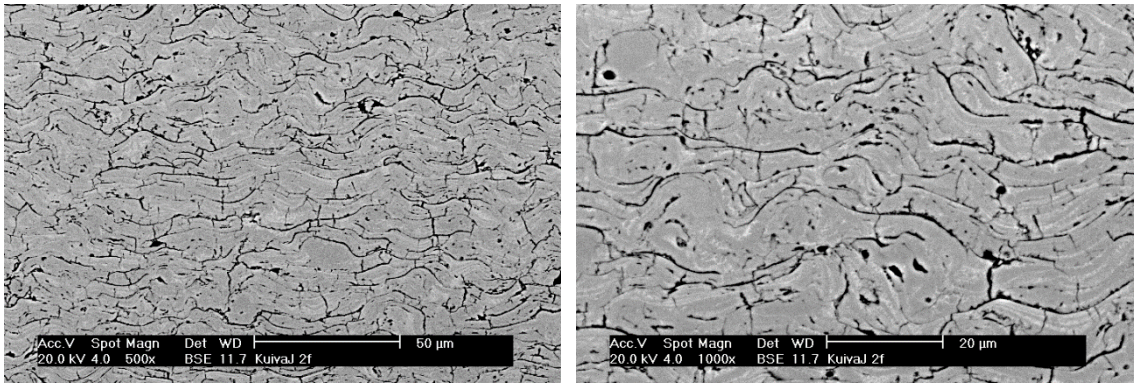

Figure 81: Sample 2f: 130 mm, snow, 4 bar, 40 kg/h, reversed

2nd spraying set:

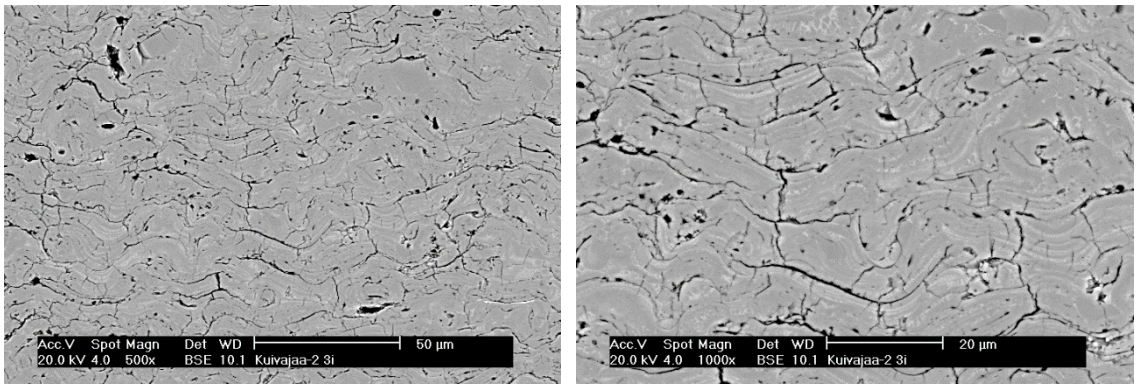

Figure 82: Sample 3i: 70 mm, ice, 4 bar, 40 kg/h

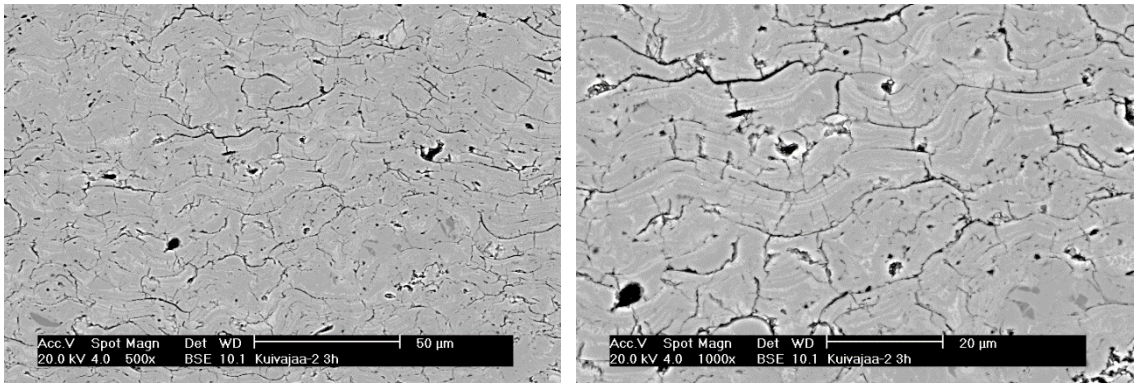

Figure 83: Sample 3h: 90 mm, ice, 3 bar, 40 kg/h

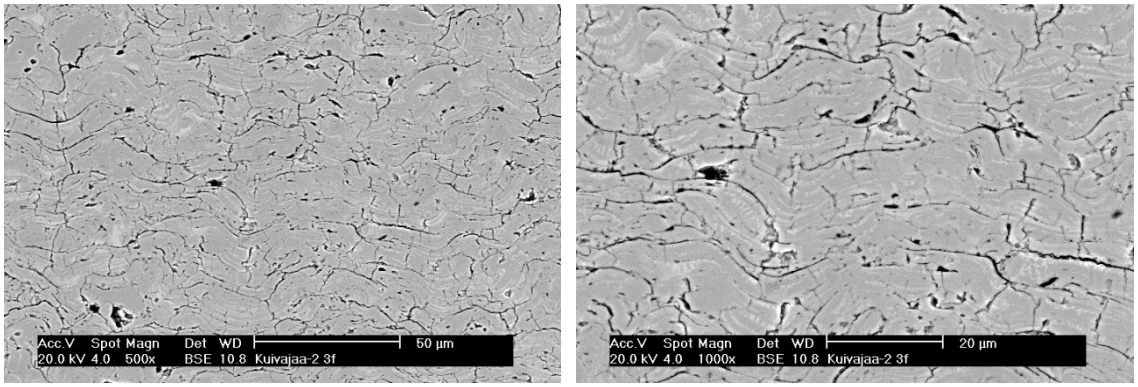

Figure 84: Sample 3f: 90 mm, ice, 4 bar, 40 kg/h

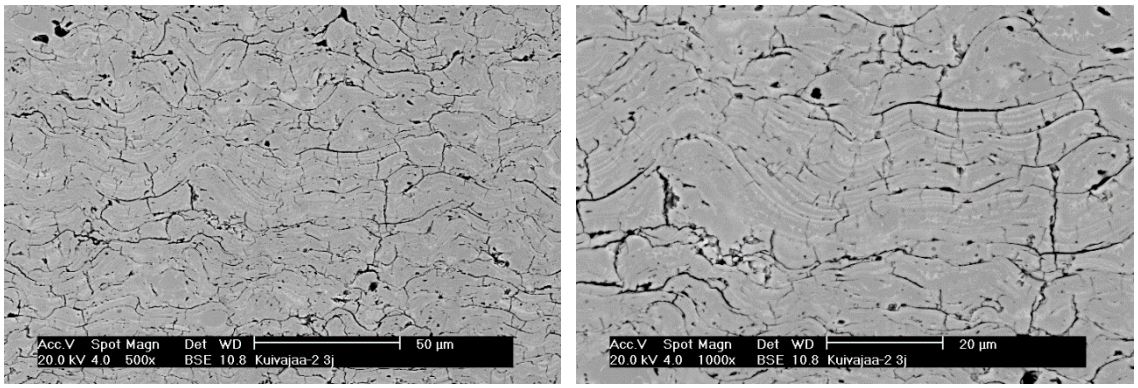

Figure 85: Sample 3j: 90 mm, ice, 6 bar, 40 kg/h

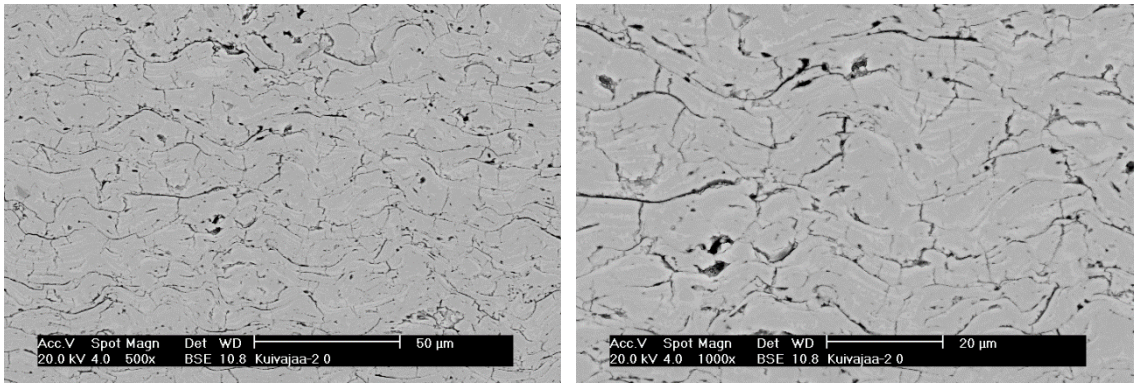

Figure 86: Sample 0: 110 mm, air, 6 bar, spread out cooling

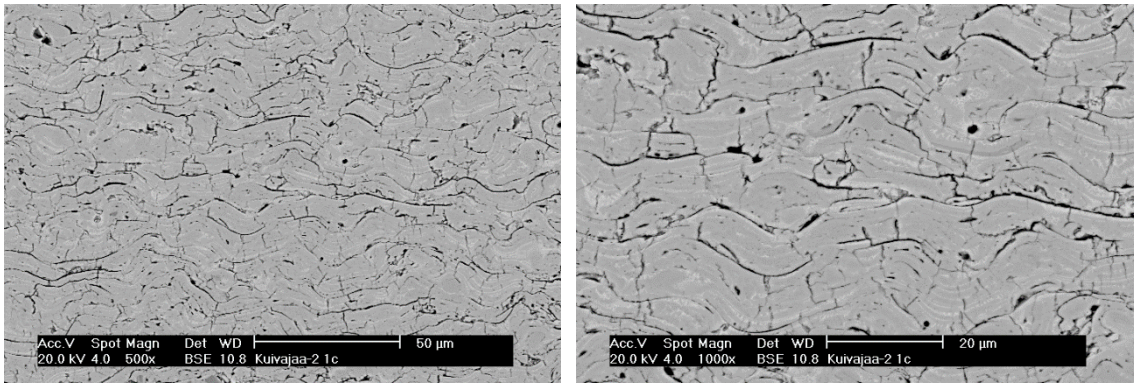

Figure 87: Sample 1c: 110 mm, air, 6 bar, nozzle

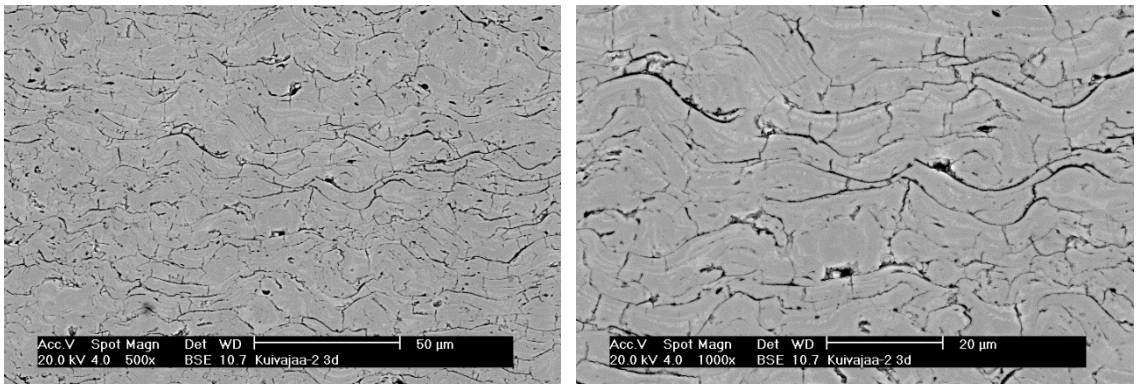

Figure 88: Sample 3d: 110 mm, ice, 3 bar, 40 kg/h

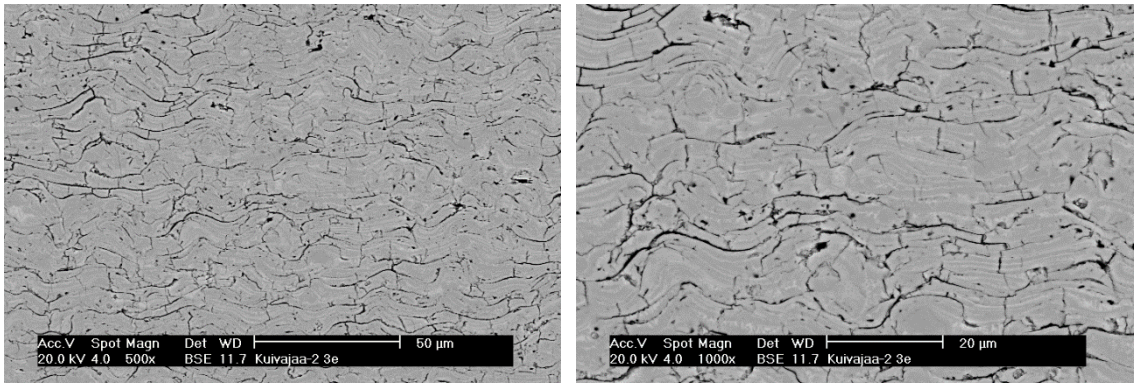

Figure 89: Sample 3e: 110 mm, ice, 3 bar, 60 kg/h

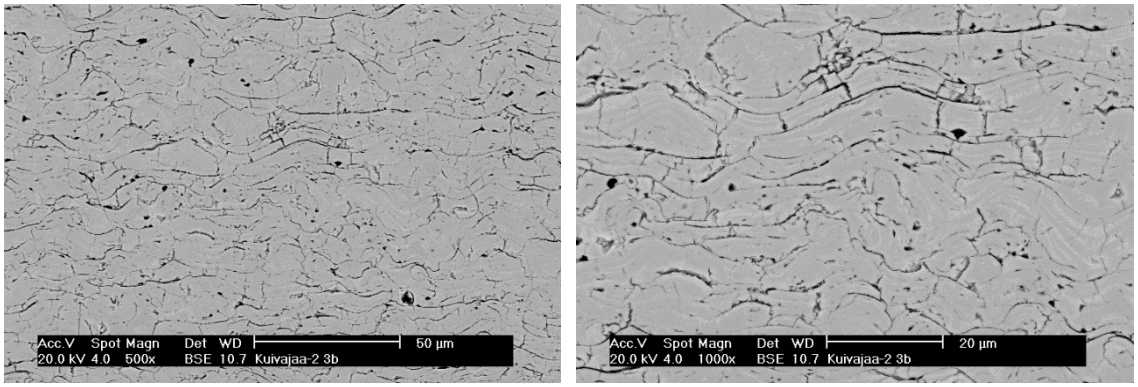

Figure 90: Sample 3b: 110 mm, ice, 4 bar, 40 kg/h

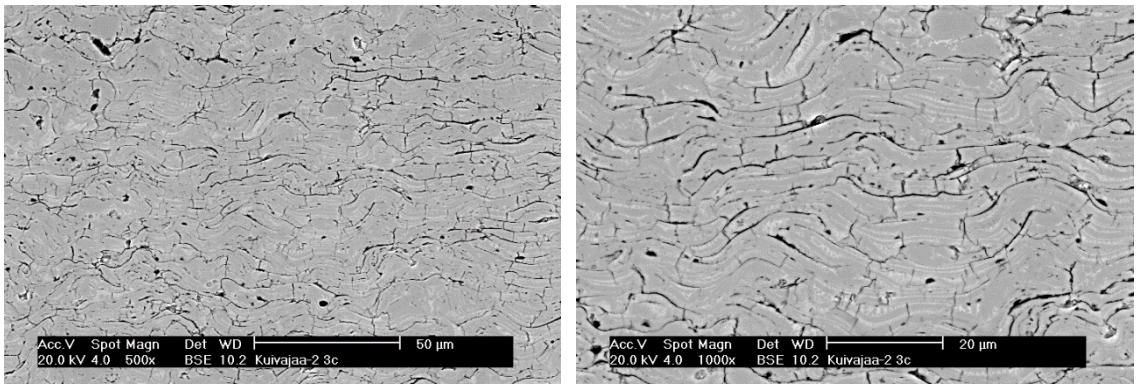

Figure 91: Sample 3c: 110 mm, ice, 4 bar, 40 kg/h, 1,5 mm

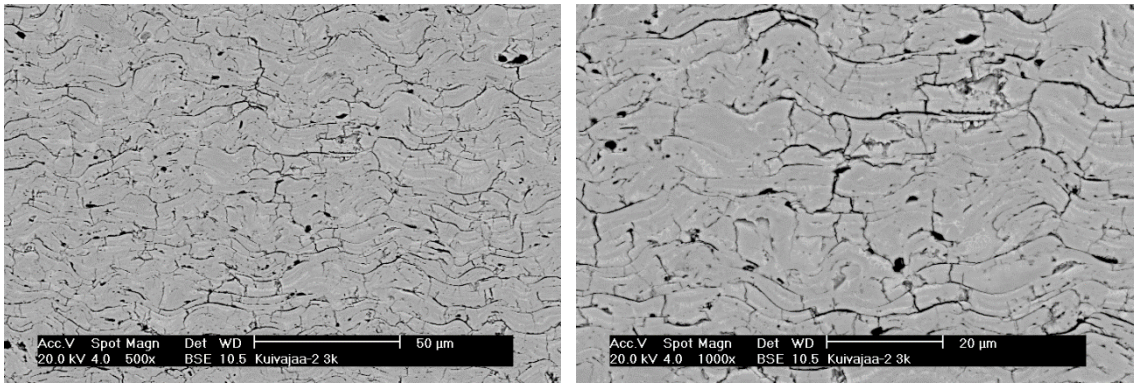

Figure 92: Sample 3k: 110 mm, ice, 6 bar, 40 kg/h

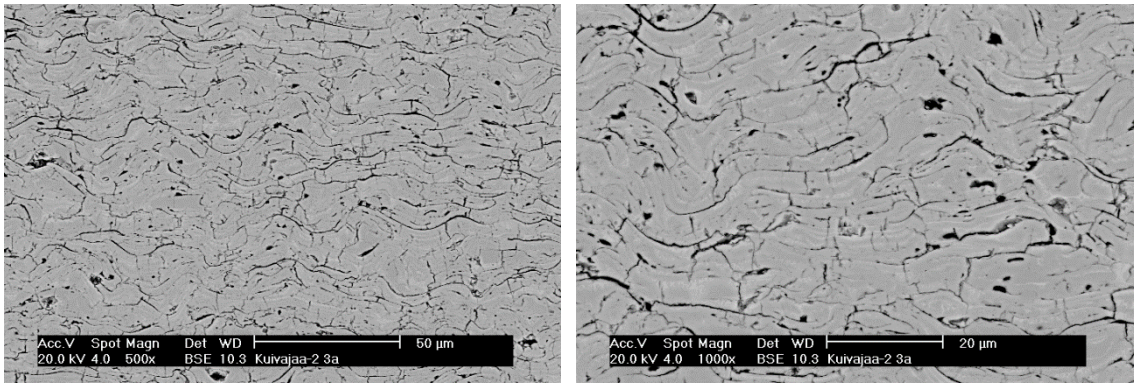

Figure 93: Sample 3a: 130 mm, ice, 4 bar, 40 kg/h

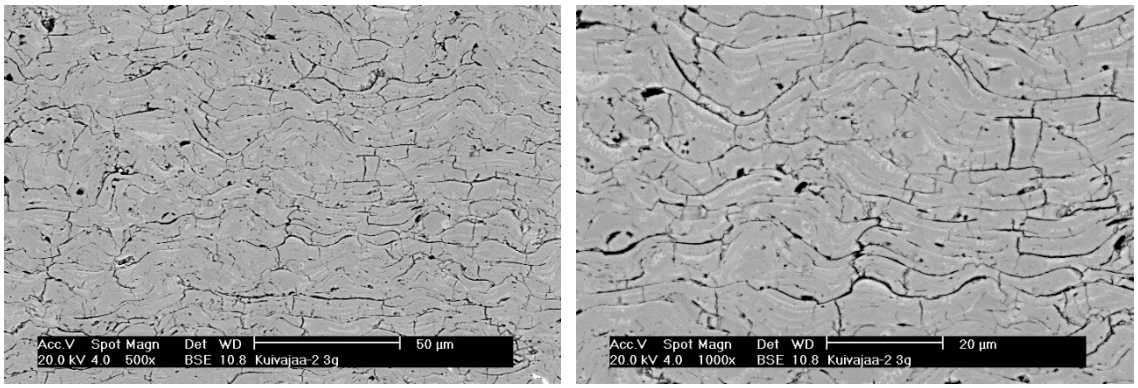

Figure 94: Sample 3g: 90 mm, ice, 4 bar, 40 kg/h, reversed

3rd spraying set:

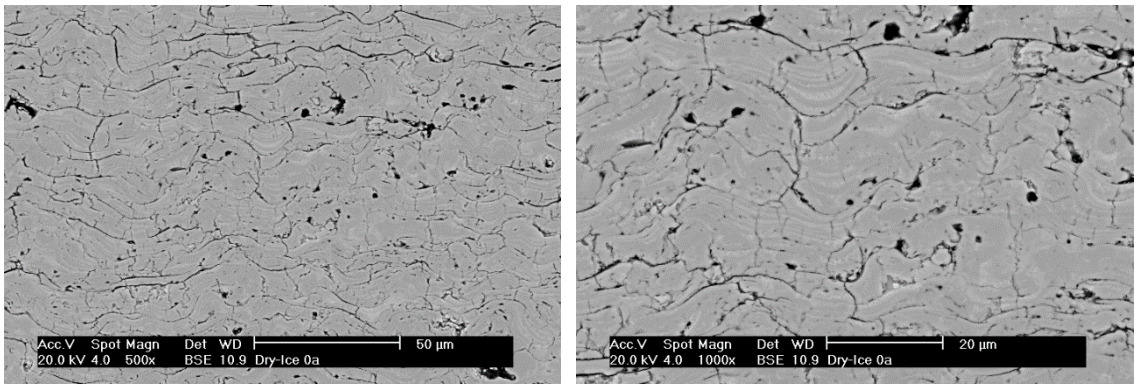

Figure 95: Sample 0a: 110 mm, air, 6 bar, spread out cooling, 60 m/min

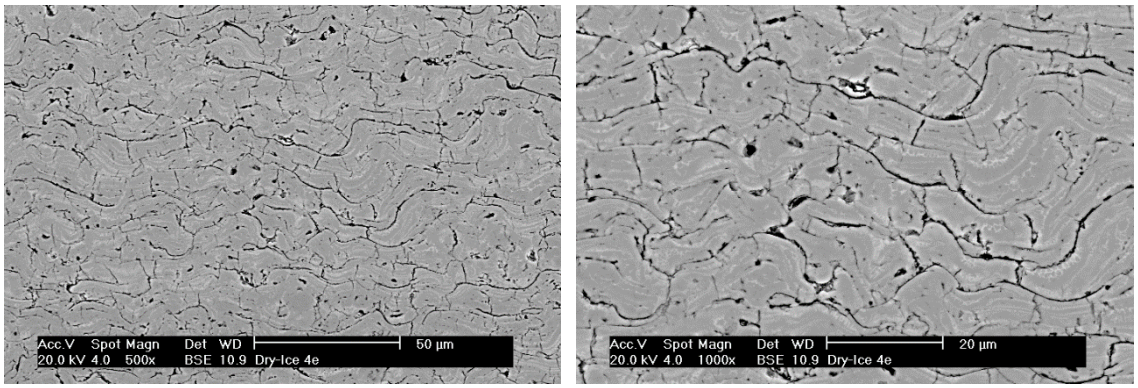

Figure 96: Sample 4e: 110 mm, ice, 2 bar, 20 kg/h, 60 m/min

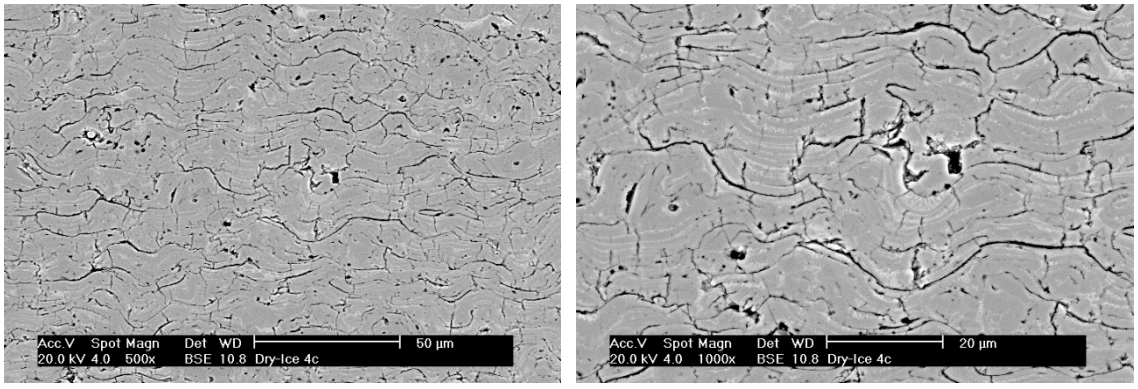

Figure 97: Sample 4c: 110 mm, ice, 2 bar, 20 kg/h, 90 m/min

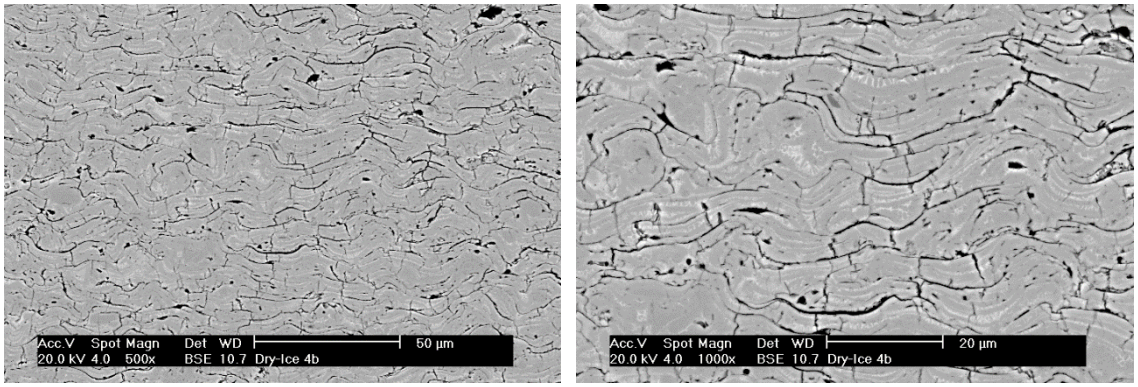

Figure 98: Sample 4b: 110 mm, ice, 4 bar, 20 kg/h, 90 m/min

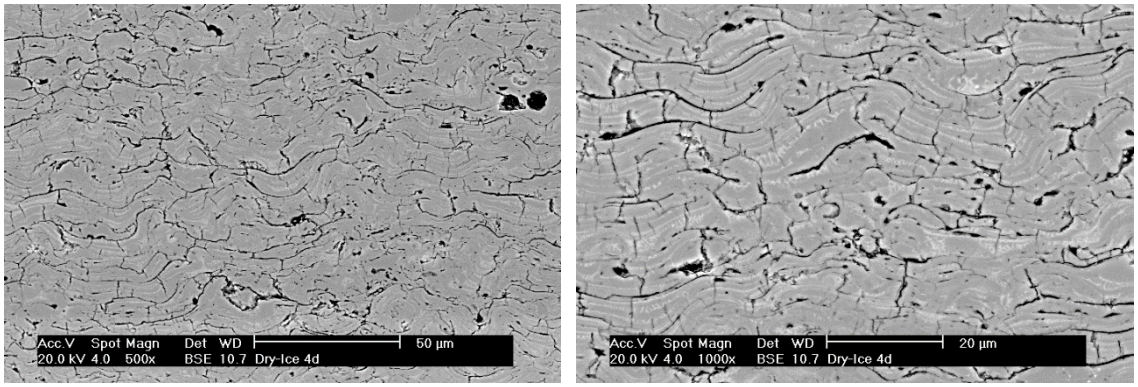

Figure 99: Sample 4d: 110 mm, ice, 4 bar, 40 kg/h, 60 m/min

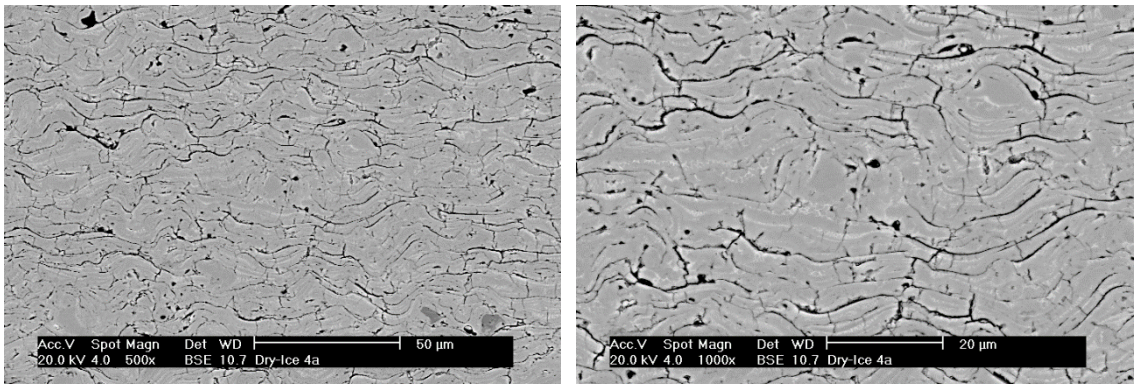

Figure 100: Sample 4a: 110 mm, ice, 4 bar, 40 kg/h, 90 m/min